Oil & Natural Gas Technology

DOE Award No.: DE-FC26-03NT15403

Final Report

Development of Next Generation Multiphase Pipe Flow Prediction Tools

Submitted by:
Tulsa University Fluid Flow Projects
800 South Tucker Drive
Tulsa, Oklahoma 74104

Prepared for:
United States Department of Energy
National Energy Technology Laboratory

November 1, 2008

Office of Fossil Energy

DISCLAIMER

TABLE OF CONTENTS

LIST OF TABLES

LIST OF FIGURES

EXECUTIVE SUMMARY

The developments of fields in deep waters (5000 ft and more) is a common occurrence. It is inevitable that production systems will operate under multiphase flow conditions (simultaneous flow of gas-oil-and water possibly along with sand, hydrates, and waxes). Multiphase flow prediction tools are essential for every phase of the hydrocarbon recovery from design to operation. The recovery from deep-waters poses special challenges and requires accurate multiphase flow predictive tools for several applications including the design and diagnostics of the production systems, separation of phases in horizontal wells, and multiphase separation (topside, seabed or bottom-hole). It is very crucial to any multiphase separation technique that is employed either at topside, seabed or bottom-hole to know inlet conditions such as the flow rates, flow patterns, and volume fractions of gas, oil and water coming into the separation devices.

The overall objective was to develop a unified model for gas-oil-water three-phase flow in wells, flow lines, and pipelines to predict the flow characteristics such as flow patterns, phase distributions, and pressure gradient encountered during petroleum production at different flow conditions (pipe diameter and inclination, fluid properties and flow rates).

The project was conducted in two periods. In Period 1 (four years), gas-oil-water flow in pipes were investigated to understand the fundamental physical mechanisms describing the interaction between the gas-oil-water phases under flowing conditions, and a unified model was developed utilizing a novel modeling approach. A gas-oil-water pipe flow database including field and laboratory data was formed in Period 2 (one year). The database was utilized in model performance demonstration.

Period 1 primarily consisted of the development of a unified model and software to predict the gas-oil-water flow, and experimental studies of the gas-oil-water project, including flow behavior description and closure relation development for different flow conditions.

Modeling studies were performed in two parts, Technology Assessment and Model Development and Enhancement. The results of the Technology assessment study indicated that the performance of the current state of the art two-phase flow models was poor especially for three-phase pipeline flow when compared with the existing data.

As part of the model development and enhancement study, a new unified model for gas-oil-water three-phase pipe flow was developed. The new model is based on the dynamics of slug flow, which shares transition boundaries with all the other flow patterns. The equations of slug flow are used not only to calculate the slug characteristics, but also to predict transitions from slug flow to other flow patterns.

An experimental program including three-phase gas-oil-water horizontal flow and two-phase horizontal and inclined oil-water flow testing was conducted utilizing a Tulsa University Fluid Flow Projects Three-phase Flow Facility. The experimental results were incorporated into the unified model as they became available, and model results were used to better focus and tailor the experimental study.

Finally, during the Period 2, a new three-phase databank has been developed using the data generated during this project and additional data available in the literature. The unified model to predict the gas-oil-water three phase flow characteristics was tested by comparing the prediction results with the data. The results showed good agreements.

MODELING

TECHNOLOGY ASSESSMENT

OBJECTIVES

The objectives of the Technology Assessment are four-fold

- Collect experimental data and review theoretical models for gas-oil-water pipe flow from open literature.
- Evaluate existing models with experimental results.
- Identify limitations and shortcomings of the models.
- Suggest modifications and new developments for future studies.

APPROACH

The approach to accomplish the set objectives of the Technology Assessment is given in four consecutive steps.

- Literature Review: This provides the state of the art in the area of gas-oil-water modeling studies.
- Data Collection: There are data available in the open literature and from other academic institutions. A TUFFP gas-oil-water databank will be created. The databank will be expandable for future data collection and TUFFP experimental results.
- Evaluation of Existing Models with the Collected Data: The applicability of existing multiphase flow models for gas-oil-water flows will be studied. This evaluation will help develop better models to predict gas-oil-water flow characteristics.
- Implementation of Existing Models: The selected multiphase models will be programmed, if necessary, to evaluate the models against the databank.

INTRODUCTION

Three-phase (gas-oil-water) flow is a common occurrence in the petroleum industry. Perhaps the most relevant practice is the transportation of natural gas-oil-water mixtures through pipelines. Three-phase flow may also be encountered in pumping systems, especially in surface gathering lines, and in wellbores and surface gathering systems of many flowing and gas lift wells which produce water along with oil and gas.

Because of the importance and wide applications of three-phase gas-oil-water flow behavior, a reliable model is needed for predicting gas-oil-water flows. There are some experimental measurements and theoretical modeling that have been done in the past. In this project, a literature review was conducted to survey previous studies involving three-phase flow. Several data sets were collected from the open literature for horizontal and near-horizontal flows. The data for vertical three-phase flows were extracted from the Tulsa University Fluid Flow Projects (TUFFP) Well Databank. The selected data are used to assess the models of their applicability and validity of the models.

LITERATURE REVIEW

Following is a summary of the literature reviewed.

Sobocinski (1955) conducted an experimental study of water, gas-oil, and air in a horizontal co-current flow. This was one of the early studies conducted on three-phase flow. This study provided data

of both pressure drop and holdup. Experiments were conducted in a 3-in. diameter transparent plastic pipe using air, water and diesel oil. The flow patterns included stratified smooth, stratified wavy and semi annular flows.

Malinowsky (1975) conducted an experimental study of oil-water and air-oil-water flowing mixtures in horizontal pipes at TUFFP. Pressure gradients were measured for the three-phase tests. Tests were conducted using a 1.5-in. ID. transparent acrylic pipe. The approach in this study was to back calculate an effective viscosity using the Beggs and Brill correlation.

Laflin and Oglesby (1976) used the same approach as Malinowsky. They also used the same testing facilities and produced more data for their study. They investigated flow rates near the inversion point and concluded that the viscosity peaks near those points.

Taitel *et al*. (1995) calculated stratified three-phase flow holdups as a step to find transition criteria. Three theoretical steady-state configurations can be obtained. Only the configuration with the thinnest total liquid layer is stable.

Langsholt *et al*. (2001) performed three-phase-oil-water-gas flow in a 100-mm diameter pipe at various inclinations up to 30^{o} uphill. The study showed that total holdup increases with increasing water flow.

Hall (1992) studied multiphase flow of gas-oil-water flow in horizontal pipes. He compared his experimental measurements with predictions of the steady-state three-phase stratified flow momentum equations. This study also provides test points from the literature.

Stapelberg (1991) studied the horizontal three-phase flow of air, water and oil. The oil viscosity was 27.8 mPas and the oil specific gravity was 0.846. The experiments were run in a 23.8-mm ID pipe. This study concentrated on three-phase slug flow.

In the Valle (2000) study of gas-crude oil-water flow in pipes, the liquid-liquid flow interactions were observed, and global models were proposed to address the phenomena.

Kvandal *et al*. (1998) conducted gas-oil-water field experiments in an operating North Sea field. The experiments were run in a pipeline with an ID of 254 mm. The oil viscosity ranged from 3 to5 mPa while the oil specific gravity ranged from 0.85 to 0.875. A total of 15 tests were conducted, reporting gas, oil and water flow rates and pressure drop.

Acikgoz *et al*. (1992) conducted gas-oil-water tests to generate flow pattern maps at various oil flow rates. The oil specific gravity and viscosity used were 0.864 and 0.1167 Pas, respectively. A total of 124 tests were completed reporting gas, oil and water superficial velocities and the corresponding flow patterns.

DATA BANKS

The data banks used for the model evaluation are the TUFFP well data bank (401 out of 2052 are gas-oil-water three-phase data) and the horizontal three-phase flow databank. The horizontal three-phase flow databank was developed in this study. Tables 1 and 2 summarize these two data banks.

TWO-PHASE FLOW MODELS

Predictions by existing two-phase flow models or correlations were compared with the collected three-phase experimental data. The correlations and models selected for comparison with vertical three-phase flow data include Beggs and

Brill (1973), modified Hagedorn and Brown (1964), Kaya (1998) and Zhang et al. (2003b). For horizontal and near-horizontal flows, the correlation developed by Beggs and Brill (1973) and the unified model developed by Zhang et al. (2003b) were selected for comparisons with experimental data. In order to conduct the evaluation, the physical properties of the liquid mixture must be estimated. Estimation of the liquid mixture density, liquid mixture viscosity and liquid mixture surface tension are as follows:

- Density of oil/water mixture:

$$\rho_L = \rho_W C_W + \rho_O (1 - C_W)$$

where, $C_W = Q_W / (Q_O + Q_W)$

- Liquid Viscosity

$$\mu_L = \mu_W C_W + \mu_O (1 - C_W)$$

- Liquid Surface Tension:

$$\sigma_L = \sigma_W C_W + \sigma_O (1 - C_W)$$

COMPARISONS

CRITERIA

The evaluation is being carried out by comparing the measured and predicted pressure gradients for the horizontal flow and the pressure drops for the vertical flow. Below are the definitions of the statistical parameters used for the comparisons:

$$\varepsilon_1 = \left[\frac{1}{N} \sum_{j=1}^{N} e_{rj} \right] \times 100$$

where

$$e_{rj} = \frac{\Delta p_{j,calc} - \Delta p_{j,meas}}{\Delta p_{j,meas}}$$

$$\varepsilon_2 = \frac{1}{N} \sum_{j=1}^{N} \left| e_{rj} \right| \times 100$$

$$\varepsilon_3 = \sqrt{\frac{\sum_{j=1}^{N} \left[e_{rj} \times 100 - \varepsilon_1 \right]^2}{N-1}}$$

$$\varepsilon_4 = \frac{1}{N} \sum_{i=1}^{N} e_i$$

where $e_i = \Delta p_{i,calc} - \Delta p_{i,meas}$

$$\varepsilon_5 = \frac{1}{N} \sum_{i=1}^{N} \left| e_i \right|$$

$$\varepsilon_6 = \sqrt{\frac{\sum_{i=1}^{N} \left[e_i - \varepsilon_4 \right]^2}{N-1}}$$

In order to compare the performances of different models, a Relative Performance Factor (RPF) is defined as:

$$RPF_i = \frac{\left|\varepsilon_{1i}\right| - \left|\varepsilon_{1MIN}\right|}{\left|\varepsilon_{1MAX}\right| - \left|\varepsilon_{1MIN}\right|} + \frac{\varepsilon_{2i} - \varepsilon_{2MIN}}{\varepsilon_{2MAX} - \varepsilon_{2MIN}} + \frac{\varepsilon_{3i} - \varepsilon_{3MIN}}{\varepsilon_{3MAX} - \varepsilon_{3MIN}} + \frac{\left|\varepsilon_{4i}\right| - \left|\varepsilon_{4MIN}\right|}{\left|\varepsilon_{4MAX}\right| - \left|\varepsilon_{4MIN}\right|} + \frac{\varepsilon_{5i} - \varepsilon_{5MIN}}{\varepsilon_{5MAX} - \varepsilon_{5MIN}}$$

The value of RPF should be between 0 and 6 which correspond to the best and the worst comparisons.

UPWARD VERTICAL FLOWS

The models used to calculate pressure drops for upward vertical flow are Zhang et al. (2003b), Kaya (1998), Beggs and Brill (1973), and The modified Hagedorn and Brown (1964).

Table 3 shows the statistical parameters for the models evaluated. Kaya (1998) model has the smallest values of ε_1, ε_2, ε_5 and ε_6. Figure 1 shows predicted pressure drops by Kaya vs. measured pressure drops.

Zhang *et al*. (2003) unified model is the second best method with the lowest value of E4 and second lowest values of ε_1, ε_3, ε_5 and ε_6. Figure 2 shows the predictions of the Zhang *et al*. model vs. the measured pressure drops.

The third best predictive method is the Beggs and Brill (1973) correlation (comparisons shown in Fig. 3) with the smallest value of ε_3. The modified Hagedorn and Brown (1964) correlation is the least accurate method (shown in Fig. 4).

HORIZONTAL AND NEAR-HORIZONTAL FLOWS

For horizontal and near-horizontal three-phase flow, pressure gradient data were collected from the open literature. Studies conducted by Sobocinski (1955), Malinowiski (1975), Laflin and Oglesby (1976), Hall (1992) and Khor (1998) generated 438 data points as listed in Table 2. The measured pressure gradients were compared with calculated pressure gradients by the model of Zhang et al. (2003b) and the correlation of Beggs and Brill (1973).

Table 4 shows the values of ε_1, ε_2, ε_3, ε_4, ε_5 and ε_6 for both methods. The performance of the Zhang et al. (2003b) unified model is better than the performance of the Beggs and Brill (1973) correlation. Both methods over-predict pressure gradients. Figure 5 shows the comparisons between the predicted pressure gradients by the Zhang *et al*. model and the measured pressure gradients. Figure 6 shows the performance of the Beggs and Brill correlation in comparison with the measured pressure gradients.

Figure 7 is a close-up view of Fig. 5 for low pressure gradient comparisons. It is seen that the discrepancies between the calculated and measured pressure gradients are very significant. The flow patterns corresponding to low pressure gradient are mostly stratified flow.

All of Hall's (1992) experimental data corresponded to three-phase slug flow. Table 5 summarizes the statistical parameters for the comparisons between model predictions and Hall's data only. Zhang et al. (2003b) unified model gives much better predictions of pressure gradients for slug flows than for general three-phase horizontal/near-horizontal flows.

Khor (1998) conducted experiments for horizontal and near-horizontal three-phase stratified flows. Figure 8 shows the comparison between predicted pressure gradients by Zhang et al. (2003b) model and Khor's data for horizontal flows. It can be seen that the discrepancies are significant.

SUMMARY

As can be seen from above comparisons, the existing two-phase gas-liquid correlations and models perform poorly for three-phase flow of gas-oil-water. The following sections describe the new model for the three-phase flow of gas-oil-water in pipes.

Table 1 - Vertical Three-Phase Flow Data from TUFFP Well Data Bank

Data Sources	Tubing Diameter (in)	No. of Data	Fluids Used
Poettmann and Carpenter (1952)	1.995-2.441	14	Air-Oil-Water
Fancher (1963)	1.944	82	Air-Oil-Water
Orkizewski (1967)	8.76	2	Air-Oil-Water
Español (1970)	2.38	8	Air-Oil-Water
Oil Companies*	1.995~2.441	106	Air-Oil-Water
Govier et al. (1975)	1.992-4.404	49	Air-Oil-Water
Chierici et al. (1974)	4.89	1	Air-Oil-Water
Prudhoe Bay	3.96-7.88	139	Air-Oil-Water
	Total Data	**401**	

*Marathon, Exxon, Amoco, Chevron, Unocal, Union Oil

Table 2 – Horizontal/Near-Horizontal Three-Phase Flow Data Bank

Data Sources	Pipe ID (mm)	No. of Data	Fluids Used
Sobocinski (1955)	76.2	114	Air-Oil-Water
Malinowsky (1975)	38	34	Air-Oil-Water
Laflin and Oglesby (1976)	38	79	Air-Oil-Water
Hall (1992)	79	93	Air-Oil-Water
Khor (1998)	79	118	Air-Oil-Water
	Total Data	**438**	

Table 3 - Model Comparisons for Vertical Three-Phase Flow (401 Cases)

Correlation/Model	Zhang et al.	Kaya	Beggs and Brill	Hagedorn and Brown
ε_1 (%)	2.53	**-2.29**	15.07	-6.89
ε_2 (%)	13.02	**11.36**	20.43	17.93
ε_3 (%)	18.53	15.33	**12.13**	21.30
ε_4 (psi)	**-29.02**	-52.15	107.46	-208.20
ε_5 (psi)	164.36	**136.97**	210.04	289.47
ε_6 (psi)	273.48	**240.57**	287.73	397.45
RPF	1.29	**0.12**	3.22	4.01

Table 4 - Model Comparisons for Horizontal/Near-Horizontal Three-Phase Flow (438 Cases)

Correlation/Model	Zhang et al.	Beggs and Brill
ε_1 (%)	**58.3**	218.5
ε_2 (%)	**123.3**	232.9
ε_3 (%)	**289.6**	413.9
ε_4 (Pa/m)	**139**	277.9
ε_5 (Pa/m)	**216.9**	301.5
ε_6 (Pa/m)	527.7	**526.5**

Table 5 - Comparisons with Hall's Data for Three-Phase Slug Flow (107 Cases)

Correlation/Model	ZHANG	BBRIL
ε_1 (%)	**15.4**	84.5
ε_2 (%)	**33.3**	92.9
ε_3 (%)	**37**	59
ε_4 (Pa/m)	**10.9**	127.2
ε_5 (Pa/m)	**79**	161.7
ε_6 (Pa/m)	**113.93**	141.4

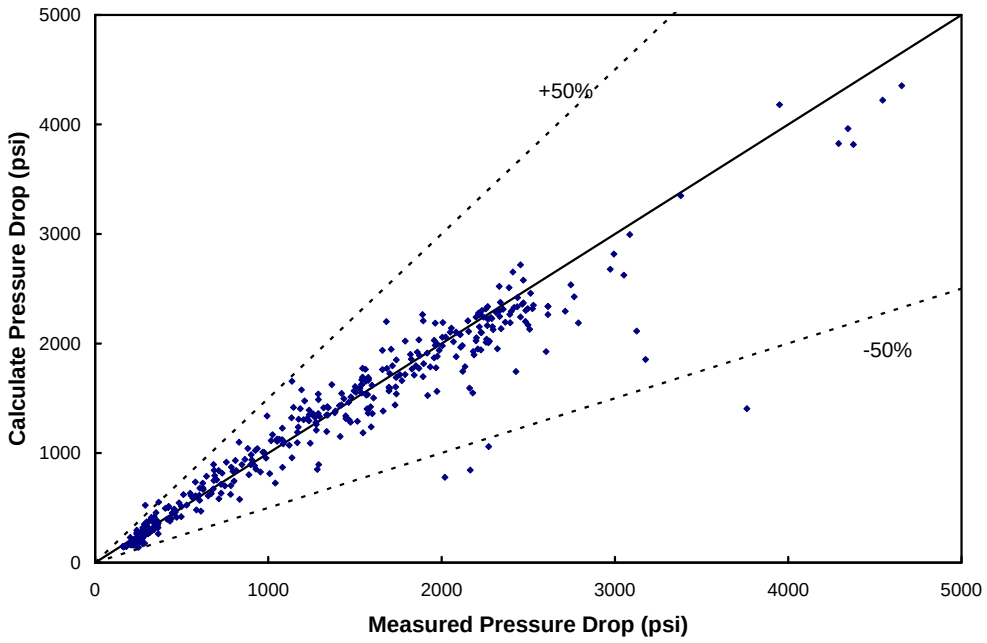

Figure 1 – Kaya Model Predictions vs. TUFFP Well Databank

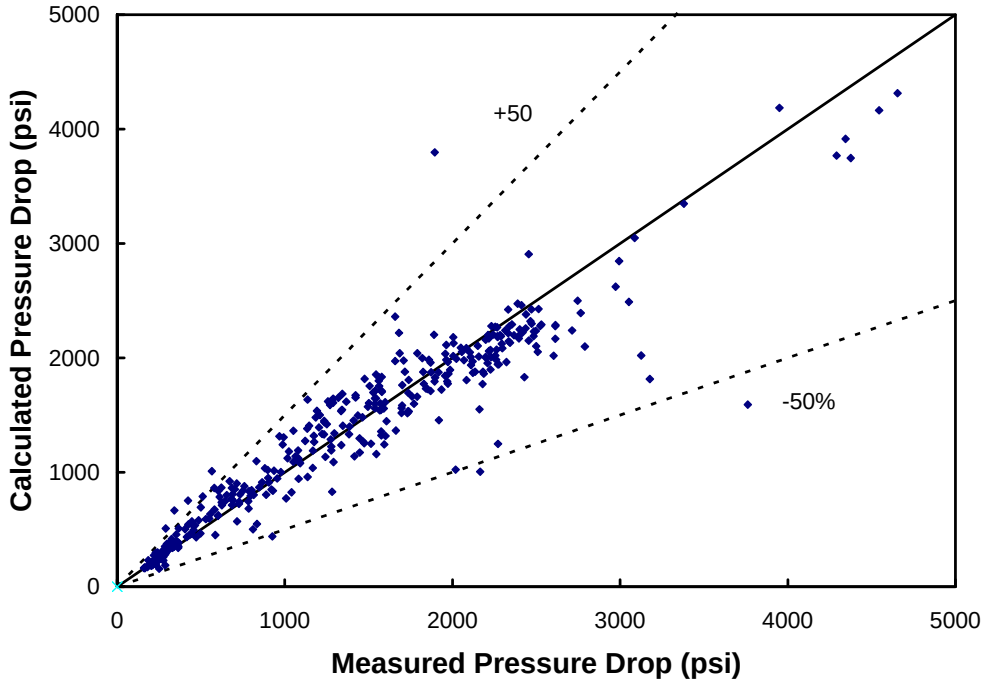

Figure 2 – Zhang et al. Model Predictions vs. TUFFP Well Databank

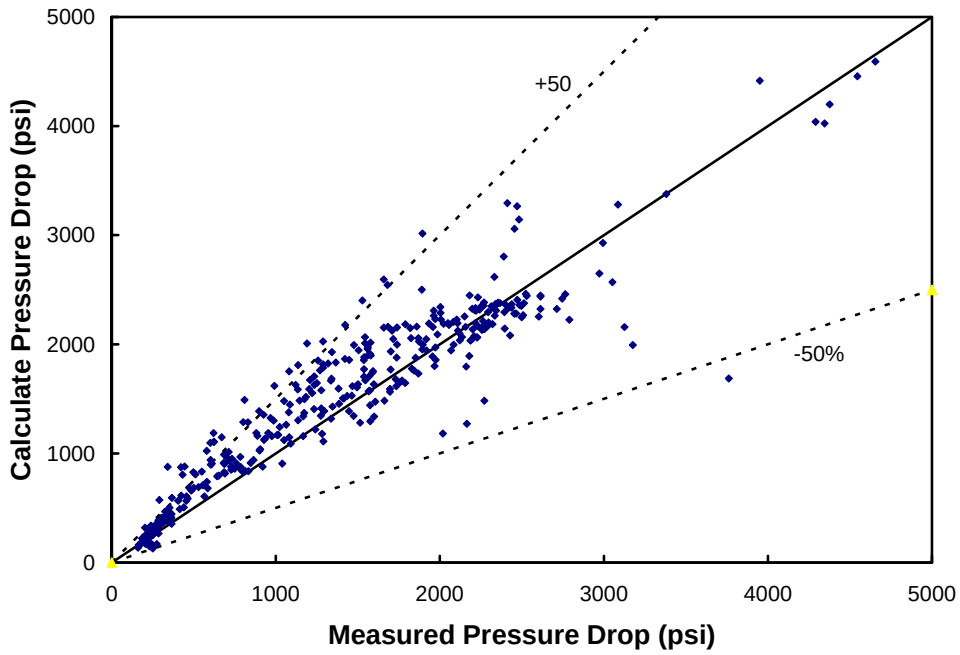

Figure 3 – Beggs and Brill Predictions vs. TUFFP Well Databank

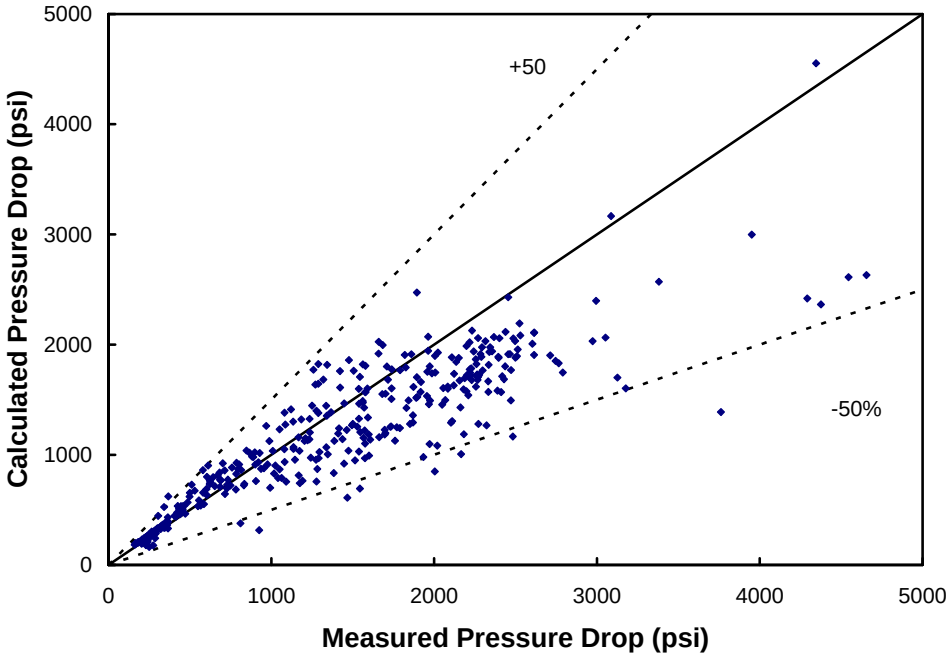

Figure 4 – Hagedorn and Brown Predictions vs. TUFFP Well Databank

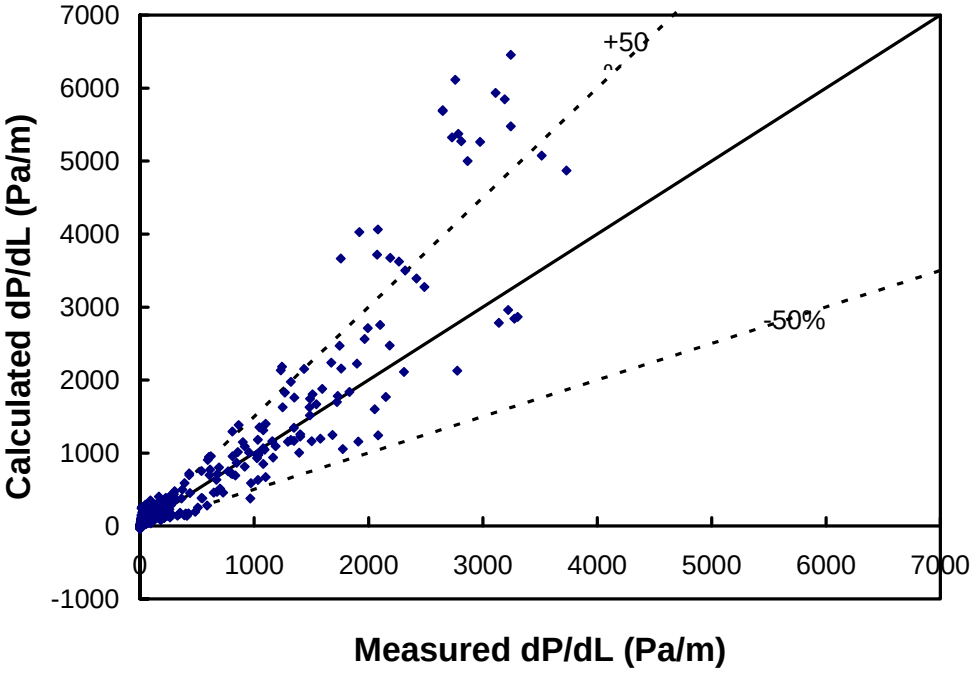

Figure 5– Zhang et al. Model vs. Horizontal Databank

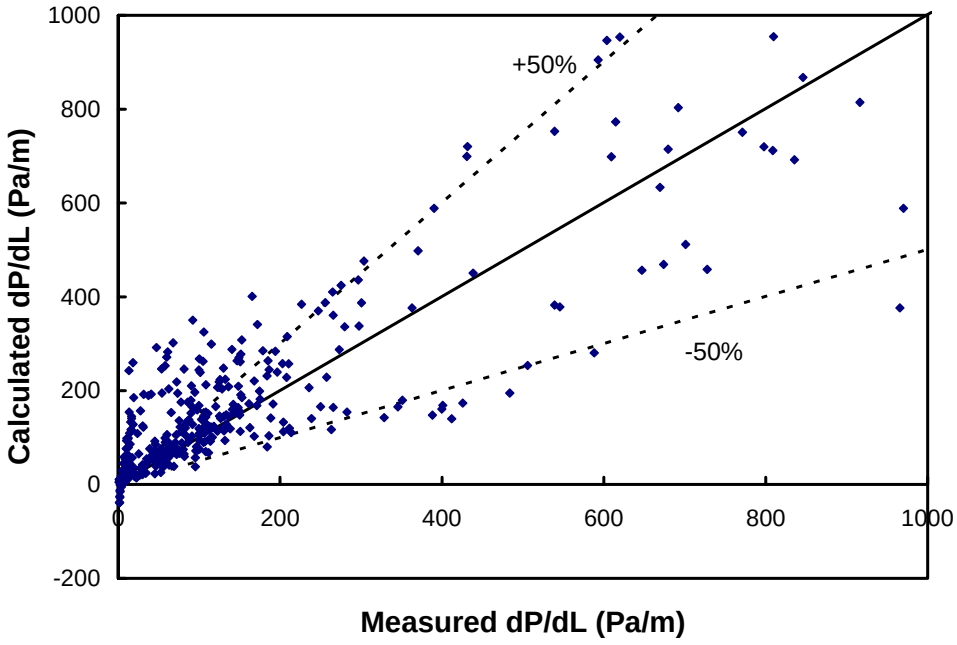

Figure 6 – Zhang et al. Model vs. Horizontal Databank (Close-up)

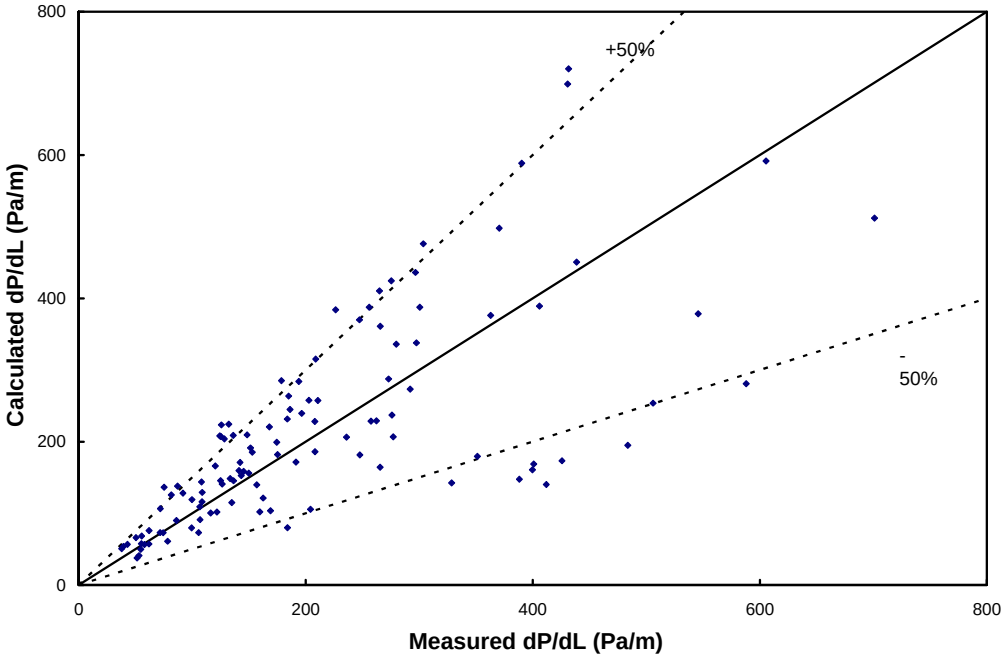

Figure 7 – Zhang et al. Model vs. Hall's Data for Three-Phase Slug Flow

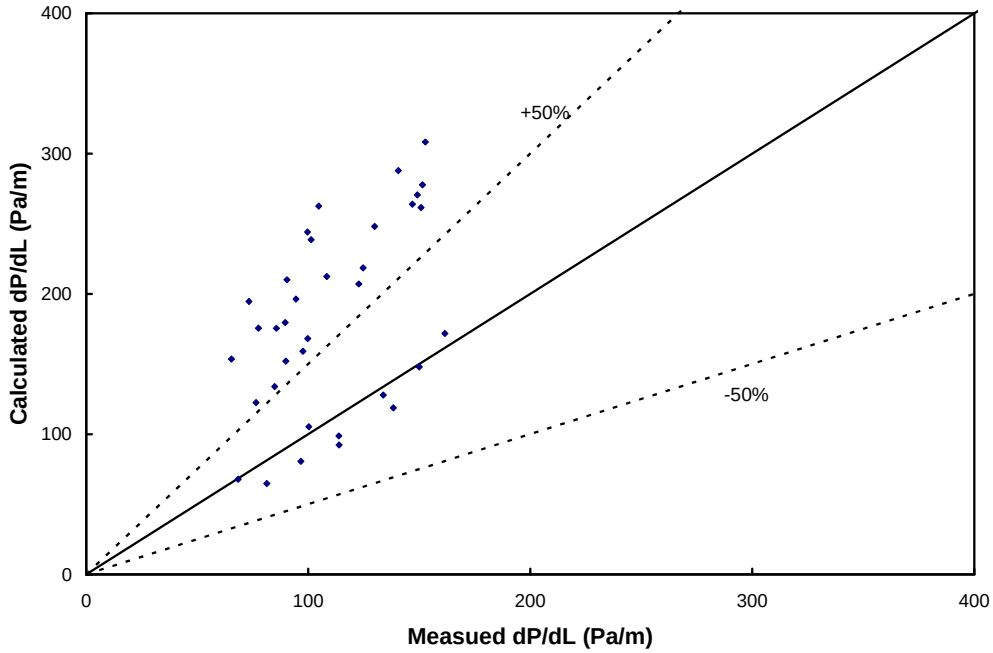

Figure 8 – Zhang et al. Model vs. Khor's Data for Three-Phase Stratified Flow

MODEL DEVELOPMENT AND ENHANCEMENT – UNIFIED MODELING

Experimental observations have shown that the flow structures of three-phase pipe flow are much more complicated than that of two-phase pipe flow. Açikgöz *et al*. (1992) classified flow patterns of horizontal three-phase flow into 10 categories. Pan *et al*. (1995) identified 7 flow patterns for horizontal air-oil-water flow. For vertical air-oil-water flow, Woods *et al*. (1998) identified 8 flow patterns. Multiphase flow hydrodynamic modeling is based on flow pattern definitions. More flow patterns imply more discontinuities and greater complexity in the hydrodynamic models. A successful model should unify the predictions of both flow pattern transitions and hydrodynamic behavior and minimize these discontinuities at the same time.

A unified gas-liquid two-phase flow model has been developed by Zhang *et al*. (2003b) for predictions of flow pattern transitions, pressure gradient, liquid holdup and slug characteristics for all inclination angles from –90° to 90° from horizontal. The model is based on the dynamics of slug flow, which shares transition boundaries with all the other flow patterns. The equations of slug flow are used not only to calculate the slug characteristics, but also to predict transitions from slug flow to other flow patterns.

Similar methodology can also be used for gas-oil-water three-phase flow. In three-phase pipe flow, the gas versus liquid phase distribution and structures may be of primary importance compared with the distribution between liquid phases due to the differences among the physical properties of the three phases. Therefore, we can adopt gas-liquid two-phase flow patterns to describe gas-oil-water three-phase flow, and use additional closure relationships to describe the distribution between the liquid phases, namely mixing and inversion.

Gas-oil-water three-phase flow can be treated as gas-liquid two-phase flow if the two liquids are fully mixed. This is probably true for vertical and steeply inclined flows, and slug and annular flows at high flow rates. The physical properties of the liquid mixture can be calculated based on the fractions and the individual physical properties of the two liquids.

The other extreme is to treat three-phase flow as a three-layer stratified flow with gas on the top, oil in the middle and water at the bottom. This can be done for immiscible liquids flowing in horizontal or slightly inclined pipe with low gas, oil and water flow rates. Among others, Hall (1992), Taitel *et al*. (1995) and Khor *et al*. (1997) modeled stratified three-phase flow in pipes by use of momentum equations for the three layers.

Most three-phase flows fit between the above two extremes: partially mixed with slippage between the two liquid phases. Some flows, such as slug flow, may display different states in different regions, e.g. stratified in the film region and fully mixed in the slug body.

EQUATIONS FOR SLUG FLOW WITH STRATIFIED OIL AND WATER

CONTINUITY EQUATIONS

As shown in Fig. 9, the entire liquid film zone (including liquid film and gas pocket) of a slug unit is used as the control volume. Continuity equations are derived relative to a coordinate system moving with the translational velocity, v_T. For steady state three-phase flow, the mass input and output rates at the left and right boundaries of the film region must be the

same for each phase. Assuming no liquid entrainment in the gas core at relatively low flow rate, the continuity equations for the oil, water and gas phases in the film zone can be obtained, respectively, as

$$(1-H_{WGS})(1-\alpha_{OS})(v_T-v_{OS})=H_{OF}(v_T-v_{OF}), \quad (1)$$

$$H_{WGS}(1-\alpha_{WS})(v_T-v_{WS})=H_{WF}(v_T-v_{WF}), \quad (2)$$

$$\begin{aligned}&(1-H_{WGS})\alpha_{OS}(v_T-v_{OS})+H_{WGS}\alpha_{WS}(v_T-v_{WS})\\&=(1-H_{OF}-H_{WF})(v_T-v_G)\end{aligned}. \quad (3)$$

The mixture velocity is

$$v_M=v_{SG}+v_{SO}+v_{SW}. \quad (4)$$

The mixture velocity is also related to the local velocities in the slug body and the film zone, respectively, as

$$v_M=(1-H_{WGS})v_{OS}+H_{WGS}v_{WS} \quad (5)$$

and

$$v_M=H_{OF}v_{OF}+H_{WF}v_{WF}+(1-H_{OF}-H_{WF})v_G. \quad (6)$$

Considering the passage of a slug unit at an observation point, the following relationships hold for the oil, water and gas phases, respectively,

$$l_U v_{SO}=l_S(1-H_{WGS})(1-\alpha_{OS})v_{OS}+l_F H_{OF}v_{OF}, \quad (7)$$

$$l_U v_{SW}=l_S H_{WGS}(1-\alpha_{WS})v_{WS}+l_F H_{WF}v_{WF}, \quad (8)$$

$$\begin{aligned}&l_U v_{SG}=l_S[(1-H_{WGS})\alpha_{OS}v_{OS}+H_{WGS}\alpha_{WS}v_{WS}]\\&+l_F(1-H_{OF}-H_{WF})v_G\end{aligned} \quad (9)$$

The slug unit length is given by

$$l_U=l_S+l_F. \quad (10)$$

MOMENTUM EQUATIONS

Applying the oil phase continuity equation, Eq. 1, the momentum exchange per unit time between the oil phase in the slug body and the oil phase in the film region is

$$\rho_O H_{OF}A(v_T-v_{OF})(v_{OS}-v_{OF}).$$

The frictional force acting on the oil film at the wall (in the opposite direction of z) is

$$-\tau_{OF}S_{OF}l_F.$$

The frictional force acting on the film at the interface between the gas and oil (in the same direction as z) is

$$\tau_{I1}S_{I1}l_F.$$

The frictional force acting on the film at the interface between the oil and water (in the opposite direction of z) is

$$-\tau_{I2}S_{I2}l_F.$$

The gravitational force is

$$-\rho_O H_{OF}Al_F g\sin\theta.$$

All the above forces should be in balance for fully developed slug flow. Therefore, the momentum equation for the oil film in the gas pocket region can be obtained,

$$\begin{aligned}\frac{(p_2-p_1)}{l_F}&=\frac{\rho_O(v_T-v_{OF})(v_{OS}-v_{OF})}{l_F}\\&+\frac{\tau_{I1}S_{I1}-\tau_{I2}S_{I2}-\tau_{OF}S_{OF}}{H_{OF}A}-\rho_O g\sin\theta\end{aligned}. \quad (11)$$

Similarly, the momentum equation for the water film in the gas pocket region can be written as

$$\begin{aligned}\frac{(p_2-p_1)}{l_F}&=\frac{\rho_W(v_T-v_{WF})(v_{WS}-v_{WF})}{l_F}\\&+\frac{\tau_{I2}S_{I2}-\tau_{WF}S_{WF}}{H_{WF}A}-\rho_W g\sin\theta\end{aligned}. \quad (12)$$

The momentum exchange between the slug body and the gas pocket is negligible since the gas density is much smaller than the liquid density. The momentum equation for the gas pocket can be written as

$$\frac{(p_2-p_1)}{l_F}=-\frac{\tau_{I1}S_{I1}+\tau_G S_G}{(1-H_{OF}-H_{WF})A}-\rho_G g\sin\theta. \quad (13)$$

From Eqs. 11 and 12, we can obtain

$$\frac{(p_2-p_1)}{l_F}=$$
$$\frac{\rho_O H_{OF}(v_T-v_{OF})(v_{OS}-v_{OF})+\rho_W H_{WF}(v_T-v_{WF})(v_{WS}-v_{WF})}{l_F(H_{OF}+H_{WF})}$$
$$+\frac{\tau_{I1}S_{I1}-\tau_{OF}S_{OF}-\tau_{WF}S_{WF}}{(H_{OF}+H_{WF})A}-\frac{(\rho_O H_{OF}+\rho_W H_{WF})g\sin\theta}{H_{OF}+H_{WF}}. \quad (14)$$

Then, a combined momentum equation for gas and liquid streams can be obtained from Eqs. 13 and 14,

$$\frac{\rho_O H_{OF}(v_T-v_{OF})(v_{OS}-v_{OF})+\rho_W H_{WF}(v_T-v_{WF})(v_{WS}-v_{WF})}{l_F(H_{OF}+H_{WF})}$$
$$-\frac{\tau_{OF}S_{OF}+\tau_{WF}S_{WF}}{(H_{OF}+H_{WF})A}+\frac{\tau_{I1}S_{I1}}{A}\left(\frac{1}{H_{OF}+H_{WF}}+\frac{1}{1-H_{OF}-H_{WF}}\right)$$
$$+\frac{\tau_C S_C}{(1-H_{OF}-H_{WF})A}-\left(\frac{\rho_O H_{OF}+\rho_W H_{WF}}{H_{OF}+H_{WF}}-\rho_G\right)g\sin\theta=0. \quad (15)$$

Another combined momentum equation for oil and water streams can be obtained from Eqs. 11 and 12,

$$\frac{\rho_W(v_T-v_{WF})(v_{WS}-v_{WF})-\rho_O(v_T-v_{OF})(v_{OS}-v_{OF})}{l_F}$$
$$-\frac{\tau_{WF}S_{WF}}{H_{WF}A}+\frac{\tau_{OF}S_{OF}-\tau_{I1}S_{I1}}{H_{OF}A}$$
$$+\frac{\tau_{I2}S_{I2}}{A}\left(\frac{1}{H_{WF}}+\frac{1}{H_{OF}}\right)-(\rho_W-\rho_O)g\sin\theta=0. \quad (16)$$

For stratified oil and water flows in the slug body, the momentum equations can be obtained as

$$\frac{(p_1-p_0)}{l_S}=\frac{\rho_O(v_T-v_{OS})(v_{OF}-v_{OS})}{l_S}$$
$$-\frac{\tau_{I0}S_{I0}+\tau_{OS}S_{OS}}{(1-H_{WGS})A}-\rho_O g\sin\theta \quad (17)$$

and

$$\frac{(p_1-p_0)}{l_S}=\frac{\rho_W(v_T-v_{WS})(v_{WF}-v_{WS})}{l_S}$$
$$+\frac{\tau_{I0}S_{I0}-\tau_{WS}S_{WS}}{H_{WGS}A}-\rho_W g\sin\theta. \quad (18)$$

The combined momentum equation for the slug body can be obtained from Eqs. (17) and (18),

$$\frac{\rho_W(v_T-v_{WS})(v_{WF}-v_{WS})-\rho_O(v_T-v_{OS})(v_{OF}-v_{OS})}{l_S}$$
$$-\frac{\tau_{WS}S_{WS}}{H_{WGS}A}+\frac{\tau_{OS}S_{OS}}{(1-H_{WGS})A}$$
$$+\frac{\tau_{I0}S_{I0}}{A}\left(\frac{1}{H_{WGS}}+\frac{1}{(1-H_{WGS})}\right)$$
$$-(\rho_W-\rho_O)g\sin\theta=0. \quad (19)$$

There are 7 unknowns in the above set of equations,

$$H_{WGS},\ v_{WS},\ l_F,\ H_{OF},\ H_{WF},\ v_{OF},\ v_{WF}.$$

These unknowns can be calculated by solving 7 independent equations, which include 4 of the 6 continuity equations (two of Eqs. 1, 2, 3, and two of Eqs. 7, 8, 9) and the 3 combined momentum equations (Eqs. 15, 16, and 19).

EQUATIONS FOR THREE-LAYER STRATIFIED FLOW

The two combined momentum equations for three-layer (gas, oil and water) stratified flow are the same as the two combined momentum equations for the gas pocket region of slug flow if the momentum exchange terms are removed from Eqs. 15 and 16,

$$-\frac{\tau_{OF}S_{OF}+\tau_{WF}S_{WF}}{(H_{OF}+H_{WF})A}+$$
$$\frac{\tau_{I1}S_{I1}}{A}\left(\frac{1}{H_{OF}+H_{WF}}+\frac{1}{1-H_{OF}-H_{WF}}\right)+$$
$$\frac{\tau_G S_G}{(1-H_{OF}-H_{WF})A}-$$
$$\left(\frac{\rho_O H_{OF}+\rho_W H_{WF}}{H_{OF}+H_{WF}}-\rho_G\right)g\sin\theta=0 \quad (20)$$

$$-\frac{\tau_{WF}S_{WF}}{H_{WF}A}+\frac{\tau_{OF}S_{OF}-\tau_{I1}S_{I1}}{H_{OF}A}$$
$$+\frac{\tau_{I2}S_{I2}}{A}\left(\frac{1}{H_{WF}}+\frac{1}{H_{OF}}\right)-(\rho_W-\rho_O)g\sin\theta=0. \quad (21)$$

The holdups of oil and water can be calculated from Eqs. 20 and 21.

EQUATION FOR OIL-WATER STRATIFIED FLOW

The combined momentum equation for oil-water (with possible gas entrapment) stratified flow are the same as the combined momentum equations for the slug body if the momentum exchange term is removed from Eq. 19,

$$-\frac{\tau_{WS}S_{WS}}{H_{WG}(1-\alpha_{WS})A}+\frac{\tau_{OS}S_{OS}}{H_{OG}(1-\alpha_{OS})A}+\frac{\tau_{I0}S_{I0}}{A}\left(\frac{1}{H_{WG}(1-\alpha_{WS})}+\frac{1}{H_{OG}(1-\alpha_{OS})}\right)-(\rho_W-\rho_O)g\sin\theta=0. \quad (22)$$

SLUG FLOW WITH FULLY MIXED OIL AND WATER

The continuity and momentum equations are the same as for gas-liquid two-phase flow. The effective (or apparent) physical properties of the liquid mixture have to be used. Since this condition normally corresponds to high gas and liquid velocities, liquid entrainment in the gas core needs to be considered.

ANNULAR FLOW

In annular flow, oil and water can be assumed as fully mixed due to the high turbulence. Therefore, combined momentum equation for gas-liquid two-phase flow can be used. Entrainment of liquid droplets in the gas core must be considered.

BUBBLE FLOW WITH FULLY MIXED OIL AND WATER

The liquid holdup and pressure gradient for dispersed bubble flow are calculated assuming that the gas and liquid phases are homogeneously mixed. For bubbly flow, the bubble rise velocity, v_o, relative to the liquid must be considered.

Even for dispersed oil-water flow, the average velocities of oil and water may not be the same due to their distributions across the pipe section. The continuous phase is typically slower due to its contact with the pipe wall.

SHEAR STRESSES

The shear stresses in the combined momentum equations are evaluated as

$$\tau_{OF}=f_{OF}\frac{\rho_O v_{OF}^2}{2}, \quad (23)$$

$$\tau_{WF}=f_{WF}\frac{\rho_W v_{WF}^2}{2}, \quad (24)$$

$$\tau_G=f_G\frac{\rho_G v_G^2}{2}, \quad (25)$$

$$\tau_{OS}=f_{OS}\frac{\rho_O v_{OS}^2}{2}, \quad (26)$$

$$\tau_{WS}=f_{WS}\frac{\rho_W v_{WS}^2}{2}, \quad (27)$$

$$\tau_{I1}=f_{I1}\frac{\rho_G(v_G-v_{OF})|v_G-v_{OF}|}{2}, \quad (28)$$

$$\tau_{I2}=f_{I2}\frac{\rho_O(v_{OF}-v_{WF})|v_{OF}-v_{WF}|}{2}, \quad (29)$$

$$\tau_{I0}=f_{I0}\frac{\rho_O(v_{OS}-v_{WS})|v_{OS}-v_{WS}|}{2}. \quad (30)$$

The friction factors, f_{OF}, f_{WF}, f_G, f_{OS} and f_{WS}, at the wall in contact with oil, water or gas in the film region and slug body are estimated with the correlation developed by Churchill (1977) for both laminar and turbulent flow regimes,

$$f=2\left[\left(\frac{8}{Re}\right)^{12}+\frac{1}{(Term1+Term2)^{1.5}}\right]^{1/12}, \quad (31)$$

where

$$Term1=\left[2.457\ln\left(\left(\frac{7}{Re}\right)^{0.9}+0.27\left(\frac{\varepsilon}{D}\right)\right)^{-1}\right]^{16},$$

$$Term2=\left(\frac{37530}{Re}\right)^{16}.$$

The interfacial friction factor at the gas-liquid interface, f_{WF}, is estimated with the same correlations used in Zhang *et al*. (2003b) for stratified and annular flows. The interfacial friction factors between oil and water of liquid film and slug body are assumed to be a constant 0.0142 in this study.

CLOSURE RELATIONSHIPS

When liquid entrainment in the gas core becomes significant, the oil and water can probably be treated as a pseudo single-phase liquid. The empirical correlation proposed by Oliemans et al. (1986) may be used with modifications of the liquid physical properties (See in Zhang et al. (2003b)).

For stratified oil and water in the slug body, different gas void fractions will be caused for the oil and water layers due to different interactions between gas and the two liquid phases. Only one gas void fraction is needed if the oil and water in the slug body becomes fully mixed. For both cases, the mechanistic approach proposed by Zhang *et al*. (2003a) is extended for predictions of the void fractions.

The same closure relationships of slug translational velocity and slug length in gas-liquid two-phase flow are used for gas-oil-water three-phase flow in this study.

The efforts in developing new closure relationships are presented later in this report.

FLOW PATTERN TRANSITIONS

The three-phase flow patterns and structures can be described with two layers of phenomena: gas-liquid flow patterns and oil-water mixing status.

GAS-LIQUID FLOW PATTERN TRANSITIONS

Oil and water are treated as one pseudo liquid phase. The prediction methods for gas-liquid flow pattern transitions are similar to those employed in the unified model for gas-liquid pipe flow. When the transition from slug flow to stratified (or annular) flow occurs, the film length l_F becomes infinitely long. The momentum exchange term in the combined momentum equations (Eqs. 15 and 16) becomes zero. Given the superficial gas velocity and water cut, the superficial oil velocity corresponding to the transition boundary can be obtained with several iterations.

If a film length, l_F, as small as half the pipe diameter is given, the transition from slug flow to dispersed bubble flow can be predicted using the combined momentum equations. Also, this transition boundary can be predicted by use of a much simpler model developed by Zhang *et al* (2003b).

The transition from stratified to annular flow is determined by the spread of the liquid film around the pipe. Therefore, the transition boundary can be estimated using a correlation for wetted wall fraction, such as the Grolman (1994) correlation, with necessary adjustment of the liquid physical properties.

OIL-WATER MIXING

Zhang et al. (2003a) proposed a model for prediction of the gas void fraction in slug body based on the balance between the total turbulent energy of the liquid in slug body and the total free surface energy of the gas bubbles dispersed in the slug body. The same concept is used to model the mixing status of oil and water in three-phase pipe flow. Water (or oil) can be assumed to be dispersed in oil (or water) when the total turbulent energy is greater than the total surface free energy. Therefore, the following criterion can be

derived that one liquid becomes dispersed in the other liquid phase when liquid mixture velocity is higher than a certain value,

$$v_{LM} > \left\{ \frac{6.325 C_e \phi_{Int} [\sigma_{OW} (\rho_W - \rho_O) g]^{1/2}}{f_{LM} \rho_{LM}} \right\}^{1/2}, \qquad (32)$$

where v_{LM}, f_{LM} and ρ_{LM} are the liquid mixture velocity, friction factor and density. σ_{OW} is the oil-water interfacial tension. ϕ_{Int} is the volumetric fraction of the internal phase.

OIL-WATER MIXTURE VISCOSITY

In this study, Brinkman's (1952) correlation is used to calculate the apparent viscosity of the mixture based on the viscosities of the continuous phase and the dispersed phase and the phase fractions, if the oil and water are fully mixed,

$$\frac{\mu_{LM}}{\mu_c} = (1.0 - \phi_{Int})^{-2.5} \qquad (33)$$

where μ_c and μ_{LM} are the viscosities of the continuous phase and the liquid mixture, respectively.

PHASE INVERSION

A criterion for the inversion point between continuous phase and dispersed phase of the fully mixed oil and water mixture is required for the estimation of the apparent viscosity of the liquid mixture. In Brauner and Ullmann's (2002) study, the criterion of minimum system free energy was combined with a model for drop size in dense dispersions to predict the critical conditions for phase inversion,

$$\phi_{OI} = \frac{\tilde{\rho}^{0.6} \tilde{\mu}^{0.4}}{1 + \tilde{\rho}^{0.6} \tilde{\mu}^{0.4}},$$

where ϕ_{OI} is the critical oil holdup in the oil-water mixture, corresponding to the inversion from oil continuous to water continuous or vice versa. $\tilde{\rho}$ and $\tilde{\mu}$ are the density ratio and viscosity ratio between oil and water,

$$\tilde{\rho} = \frac{\rho_O}{\rho_W}, \quad \tilde{\mu} = \frac{\mu_O}{\mu_W}.$$

Inversion prediction is related to viscosity prediction of dispersions. Assuming the viscosity is continuous at the inversion point, the phase fraction corresponding to the inversion can be determined where the viscosities of the dispersions with continuous oil and continuous water phases are identical. Based on this reasoning, we can use Brinkman's viscosity correlation to obtain a correlation for inversion fraction,

$$\phi_{OI} = \frac{\tilde{\mu}^{0.4}}{1 + \tilde{\mu}^{0.4}}. \qquad (34)$$

This equation is almost same as the Brauner and Ullmann (2002) equation since the density difference between the two liquids is small.

SOLUTION PROCEDURE

Figure 10 shows a flow chart for general pipe flow calculation with up to three-phases of gas, oil or water. The computer program first determines whether the flow is a single-phase flow (gas, oil or water), an oil-water two-phase flow, a gas-liquid two-phase flow, or a gas-oil-water three-phase flow.

Figure 11 shows an overall flow chart of the three-phase unified model for a pipe increment. Flow pattern is determined based on the input parameters. The hydrodynamic behavior of the multiphase flow is calculated using the corresponding momentum and continuity equations.

Figure 12 is a flow chart for calculations of slug flow with stratified oil and water. This is one part of the three-phase unified model. The calculations for other flow patterns are simpler. The flow charts for

gas-liquid two-phase flow calculations can be found in Zhang *et al*. (2003b).

NEW CLOSURE RELATIONSHIP DEVELOPMENT

OIL-WATER MIXING

The mixing status of the two liquids must be predicted to determine whether the three-layer stratified model should be used or whether the two liquids should be treated as a single phase. The transition boundaries to dispersed liquid-liquid flows may be used.

Hinze (1955) showed that, in turbulent flow, deformation of a droplet depends on a critical Weber number, $We_{crit} = \rho d_{\max} / \sigma$, which gives the ratio between the surface tension force and the external force (τ) that tends to deform the droplet. We_{crit} can also be obtained by assuming a balance between the surface energy and the turbulent kinetic energy,

$$\frac{\rho_c v'^2}{2} \sim \frac{4\sigma}{d_{\max}} \tag{35}$$

Where, ρ_c is the density of the continuous phase. If the turbulent flow is assumed to be isotropic and homogeneous, the turbulent kinetic energy can be written in terms of turbulent energy dissipation (per unit mass of the continuous phase) $\bar{e}$,.

$$v'^2 = 2(\bar{e} d_{\max})^{2/3}. \tag{36}$$

Using this approach, the following equation was developed by Hinze (1955),

$$d_{\max}\left(\frac{\rho_c}{\sigma}\right)^{3/5} \bar{e}^{2/5} = C = 0.725. \tag{37}$$

Clay (1940) calculated the constant 0.725, which corresponds to $We_{crit} = \rho_c v'^2 d_{\max} / \sigma = 1.17$, by fitting experimental data of several liquid-liquid dispersions.

The mean rate of energy dissipation is a function of the frictional pressure drop,

$$\bar{e} = \frac{4\tau v_c}{D\rho_c(1-\lambda_d)} = \frac{2v_c^3 f}{D}\frac{\rho_m}{\rho_c(1-\lambda_d)} \tag{38}$$

Hinze's correlation then becomes,

$$\left(\frac{d_{\max}}{D}\right)_0 = 0.55\left(\frac{\rho_c v_c^2 D}{\sigma}\right)^{-0.6}\left[\frac{\rho_m}{\rho_c(1-\lambda_d)} f\right]^{-0.4}. \tag{39}$$

Dispersions occur at high flow rates where the drift velocity between the continuous and the dispersed phases can be neglected. Therefore, the homogeneous no-slip model can be used to obtain in-situ holdup,

$$v_c = v_d = v_{sc} + v_{sd}, \tag{40}$$

$$\lambda_d = \frac{v_{sd}}{v_{sd} + v_{sc}}, \tag{41}$$

$$\rho_m = \lambda_d \rho_d + (1-\lambda_d)\rho_c \tag{42}$$

For three-phase gas-oil-water flow,

$$v_c = v_d = v_{sc} + v_{sd} + v_{sg} \equiv v_M \tag{43}$$

The Hinze model is only valid for dilute dispersions because it considers the stability of only a single droplet in a turbulent field. Brauner (2001) extended the Hinze model for dense dispersions where droplet coalescence takes place. The turbulent energy of the continuous phase should be high enough to prevent the coalescence of droplets and to disperse the other phase. The rate of surface energy is

$$\dot{E}_s = \frac{\pi d_{\max}^2 \sigma}{\pi d_{\max}^3 / 6} Q_d = \frac{6\sigma}{d_{\max}} Q_d \tag{44}$$

Where Q_d is the dispersed liquid phase flow rate.

The rate of turbulent energy of the continuous phase is proportional to the rate of surface energy of the dispersed phase,

$$\frac{\rho_c v'^2}{2} Q_c = C_H \frac{6\sigma}{d_{\max}} Q_d \quad (45)$$

Where Q_c is the continuous liquid phase flow rate, and C_H is a constant. Substituting Eqs. 37 and 38 into Eq. 45 gives

$$\left(\frac{d_{\max}}{D}\right)_\varepsilon = 2.22 C_H^{3/5} \left(\frac{\rho_c v_c^2 D}{\sigma}\right)^{-0.6} \left[\frac{\rho_m}{\rho_c(1-\lambda_d)} f\right]^{-0.4} \left(\frac{\lambda_d}{(1-\lambda_d)}\right)^{0.6} \quad (46)$$

If a two-fluid system and operational conditions are known, the maximum droplet size is the largest of the two values obtained from Eqs. 39 and 46

$$\frac{d_{\max}}{D} = MAX\left\{\left(\frac{d_{\max}}{D}\right)_0, \left(\frac{d_{\max}}{D}\right)_\varepsilon\right\} \quad (47)$$

DROP SIZE VARIATION ACROSS THE CROSS SECTION OF THE PIPE

An empirical correlation to predict the droplet size variation with respect to pipe cross section for dispersions of o/w over a water layer was developed. The correlation was obtained by fitting the experimental data obtained in this study for this type of flow pattern.

The SMD varies from bottom to top of the pipe and is a function not only of the continuous phase velocity but also of the dispersed phase velocity. None of the compared models takes into account the dispersed phase velocity and the region where the droplets are formed. Therefore, in an attempt to improve the understanding of the distribution of droplets across the pipe diameter, the following correlation was developed,

$$v_{so}^{0.5} * SMD = a + b * \left(\frac{h}{D}\right)^3 . \quad (48)$$

Where a and b, given by Eqs. 49 and 50, are parameters that depend on the dispersed phase velocity and the continuous phase velocity,

$$a = 1.36 * v_{so}^{0.63} . \quad (49)$$

$$b = \frac{2.7 * \exp^{-0.1/v_{so}}}{v_{sw}^4} . \quad (50)$$

Figures 22 and 23 show the results for v_{sw}=1 m/s and v_{sw}=0.75 m/s respectively. The dots represent the experimental data and the continuous lines represent the predicted values from the correlation; there is a zone that represents approximately the water layer. From these figures it can be seen that the agreement between the points and the lines is reasonable for most of the cases. SMD increases as the dimensionless diameter increases. The water layer also increases when decreasing the oil superficial velocity.

The parameter b depends on the water and oil superficial velocities; by decreasing the water superficial velocity b tends to infinite giving values of SMD out of range (larger than the pipe diameter). A correlation for the determination of the free water layer should be developed in order to determine the region where the correlation previously developed is valid. The correlation has to be used only for dispersions of oil in water over a water layer.

Increasing the dispersed phase velocity increases the SMD as well as decreasing the velocity of the continuous phase. When the turbulence of the continuous phase is not enough to compete against the interfacial forces larger droplets are generated. Combined with the density difference, this leads to different profiles of droplets across the pipe diameter.

There are no other independent data. More data are needed to validate/improve this correlation and to determine the physical effects of all the parameters.

TRANSITION TO DISPERSED FLOW CRITERION

If the turbulence of the continuous phase is high enough to break the dispersed phase into droplets smaller than the critical droplet diameter, d_{crit}, the transition to dispersed flow occurs. Therefore, the transition criterion for $\mathrm{Re}_c \geq 2100$ and $1.82\mathrm{Re}_c^{-0.7} < d_{crit}/D < 0.1$ (Brauner, 2001) is given as

$$d_{\max} \leq d_{crit}. \tag{51}$$

An approach similar to Barnea's (1987) can be used to obtain the critical droplet diameter,

$$\frac{d_{crit}}{D} = MIN\left(\frac{d_{c\sigma}}{D}, \frac{d_{cb}}{D}\right). \tag{52}$$

Where $d_{c\sigma}$ is the maximum droplet diameter above which the droplets are deformed (Broadkey, 1969), and d_{cb} is the maximum droplet diameter above which the droplets move to the pipe wall due to buoyancy. $d_{c\sigma}$ and d_{cb} are given by

$$\frac{d_{c\sigma}}{D} = \left[\frac{0.4\sigma}{|\rho_c - \rho_d| g \cos\theta' D^2}\right]^{1/2} = \frac{0.224}{(\cos\theta')^{1/2} Eo_D^{1/2}} \tag{53}$$

$$Eo_D = \frac{\Delta\rho g D^2}{8\sigma}, \tag{54}$$

$$\theta' = \begin{Bmatrix} |\theta|, & |\theta| < 45^o \\ 90 - |\theta|, & |\theta| > 45^o \end{Bmatrix}, \tag{55}$$

$$\frac{d_{cb}}{D} = \frac{3}{8}\frac{\rho_c}{|\Delta\rho|}\frac{f v_c^2}{Dg\cos\theta} = \frac{3}{8} f \frac{\rho_c}{\Delta\rho g} Fr_c, \tag{56}$$

$$Fr_c = \frac{v_c^2}{Dg\cos\theta} \tag{57}$$

Where θ is the inclination angle to the horizontal (positive for downward inclination).

TRANSLATIONAL VELOCITY AND SLUG LENGTH

The translational velocity of the liquid slugs for gas-liquid two-phase flow is expressed by Nicklin (1962) as a function of mixture velocity, v_M,

$$v_T = C_S v_M + v_D \tag{58}$$

Where v_D is the drift velocity and C_S is a coefficient approximately equal to the ratio of the maximum to the mean velocity of a fully developed velocity profile. A value of 2 for laminar flow and 1.2 for turbulent flow can be used for C_S.

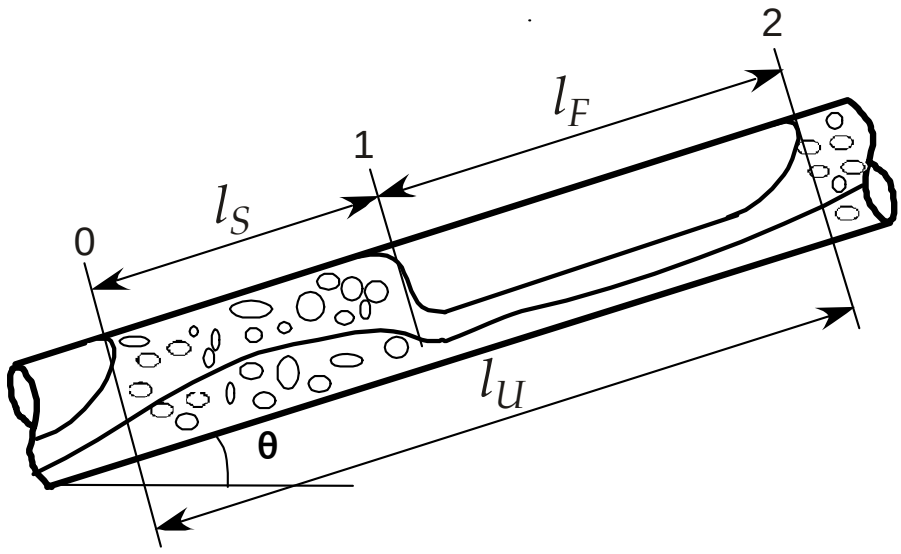

Figure 9 - Control Volumes of Gas Pocket Region and Slug Body Region Used in Modeling

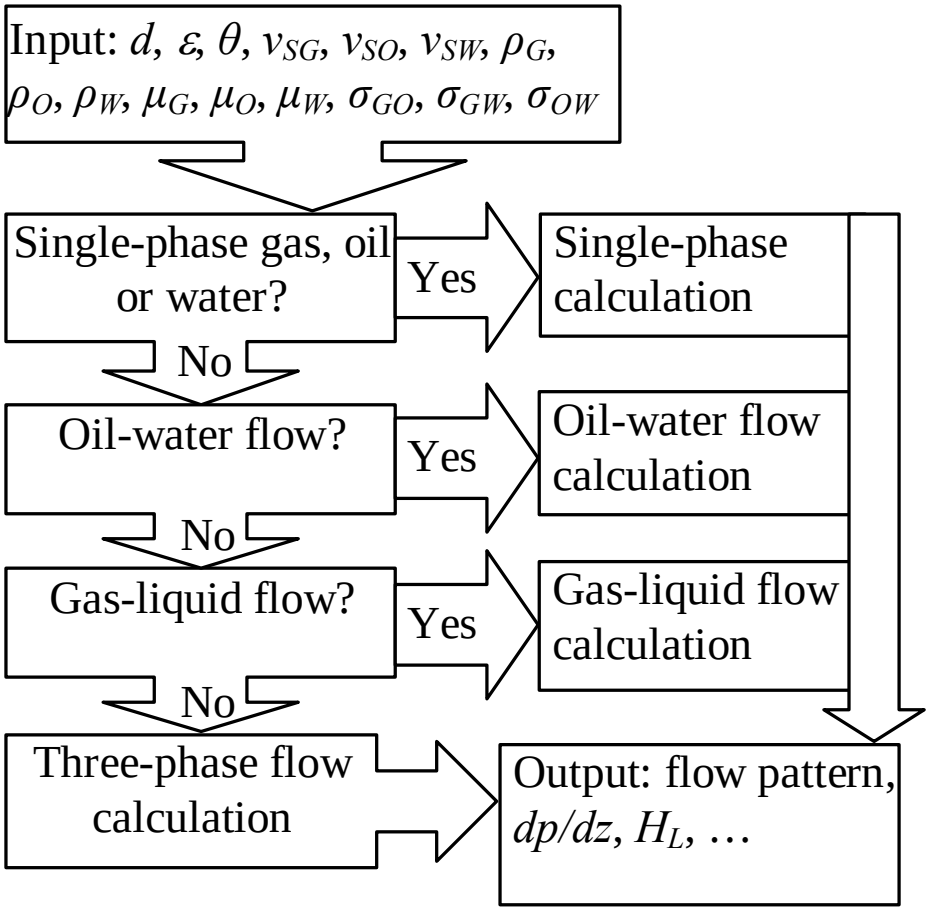

Figure 10 - General Flow Chart for Multiphase Pipe Flow Calculation

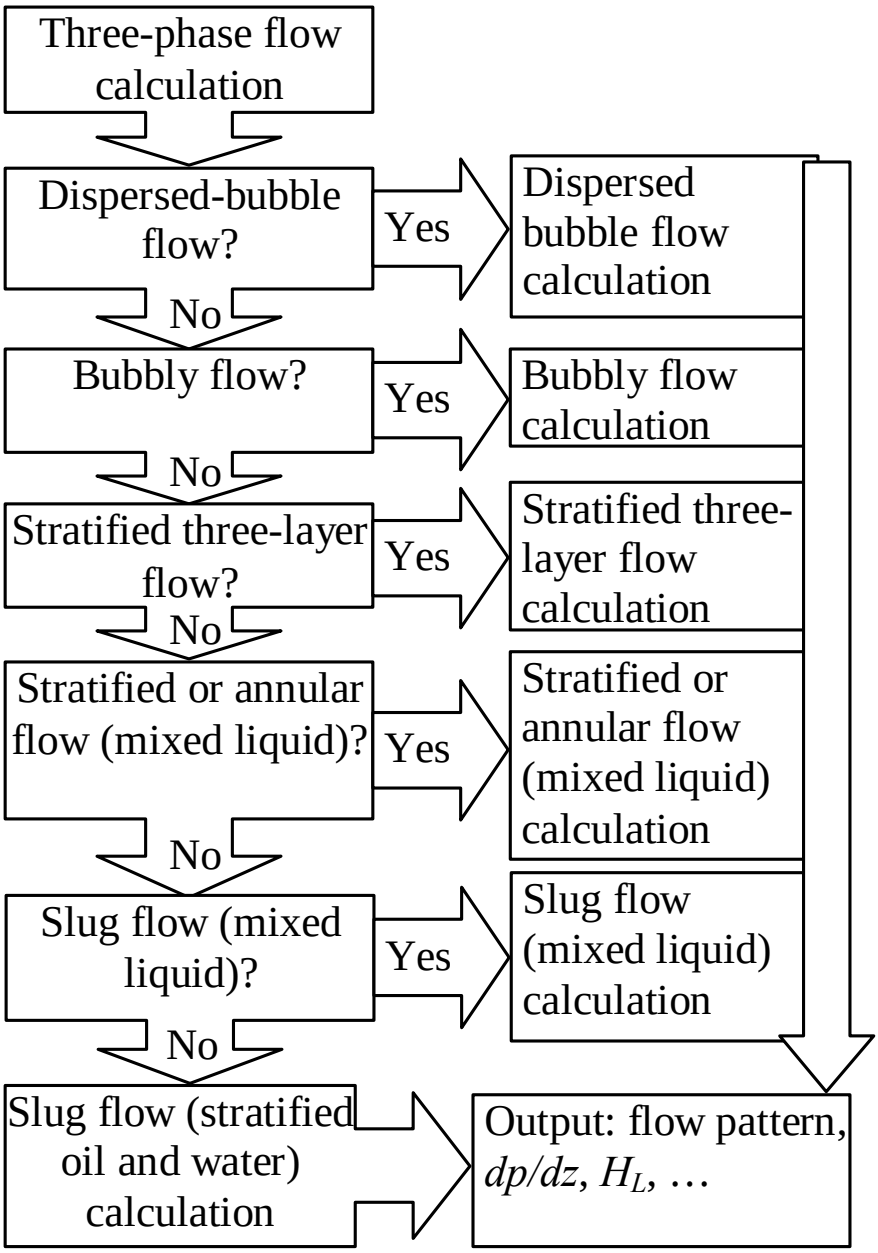

Figure 11 - Overall Flow Chart for Three-Phase Unified Model

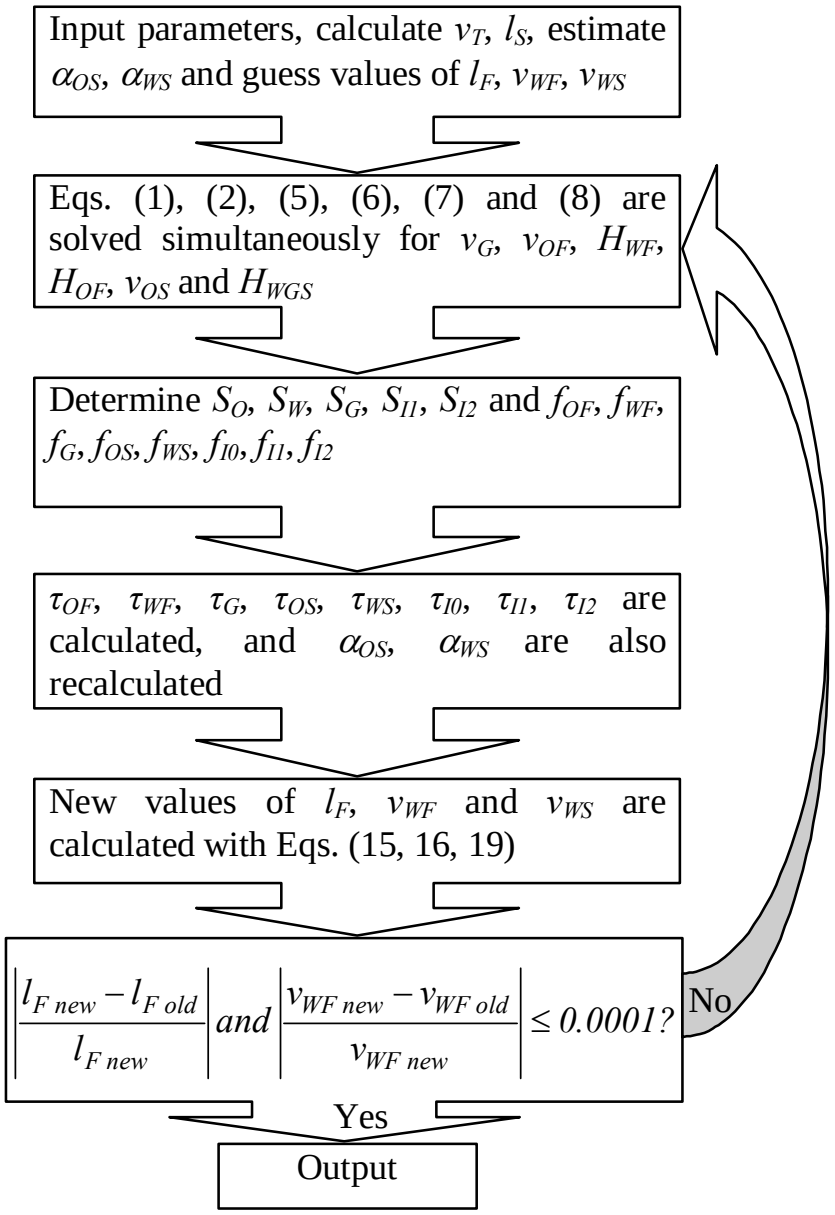

Figure 12 - Flow Chart for Calculation of Three-Phase Slug Flow with Stratified Oil and Water

EXPERIMENTAL STUDY

EXPERIMENTAL FACILITY AND FLOW LOOP

The experimental work was conducted using the TUFFP facility for gas-oil-water flow located at The University of Tulsa North Campus Research Complex. This facility was used previously for oil-water flow experiments by Trallero (1995) and Alkaya (2000) in horizontal and slightly inclined pipes and by Flores (1997) for vertical and deviated wells.

The facility consists of a closed circuit loop with the following components: pumps, heat exchangers, metering sections, filters, test section, separator and storage tanks. The test section is attached to an inclinable boom. A schematic diagram of the flow loop is given in Fig. 13.

INSTRUMENTATION AND DATA ACQUISITION

The current test section is composed of two 21.1-m (69.3-ft) long straight transparent pipes, connected by a 1.2-m (4.0-ft) long PVC bend to reduce the disturbance to the flow pattern due to a sharp turn. The pipeline has a 0.0508-m (2.0-in.) internal diameter. The upward branch of the test section consists of: a 13.8-m (45.3-ft) long flow developing section (L/D=272.0), two short pressure drop sections 5.2-m (17.0-ft) and 3.3-m (11.0-ft) long, one long pressure drop section combining the two short sections, one 5.5-m (18.1-ft) long fluid trapping section (L/D=108), and a 1.8-m (6.0-ft) long measurement section. The downward branch of the test section is designed and built similar to the upward branch. The transparent pipes are instrumented to permit continuous monitoring of temperature, pressure, differential pressure, holdup, inclination angle and spatial distribution of the phases.

Quick-closing valves, conductance probes and capacitance sensors are used to measure phase fractions and flow characteristics.

Conductance probes were developed mainly to determine the liquid phase at a point in a gas-oil-water flow. They were also used to determine the continuous phase. Three on the upward branch and one on the downward branch of the test section were installed.

The capacitance sensors were mainly used to obtain slug characteristics such as, slug length and translational velocity. A schematic diagram of the test section is given in Fig. 14.

The TUFFP high speed video system was used in identifying the flow patterns and determining the oil-water mixing status.

For data acquisition, Lab VIEW™ 7.0 software is used. A new data acquisition program was developed for the new system. New hardware, including a computer, a multiplexer and a multifunction I/O board, were installed.

TEST FLUIDS

The fluids used in the experiments consist of a refined mineral oil, fresh water, and air. Due to its good separability, a mineral oil is used as the oil phase in the tests. The physical properties of the oil are given below:

- 33.2 API gravity
- Density: 858.75 kg/m^3 @ 15.6 ^{o}C
- Viscosity: 13.5 cp @ 40 ^{o}C

- Surface tension: 29.14 dynes/cm @ 25.1 °C
- Interfacial tension with water: 16.38 dynes/cm @ 25.1 °C
- Pour point temperature: -12.2 °C
- Flash point temperature: 185 °C

UNCERTAINTY ANALYSIS

Error is the true difference between the true value of a parameter and the measurement obtained. In every measurement there is error. Neither the true value nor the error is ever known. Uncertainties are used to determine the limits of errors.

Errors are divided into two parts: random errors and systematic errors. Random errors affect the test data in a random fashion. On the other hand, systematic errors do not change during a test. Random uncertainty estimates the limits of random errors and systematic uncertainty estimates the limits of systematic errors.

RANDOM UNCERTAINTY

Experimental data can be used to obtain the random uncertainty. Assuming a Gaussian distribution for N number of data points of a parameter, the standard deviation is,

$$S_X = \left[\frac{\sum \left(X_i - \overline{X} \right)^2}{N-1} \right]^{1/2} \quad (59)$$

The standard deviation of the average can be obtained using,

$$S_{\overline{X}} = \frac{S_X}{\sqrt{N}} \quad (60)$$

SYSTEMATIC UNCERTAINTY

Systematic errors affect every measurement of a parameter equally. Therefore, experimental data cannot be used to estimate the systematic uncertainty. In this report, the calibration equations are used to calculate the systematic uncertainty for pressure, differential pressure and temperature measurements. For liquid and gas mass flow rates, and holdup measurements, the systematic uncertainties are neglected due to the fact that they are so small compared to the random uncertainties.

COMBINING RANDOM AND SYSTEMATIC UNCERTAINTIES

Random and systematic uncertainties coming from various sources should be combined to evaluate their combined effect. The combined random uncertainty can be calculated using,

$$S_{\overline{X},R} = \left[\sum \left(S_{\overline{X},i} \right)^2 \right]^{1/2} \quad (61)$$

Combined systematic uncertainty is formulated as,

$$B = \left[\sum \left(b_i \right)^2 \right]^{1/2} \quad (62)$$

Therefore, the combined uncertainty is,

$$U_{95} = \pm t_{95,\nu} \left[(B/2)^2 + \left(S_{\overline{X},R} \right)^2 \right]^{1/2} \quad (63)$$

Most of the time in uncertainty analysis, a 95% confidence interval is used. The student's $t_{95,\nu}$ can be found in any statistics handbook. The test data can be expressed as $\overline{X} - U_{95} \le X \le \overline{X} + U_{95}$. Then the X value will lie between $\left(\overline{X} - U_{95} \right)$ and $\left(\overline{X} + U_{95} \right)$ 95% of the time.

UNCERTAINTY PROPAGATION

For any experimental study, it is essential to combine the effect of different parameters in order to calculate propagation of the desired parameter. There are three commonly used methods for the uncertainty propagation: Taylor's Series uncertainty propagation,

Dithering, and Monte Carlo simulation. For this study, Taylor's Series method was used to calculate the uncertainty propagation for the pressure drop, superficial velocities, mixture velocity, holdup, holdup ratio, and actual oil and water velocities.

If *y* is a function of independent variables *a, b, c….*, the uncertainty of *y* will be described as a function of independent uncertainties of *a, b, c….*, and are expressed as follows:

$$U_y = \sqrt{\left[\left(\frac{\partial y}{\partial a}\right)^2 (U_a)^2 + \left(\frac{\partial y}{\partial b}\right)^2 (U_b)^2 + \left(\frac{\partial y}{\partial c}\right)^2 (U_c)^2 + ...\right]} \quad (64)$$

RESULTS

An uncertainty analysis for test for a representative test where v_{sg}=0.1-m/s, v_{sw}=0.03-m/s and v_{so}=0.045-m/s, is given as an example in Table 6.

Table 7 shows all the uncertainty analysis results for the measurement in oil-water experimental study. The uncertainty propagation for oil-water tests is shown in Table 8.

Table 6 - Uncertainty Analysis Results for a Sample Test

Parameters		Pressure Drop (in. H2O)	Pressure (Psi)	Temp. (˚F)	Water Flow Rate (Kg/min)	Oil Flow Rate (Kg/min)	Gas Flow Rate (Kg/min)	Liquid Holdup
Average	$\overline{X}$	0.903	19.72	90.69	3.786	4.927	0.079	0.562
Random	$S_{\overline{X}}$	0.0345	0.010	0.011	0.0177	0.0174	0.0006	N/A
	$d.f.$	999	999	999	999	999	999	N/A
Systematic	B	0.006	0.0001	0.0001	0.00038	0.00049	0.00004	0.00281
	$d.f.$	10	4	7	Infinity	Infinity	Infinity	Infinity
Combined Uncertainty (95%)	$t_{95,\nu}$	2	2	2	2	2	2	2
	U_{95}	0.069	0.021	0.022	0.0354	0.0348	0.0013	0.0028
True Value (95%)		0.834 0.972	19.70 19.74	90.66 90.71	3.750 3.821	4.892 4.961	0.077 0.080	0.559 0.565

$d.f.$**: Degree of Freedom**

Table 7 - Uncertainty Analysis Results for Oil-Water Facility

Instrument	Random Uncertainty	Systematic Uncertainty	Degrees of Freedom	Overall Uncertainty (U_{95})
PT1 (psi)	0.70%	5.26%	Infinity	5.44%
PT1_1 (psi)	0.57%	9.80%	Infinity	9.87%
PT2 (psi)	1.95%	10.34%	Infinity	11.05%
PT3 (psi)	2.57%	4.22%	Infinity	6.65%
PT4 (psi)	1.70%	2.86%	Infinity	4.44%
PT6 (psi)	2.56%	4.19%	Infinity	6.61%
PT7 (psi)	2.76%	3.74%	Infinity	6.66%
PT8 (psi)	0.00%	0.46%	Infinity	0.46%
DP1 (in H_2O)	0.08%	0.14%	Infinity	0.21%
DP2 (in H_2O)	0.03%	0.06%	Infinity	0.08%
DP3 (in H_2O)	0.03%	0.08%	Infinity	0.10%
DP4 (in H_2O)	0.02%	0.16%	Infinity	0.17%
DP5 (in H_2O)	0.03%	0.09%	Infinity	0.10%
DP6 (in H_2O)	0.02%	0.07%	Infinity	0.08%
TT1 (°F)	0.001	0.389	Infinity	0.39
TT2 (°F)	0.003	0.372	Infinity	0.37
TT3 (°F)	0.005	0.383	Infinity	0.38
TT4 (°F)	0.002	0.376	Infinity	0.38
TT5 (°F)	0.007	0.381	Infinity	0.38
TT7 (°F)	0.007	0.382	Infinity	0.38
TT8 (°F)	0.005	0.375	Infinity	0.38
WFM (gpm)	0.11%	0.16%	Infinity	0.27%
OFM (gpm)	0.11%	0.04%	Infinity	0.22%
WFM (gr/cm^3)	0.00%	0.05%	Infinity	0.05%
OFM (gr/cm^3)	0.00%	0.04%	Infinity	0.04%
Tape (inch)	1.00	0.10	Infinity	2.00
Droplet Size (mm)	0.012	0.010	Infinity	0.03

Table 8 - Uncertainty Propagation Results

Measurement	Random Uncertainty	Systematic Uncertainty	Degrees of Freedom	Overall Uncertainty (U_{95})
Pressure Drop (Pa/m)	0.00503	0.04677	Infinity	0.04784
v_{sw} (m/s)	0.00003	0.00005	Infinity	0.00008
v_{so} (m/s)	0.00003	0.00001	Infinity	0.00007
v_M (m/s)	0.00005	0.00005	Infinity	0.00011
H_w	0.00459	0.02294	Infinity	0.02470
C_w/H_w	0.00644	0.02359	Infinity	0.02688

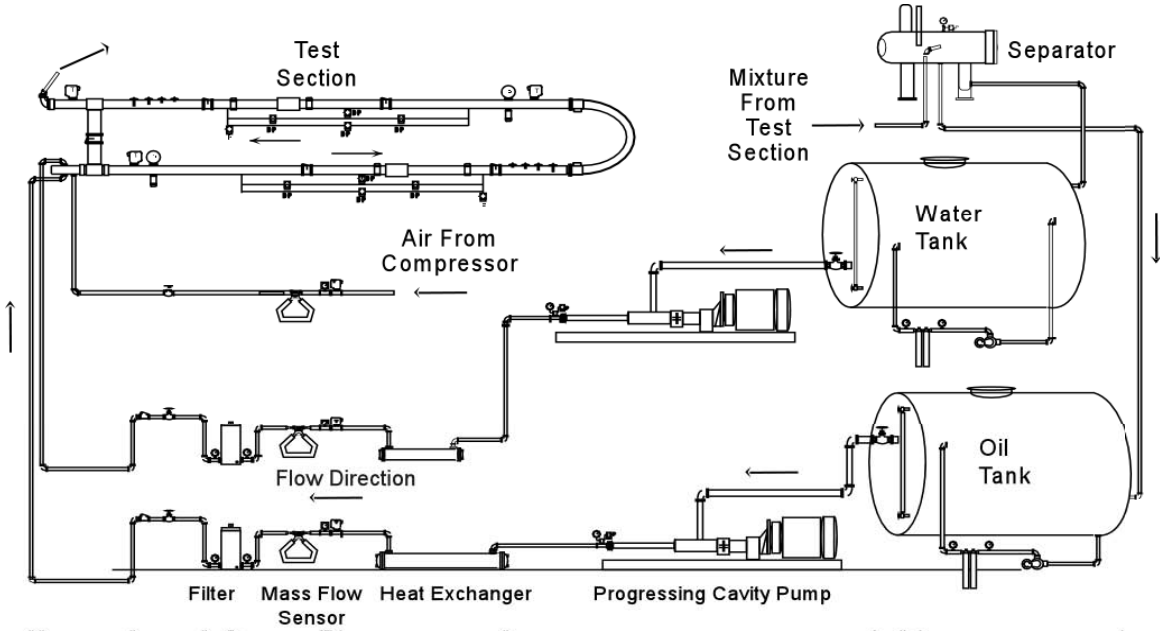

Figure 13 - Schematic Representation of Experimental Flow Loop

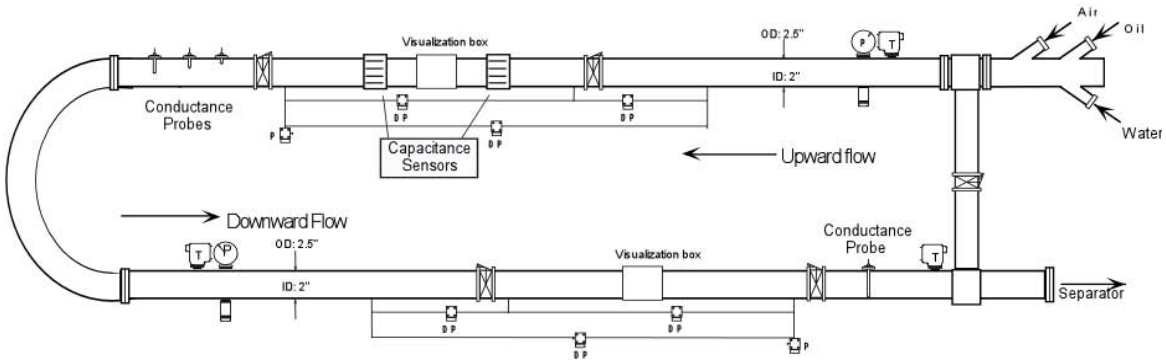

Figure 14 - Test Section

RESULTS AND DISCUSSIONS

GAS-OIL-WATER FLOW IN HORIZONTAL PIPES

GAS-OIL-WATER TEST PROGRAM

A typical test for gas-oil-water flow starts with varying the gas flow rate, keeping the oil and water flow rates and water fraction constant. Then, tests are repeated for several oil and water flow rates at constant water fraction, and continue with varying water fraction.

The testing ranges for the gas-oil-water tests conducted are as follows:

- Superficial gas velocity: 0.1 – 7.0 m/s
- Superficial oil velocity: 0.02 – 1.5 m/s
- Superficial water velocity: 0.01 – 1.0 m/s
- Water fraction: 20, 40, 50, 60 and 80 %

THREE-PHASE FLOW PATTERNS

Three-phase gas-oil-water flow patterns are actually a combination of gas-liquid and oil-water flow patterns. Gas-liquid flow patterns observed during three-phase tests in horizontal pipe are: stratified smooth (SS), stratified wavy (SW), elongated bubble (EB), and slug flow (SL). There are also annular (AN) and dispersed bubble flows (DB). Oil-water flow patterns in horizontal pipes identified by Trallero (1995) are used in this study. The name of those flow patterns are: stratified (ST), stratified flow with mixing at the interface (ST & MI), dual type of dispersions (Dw/o & Do/w), dispersion of oil in water over a water layer (Do/w & w), water in oil dispersion (w/o), and oil in water dispersion (o/w).

The combination of those gas-liquid and oil-water flow patterns gives us several different three-phase flow patterns which are not practical in use. Therefore, a new classification of gas-oil-water three-phase flow patterns is needed.

Starting with the gas-liquid flow patterns, stratified smooth and stratified wavy flow patterns can be combined under the name “stratified” to reduce the number of three-phase flow patterns. Similarly, “intermittent flow” can be used for both elongated bubble and slug flows.

There are more oil-water flow patterns than gas-liquid flow patterns, and they are more complex. Six oil-water flow patterns observed during three-phase tests were mentioned above. This number can be reduced by grouping them into three. When oil and water flow separately in the pipe with even few droplets only at the interface, the flow pattern is called “stratified” oil-water flow. Stratified (ST) and stratified flow with mixing at the interface (ST & MI) flow patterns fall into this group. In an oil-water pipe flow, if there is an oil-water interface, and if oil droplets are observed in water and/or water droplets are observed in oil away from the interface, that means there are two continuous phases. This flow is called “dual continuous”. Trallero’s (1995) dual type of dispersions (Dw/o & Do/w) and dispersion of water in oil over a water layer (Dw/o & w) flow patterns fall into this group. When there is no oil-water interface and when one liquid phase is completely dispersed in the other liquid phase, we have mono continuous flow. The continuous phase is either oil or water. Dispersion of oil in water over a water layer (Do/w & w), water in oil dispersion (w/o) and oil in water dispersion (o/w)

flow patterns are examples of this kind of flow.

Based on the above classifications, 12 individual three-phase gas-oil-water flow patterns in horizontal pipes have been identified and listed below. The names of the gas-oil-water flow patterns consist of two words. First word stands for gas-liquid flow pattern and the second word indicates oil-water flow pattern. The sketches of the gas-oil-water flow patterns and the gas-oil-water flow pattern maps for 20, 40, 50, 60 and 80 % water cut tests are given in Figs. 15 to 20 and Figs. 21 to 25, respectively.

- Stratified-Stratified (ST-ST)
- Stratified-Dual Continuous (ST-DC)
- Stratified-Oil Continuous (ST-OC)
- Stratified-Water Continuous (ST-WC)
- Intermittent-Stratified (IN-ST)
- Intermittent-Dual Continuous (IN-DC)
- Intermittent-Oil Continuous (IN-OC)
- Intermittent-Water Continuous (IN-WC)
- Annular-Oil Continuous (AN-OC)
- Annular-Water Continuous (AN-WC)
- Dispersed Bubble-Oil Continuous (DB-OC)
- Dispersed Bubble-Water Continuous (DB-WC)

PRESSURE GRADIENT

The pressure gradients increase with increasing gas and liquid flow rates. From a flow pattern point of view, the pressure gradients increase slightly for stratified and partially mixed oil-water flows where both gas and liquid flow rates are relatively low. At superficial gas velocities higher than 1.0 m/s where slug and fully mixed oil-water flows are observed, the increase in the pressure gradients is quite sharp. This might be due to the rise in effective viscosity as the water-in-oil dispersion occurs, or just because of the increase in gas flow rate. Another observation is that, the pressure gradients for water in oil dispersions are relatively higher than the pressure gradients for oil in water dispersions at similar gas and liquid flow rates most probably due to the change of the continuous phase. The pressure gradient change with water cut at various superficial gas velocities for constant 0.05 m/s superficial liquid velocity is given in Fig. 26 where the flow patterns are mostly ST-ST. In Fig. 27, the same graph is plotted for constant 1.25 m/s superficial liquid velocity where the flow patterns are IN-OC for 20 % and 40 % water cuts and IN-WC for 60 % and 80 % water cuts.

HOLDUP MEASUREMENTS

Local holdup measurements were performed using the quick closing ball valves located on the downward branch of the test section by lifting the test section to vertical or close to the vertical position. One particular problem encountered during the measurements for intermittent flows was the variation of the trapped volume of liquid depending on whether or not a liquid slug was trapped, due to the ratio of the length of the trapping section (5.56 m) to the length and frequency of slugs.

WETTED PERIMETER MEASUREMENTS

Wetted perimeter, which is the pipe periphery wetted by the liquid phases, is measured by a measurement tape attached to the outer surface of the pipe. The oil and water wetted perimeters are measured separately when one of the liquid phases is not dispersed in the other liquid phase. For intermittent flows, the wetted perimeter measurements are performed only for the liquid film unless the liquid phases in slug body are separated.

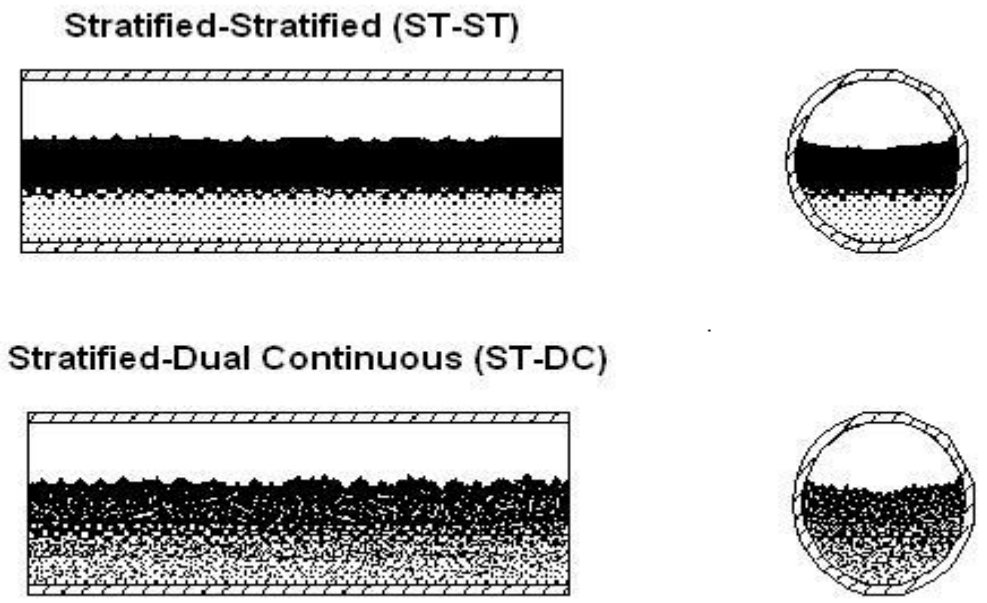

Figure 15 - Stratified-Stratified (ST-ST) and Stratified-Dual Continuous (ST-DC) Gas-Oil-Water Flow Patterns

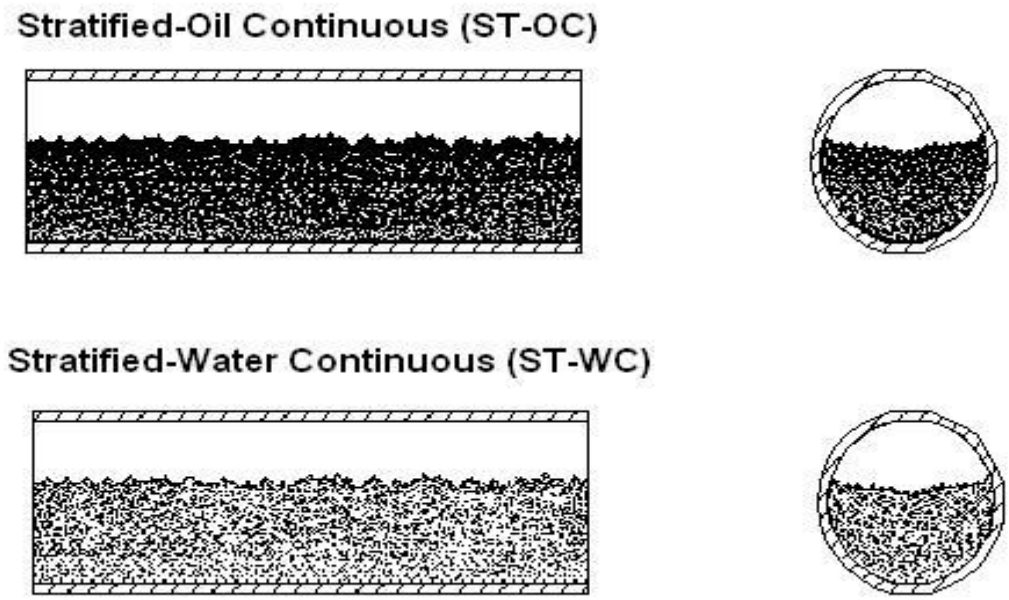

Figure 16 - Stratified-Oil Continuous (ST-OC) and Stratified-Water Continuous (ST-WC) Gas-Oil-Water Flow Patterns

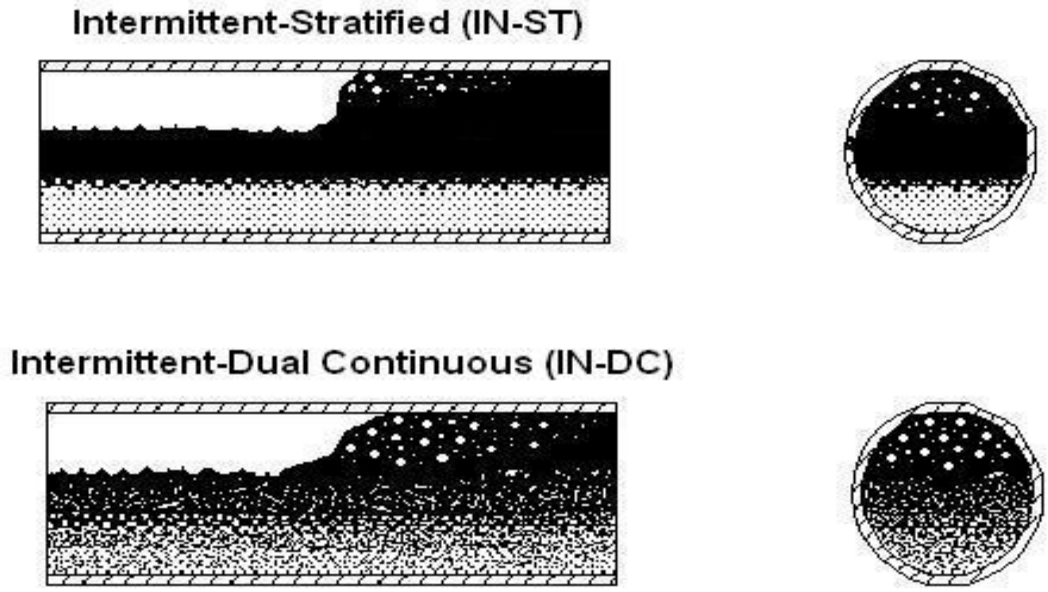

Figure 17 - Intermittent-Stratified (IN-ST) and Intermittent-Dual Continuous (IN-DC) Gas-Oil-Water Flow Patterns

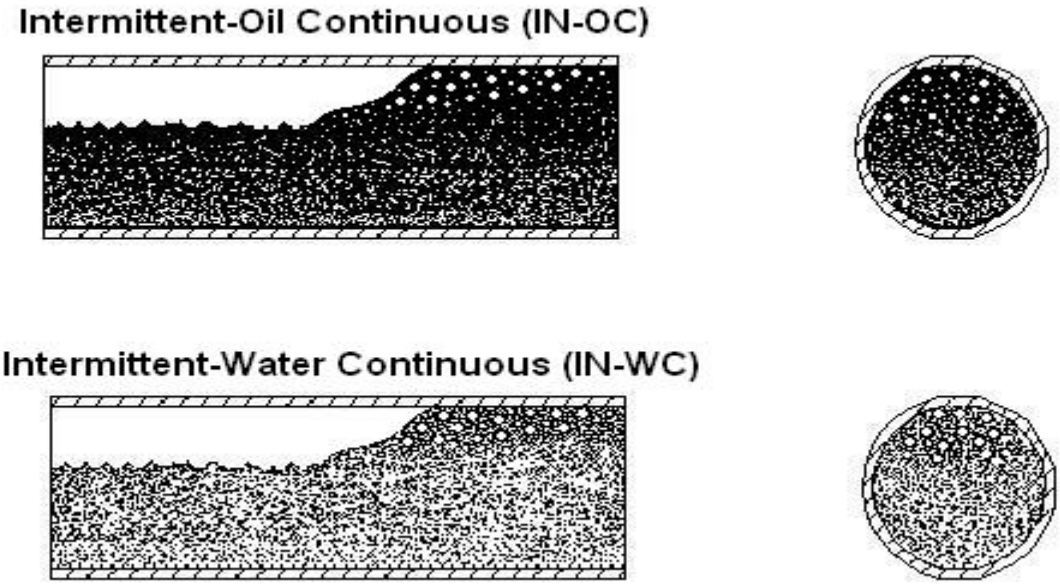

Figure 18 - Intermittent-Oil Continuous (ST-OC) and Intermittent-Water Continuous (ST-WC) Gas-Oil-Water Flow Patterns

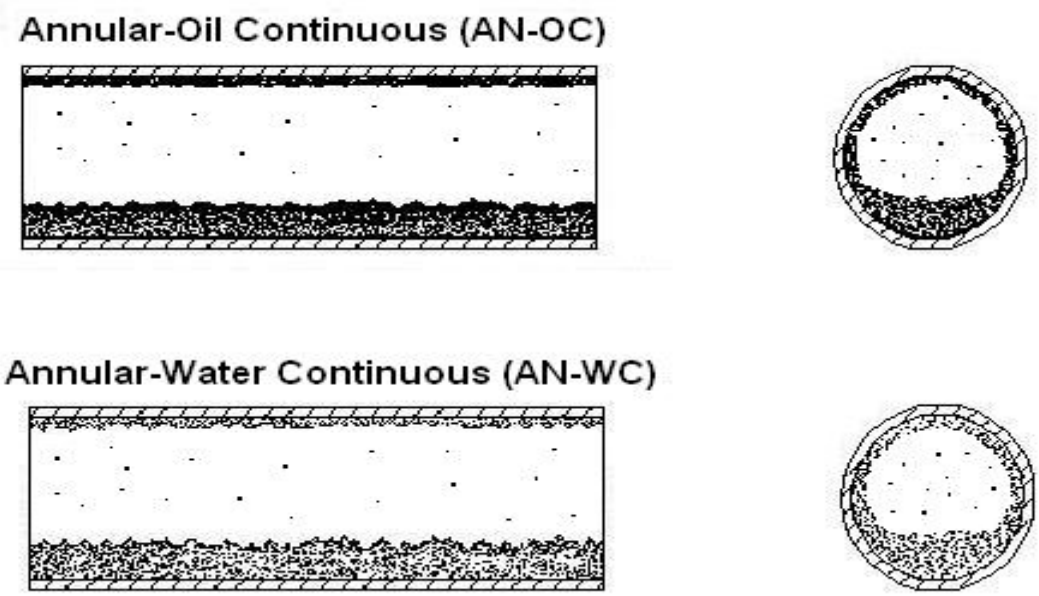

Figure 19 - Annular-Oil Continuous (AN-OC) and Annular -Water Continuous (AN-WC) Gas-Oil-Water Flow Patterns

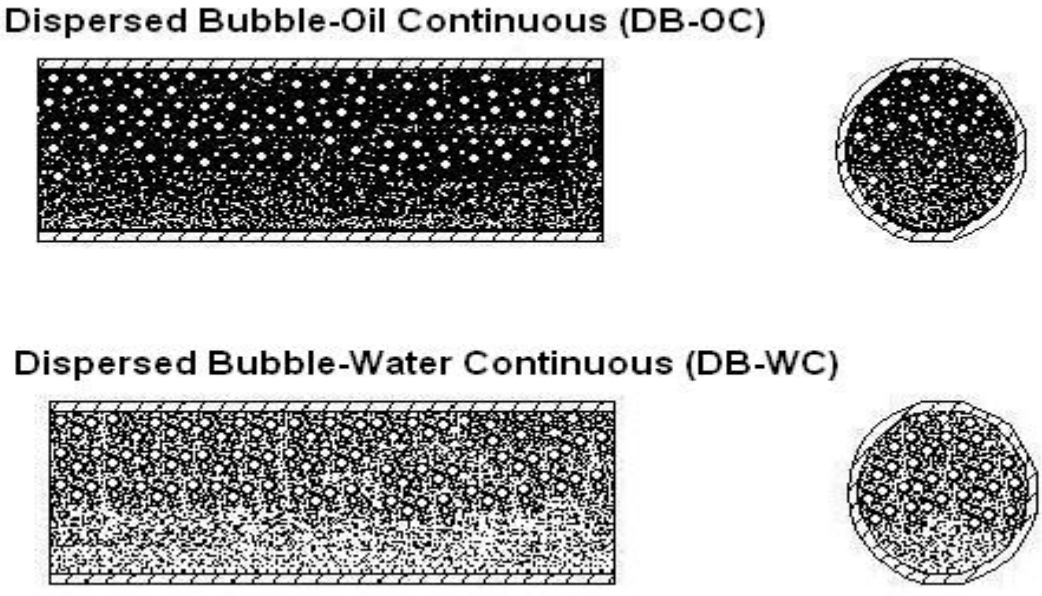

Figure 20 - Dispersed Bubble-Oil Continuous (DB-OC) and Dispersed Bubble-Water Continuous (DB-WC) Gas-Oil-Water Flow Patterns

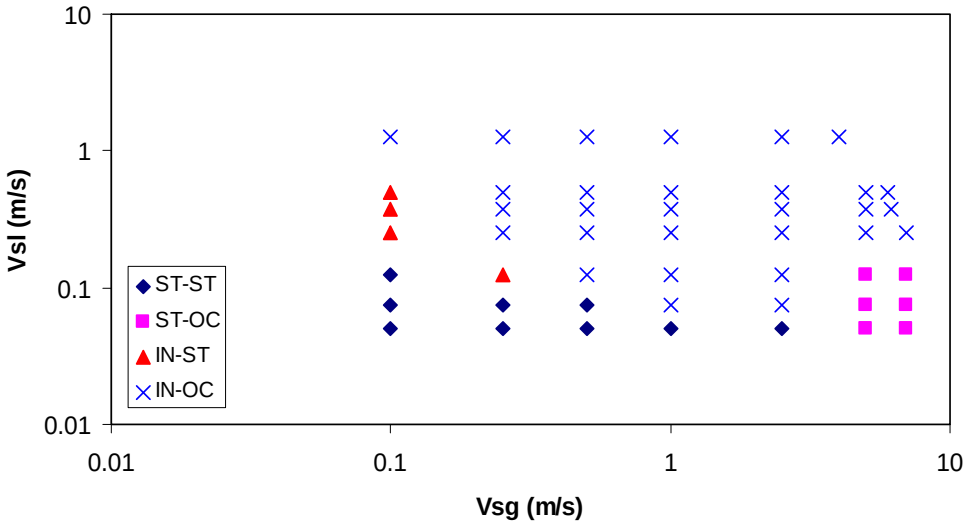

Figure 21 - Gas-Oil-Water Flow Pattern Map for 20 % Water Fraction

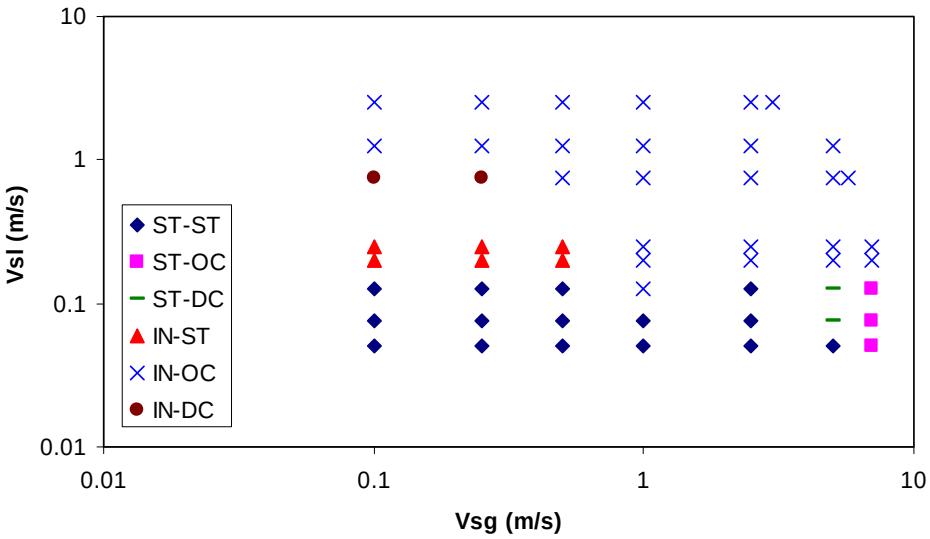

Figure 22 - Gas-Oil-Water Flow Pattern Map for 40 % Water Fraction

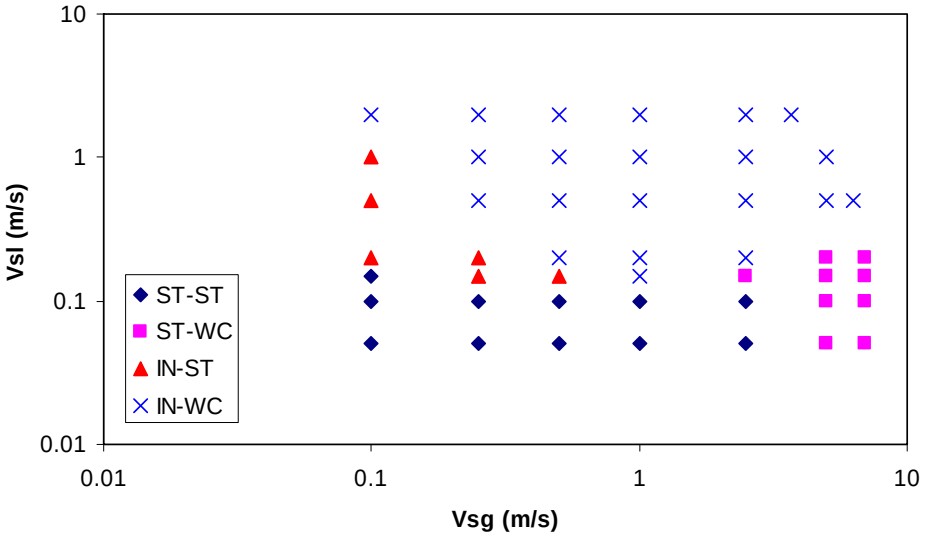

Figure 23 – Gas-Oil-Water Flow Pattern Map for 50 % Water Fraction

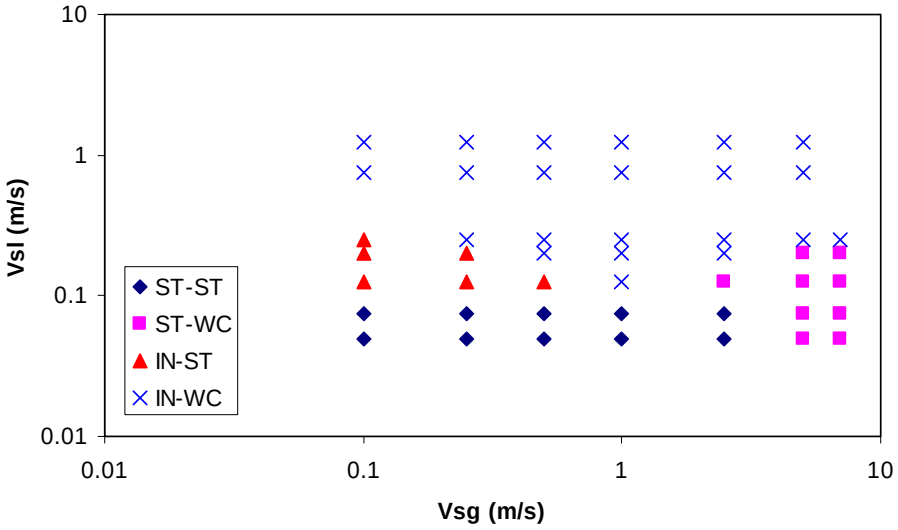

Figure 24 - Gas-Oil-Water Flow Pattern Map for 60 % Water Fraction

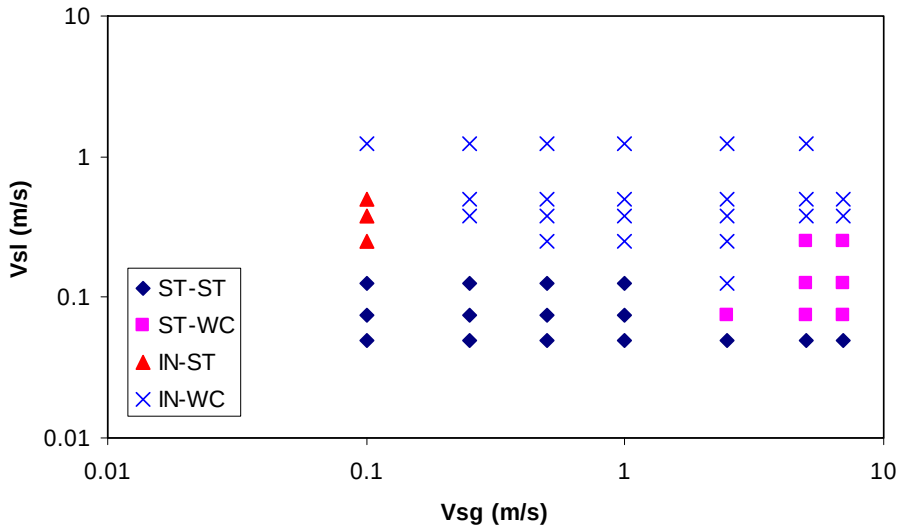

Figure 25 - Gas-Oil-Water Flow Pattern Map for 80 % Water Fraction

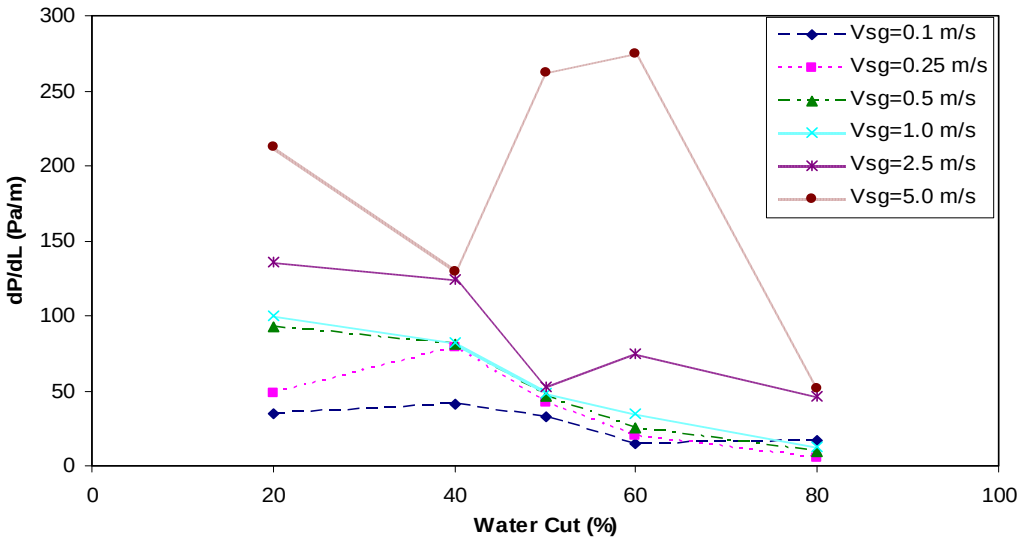

Figure 26 – Pressure Gradient vs. Water Cut (vSL = 0.05 m/s)

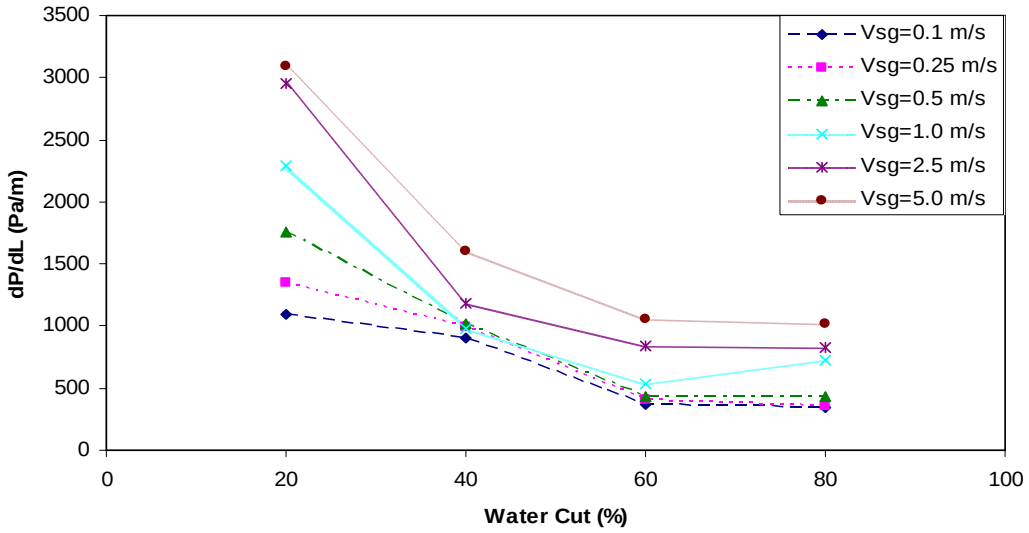

Figure 27 – Pressure Gradient vs. Water Cut (vSL= 1.25 m/s)

OIL-WATER FLOW IN HORIZONTAL AND SLIGHTLY INCLINED PIPES

A large number of data points are collected at various conditions in terms of both fluid velocities and inclination angles. The inclination angles were 0°, ±1°, ±2° and -5°. Superficial oil and water velocities range from 0.025 to 1.75 m/sec. These oil and water flow rates were determined in order to obtain the flow pattern boundaries clearly. Moreover, the limits of the facility were taken into consideration.

The experimental data of flow pattern, pressure drop, holdup, phase distribution, drop size and distribution, actual velocities and droplet size comparison against existing models are discussed

Trallero (1995) and Zhang et al. (2003b) flow pattern prediction models were compared against the experimental data obtained in this study. Zhang et al. model was also used for pressure gradient and holdup comparison. Hinze (1955), Kubie and Gardner (1977), Angeli and Hewitt (2000), Brauner (2002) and Kouba (2003) models were used for d_{max}, d_{min} and SMD comparisons.

For the experimental results section, only representative inclination angles will be discussed for upward and downward flow. A complete set of the data and graphs can be found in Atmaca (2007).

FLOW PATTERN

Experimental flow pattern maps were generated by examining the images and videos obtained from high speed camera. The superficial velocities for each phase vary between 0.025-1.75 m/s. Figure 28 shows the experimental flow patterns for -1° of inclination angles respectively. By changing superficial velocities of each phase following flow patterns were observed:

- Stratified Flow (ST) (Fig. 29)
- Stratified with Mixing Interface (ST&MI) (Fig. 30)
- Dispersion of Oil in Water over Water Layer (DO/W&W) (Fig. 31)

- Dual Dispersion (Dispersion of oil in water and Dispersion of water in oil) (DO/W&DW/O) (Fig. 32)
- Dispersion of oil in water (DO/W) (Fig. 33)
- Dispersion of water in oil (DW/O) (Fig. 34)
- Transition stratified to stratified mixing interface (TRNS ST to ST&MI) (Fig. 35)
- Dispersion of water in oil under oil layer (DW/O&O) (Fig. 36)

Experimental flow pattern maps were compared against Trallero (1995) model and Zhang et al. (2003b) unified model. Trallero model predicted the most of the flow pattern boundaries well except stratified flow pattern (ST) (Fig. 37). Although Zhang et al. model was developed for three-phase gas-oil-water, for this study, only oil-water part is used. In oil-water unified model, there are only two boundaries, which stand for the boundaries of oil in water (O/W) and water in oil (W/O). Zhang et al. model predicted the water in oil (W/O) boundary well in all inclination angles, while oil in water (O/W) flow pattern boundary was under-predicted. Figures 38 and 39 show the comparison of experimental flow pattern against Zhang et al. unified model prediction for -2° and +2° inclination angles, respectively.

PRESSURE GRADIENTS

Figure 40 shows the pressure gradient data for v_{so}=0.025 m/s and its comparison between Trallero (1995), Alkaya (2000) and Vielma (2006) data for the similar conditions. As expected, the pressure gradient increases with increasing superficial water velocity. The differences are mainly due to the different oil viscosities. The best match was observed with Vielma since the same oil is used in this study.

Total pressure gradient for two-phase flow has three components; frictional, acceleration and gravitational pressure gradients. For horizontal oil-water flow, acceleration and gravitational components can be neglected. For inclined flows, while the acceleration component can still be neglected, the gravitational component becomes very significant. For inclined flow, the measured pressure drop was corrected for the liquid in the pipe. Since the pipe is filled with oil-water mixture, the total pressure gradient can be obtained from the measured pressure drop using;

$$\frac{\Delta p_t}{\Delta L} = \frac{\Delta p_M}{\Delta L} + \rho_M g \sin\theta \,. \tag{14}$$

Figure 41 shows the pressure drop for different superficial oil velocities as a function of superficial water velocities for +2° (upward flow). The general behavior, which is the increase in total pressure gradient with increasing superficial water velocity, is similar to that of horizontal configuration. For low superficial water and oil velocities, the dominant pressure gradient component is the gravitational component. As the velocity of each phases increase, the frictional component starts becoming dominant

Figure 42 is the pressure gradient graph for the -2° downward flow. Since negative pressure gradient values can exist, pressure drops were plotted in Cartesian scale. In downward flow, the existence of a minimum pressure gradient for a certain superficial water and oil velocities was observed.

The experimental pressure gradient data obtained in this study for different inclination angles were compared against the Zhang et al. (2003b) model. Figure 43 shows the pressure gradient comparison against Zhang et al. model for horizontal case. The model predicts the pressure gradient within ±20 % error band. Figure 44 is the comparison of pressure gradient

obtained for +1° of inclination angle with Zhang et al. model. The model predicts the pressure gradient within ±15 % error band. For most of the cases, the pressure gradients were over predicted by the model. The model predictions were observed to be reasonably well for low superficial velocities while they were worsened as the superficial velocities increased. Table 9 shows the error analysis of the Zhang et al. model against experimental data.

Figure 45 is the comparison of Zhang et al. (2003b) model against experimental data for minimum pressure gradient behavior. The model shows minimum pressure gradient behavior but not as pronounced as the experimental data. Figure 46 shows only the minimum pressure gradient area for v_{so}=0.025 m/s and v_{so}=0.100 m/s.

WATER HOLDUP

Quick closing valves are used for holdup measurements with raising the boom. A measured tape was attached parallel to the boom to measure the oil and water level in trapping section.

Figures 47-48 and Figs. 49-50 show the water holdup and water holdup ratio, which is the ratio of no-slip holdup to experimental holdup, for -2° and +2° of inclination angles, respectively. Due to separation problems, holdup data was not collected for v_{so}=1.750 m/s and v_{sw}=1.750 m/s for ±2° inclination angles. In C_w/H_w graph, for +2° inclination angle, all the values start from less than one which means oil flows faster than water. Moreover, the other values are very close to one which means there is no or negligible slippage. Water mostly flows slower than oil for +2° inclination angle. For -2° inclination angle this ratio starts more than one which means water flows faster.

For the better understanding of slippage of the phases in different operating conditions, the normalized drift velocity was plotted against the mixture velocity. The normalized drift velocity, v_N, and mixture velocity, v_M, are defined in Eqs. 15 and 16, respectively.

$$v_N = \left(v_w - v_o\right)/v_M \cdot \tag{15}$$

$$v_M = v_{sw} + v_{so} \cdot \tag{16}$$

Three different (low, medium and high) superficial oil velocities (v_{so}) were used in normalized drift velocity graphs. Figure 51 shows the normalized drift velocity -2° inclination angle. As expected, the largest v_N values can be seen for the lowest mixture velocity values for each individual superficial oil velocities. Generally, for each representative superficial oil flow rate, as the mixture velocity increases, normalized slip velocity approaches to zero which means there is no or negligible slippage between the phases. For v_{so}=0.050 m/s, the normalized slip velocity starts from high positive values, which means water flows much faster than oil. This is mainly due to the gravity effect.

Figure 52 is the normalized drift velocity graph with respect to mixture velocity for +2° inclination angle. As observed in -2° downward flow, the normalized drift velocity approaches zero with increasing mixture velocity. Normalized drift velocity for v_{so}= 0.050 m/s starts from large negative values, which means oil flows much faster than water. This difference between +2° and -2° inclination angle explains the physics of the flow. For upward flow (+2°), since the density of the water is greater than the density of oil, the gravitational force behaves like drag force for the water phase. The drag force slows the flow of the water with respect to the oil. The similar argument can be made for the downward flow (-2°).

The experimental water holdup for different inclination angles were compared against Zhang et al. model. Figures 53 and 54 show the comparisons for +1° and -1° inclination angles, respectively. Solid lines stand for the model predictions for the boundaries. The model predicts the holdups within ±15 % error band for both configurations.

Table 10 shows the performance of the Zhang et al, (2003b) model against experimental data.

PHASE DISTRIBUTION

Conductivity probes were used to determine the phase distribution across the cross section of the pipe. Conductivity probes can determine the continuous phase in the pipe during different operating conditions. For stratified (ST) and stratified with mixing interface (ST&MI) flow patterns, conductivity probes performed well. Due to the turbulence and the formation of drops, conductivity probes did not give reliable results for dispersion type flow patterns. The probes cannot detect the small droplets.

Collecting conductivity probe data for each data point is a very slow process. Therefore, the phase distribution data were collected for three different oil/water ratios (v_{so}=0.050 m/s and v_{sw}=0.050 m/s, v_{so}=0.050 m/s and v_{sw}=0.100 m/s, v_{so}=0.100 m/s and v_{sw}=0.050 m/s) for each inclination angles using the new improved grid system (Fig. 55) with 120 data points to increase the accuracy of the data points.

Figure 56 shows the phase distribution of the phases for -2° inclination angle. The estimated layer was tried to be plotted with continuous line on each figure. In the middle of the figure, concave or convex structure was observed but this is because of the interpolation between the data points. Figure 57 shows the phase distribution of each phases for +2° inclination angle for upward flow.

DROPLET SIZE DISTRIBUTION

Droplet size and its distribution is one of the main interests for this study. Image analysis technique by using high-speed camera was used to determine the droplet size and its distribution as used in Vielma. This technique was chosen because of its non-intrusive nature, which does not disturb the droplets during the flow. It is not applicable to all combination of flow rates (especially high flow rates with low water cut). Location of the high-speed camera was dependent on flow pattern. For stratified (ST), stratified mixing (ST&MI) and dispersion of oil in water over water layer (DO/W&W) flow patterns, entire pipe was shot in different shutter speed. For dispersion of oil in water (O/W) and water in oil (W/O), the camera was located close to the pipe and only small section of the pipe was shot. In oil in water (O/W) and water in oil (W/O) type of flow pattern, it was assumed that the distributions of the droplets are homogenous all around the pipe. In dual continuous (O/W&W/O) flow pattern, the pictures were taken from the bottom and the top of the pipe. The number of the droplets obtained from the pictures is flow pattern dependent, but in all cases, minimum 400 droplets were counted.

Droplets were counted by using Image ProPlus 5.1 software. In each picture every droplet was counted one by one. Since droplets are not counted automatically, the repeatability of the counting droplets should be checked. Figure 58 shows the repeatability of this technique. Droplets were counted from the same picture by two different people. Dispersion of oil in water over water layer (DO/W&W) flow pattern was selected as a

sample because it was divided into ten sections, which make it more sensitive. The top section refers to the top of the pipe and the bottom section refers to the bottom of the pipe. The agreement between two counts was good.

Figures 59 and 61 show the droplet size distribution and probability distributions for oil in water flow (O/W) and water in oil (W/O) patterns, for $+2^o$ inclination angle, respectively. The figures show all the probability distributions tested to represent droplet size data. In both cases, log-normal is the best probability distribution to represent the droplets size data. Rosin Rammler distribution type failed to represent any of the cases for water droplets.

Figure 63 shows the droplet size data and the three different probabilistic distributions for stratified with mixing interface (ST&MI) flow pattern for $+2^o$ inclination angle. As stated in the previous flow patterns, log-normal represents the droplet size data best among the selected distribution types.

For dispersion of water in oil over water layer (DO/W&W) flow pattern, different procedure was applied since the droplet size distribution is not homogenous across the pipe cross section. Figure 65 shows the behavior of SMD as function of the height from bottom to top of the pipe for $+2^o$ inclination angle. The pipe was divided into 5 sections in each picture to see the SMD behavior clearly. The top and bottom of the y-axis in the graphs refer to the top and bottom of the cross section of the pipe, respectively.

Figures 66 and 67 show the droplet size distribution and probabilistic distributions for oil droplets and water droplets, respectively, for -1^o inclination angle for dual continuous (O/W&W/O) flow pattern. The water droplets are smaller compared to oil droplets. For both of oil and water droplets, log-normal distribution worked well.

SMD was analyzed for each flow pattern. Increasing trend in SMD was observed with increasing dispersed phase superficial velocities for different inclination angles in oil in water (Fig. 60) and water in oil (Fig. 62). When the internal phase velocity increases, v_{so} and, v_{sw}, respectively, the SMD tends to increase for same continuous phase superficial velocity. As the percentage of internal phase increases, the droplets get closer, increasing the coalescence tendency, and resulting in larger droplets. No trend was observed for the effect of inclination angle. Figure 64 shows the SMD behavior with respect to v_{sw} for different inclination angles. Decreasing trend in SMD was observed with increasing superficial water velocities for different inclination angles. As the superficial water velocity increases, turbulence level increases and smaller oil droplets are formed. The size of SMD also depends on the oil layer thickness during the flow. No clear trend was observed for the effect of inclination angle. Figures 68 and 69 show the variation of SMD for oil and water droplets respectively for a constant superficial oil velocity (v_{so}=1.000 m/s) with changing superficial water velocity. Increasing trend in SMD was observed in water droplets with increasing superficial water velocities for different inclination angles. For water droplets, this can be explained by coalescence tendency as discussed in W/O type of flow pattern. Trend is not so clear for the oil droplets since there are only two data points in each inclination angles. No clear trend was observed with the change of inclination angle.

DROPLET SIZE COMPARISON

The droplet size data were compared against the predictions by the existing models for d_{max}, d_{min} and SMD. In the literature, Hinze (1955), Kubie and Garner (1977), Angeli and Hewitt (2000), Brauner (2002) and Kouba (2003) models exist to estimate the d_{max}. Kouba (2003) model is the only model to predict the $d_{min.}$ For SMD prediction, Angeli and Hewitt (2000) model, which is the only available model for SMD prediction, was used. The models work for fully dispersed cases. Therefore, the following comparisons are presented.

MAXIMUM DIAMETER COMPARISONS-O/W

Figure 70 shows the comparison of experimental d_{max} with the model predictions for -1° of inclination angle, for different superficial oil velocities. Diamond points on the graph represent the experimental data points. Angeli and Hewitt (2000), Kubie and Gardner (1977) models over-predicted, while Kouba (2003) model under-predicted the experimental data. Hinze (1955) and Brauner (2002) showed the best performance. Hinze (1955) predicted d_{max} the best among all models. Table 11 shows the error analysis for each model.

MINIMUM DIAMETER COMPARISONS-O/W

Figure 71 shows the comparison of d_{min} data against Kouba (2003) model for -1° of inclination angle, for different oil superficial velocities. The model under-predicted for most of the cases. Table 12 shows the statistical parameters for Kouba (2003) model.

SMD COMPARISONS-O/W

Figure 72 shows the comparison of experimental SMD against Angeli and Hewitt (2000) model for -1° of inclination angle. Angeli and Hewitt model over-predicted the experimental SMD data for all cases. Table 13 shows the error analysis for the comparison.

MAXIMUM DIAMETER COMPARISONS-W/O

Figure 73 shows the comparison of d_{max} against existing models for different superficial water velocities for -1°. Kubie and Gardner (1977) model over predicted the experimental d_{max} for all inclination angles, where all the other models under predicted experimental d_{max} data. Brauner (2002) model predicted the d_{max} the best among all models. An error analysis can be found in Table 14.

MINIMUM DIAMETER COMPARISONS-W/O

Figure 74 shows the comparison of d_{min} against Kouba model for varying superficial water velocities for -1°. The model under-predicted d_{min}. Table 15 shows the error analysis for Kouba model.

SMD COMPARISONS-W/O

Figure 75 shows the performance of Angeli and Hewitt (2000) model against experimental SMD obtained in this study for -1°. Angeli and Hewitt model (2000) under-predicted experimental SMD data that obtained in this study. Error analysis can be found in Table 16.

Table 9 - Pressure Gradient Evaluation against Zhang et al. (2003b) Model

	ε_1 (%)	ε_2 (%)	ε_3 (%)	ε_4 (Pa/m)	ε_5 (Pa/m)	ε_6 (Pa/m)
Pressure Gradient	73.93	125.76	863.08	155.26	194.91	319.84

Table 10 - Water Holdup Evaluation against Zhang et al. (2003b) Model

	ε_1 (%)	ε_2 (%)	ε_3 (%)	ε_4	ε_5	ε_6
Water Holdup	1.43	9.65	27.23	0.01	0.04	0.04

Table 11 - Maximum Diameter Model Evaluation for O/W Dispersions

Model	Flow Pattern	ε_1 (%)	ε_2 (%)	ε_3 (%)	ε_4 (mm)	ε_5 (mm)	ε_6 (mm)
Hinze	O/W	-9.84	19.00	24.36	-0.22	0.28	0.40
Kubie & Gardner	O/W	449.36	449.36	153.14	5.14	5.14	0.76
Angeli & Hewitt	O/W	231.94	231.94	94.74	2.58	2.58	0.42
Kouba	O/W	-84.14	84.14	6.40	-1.07	1.07	0.43
Brauner	O/W	-16.26	22.13	23.93	-0.29	0.33	0.42

Table 12 - Minimum Diameter Model Evaluation for O/W Dispersions

Model	Flow Pattern	ε_1 (%)	ε_2 (%)	ε_3 (%)	ε_4 (mm)	ε_5 (mm)	ε_6 (mm)
Kouba	O/W	-38.75	43.49	29.67	-0.05	0.05	0.05

Table 13 - SMD Model Evaluation for O/W Dispersions

Model	Flow Pattern	ε_1 (%)	ε_2 (%)	ε_3 (%)	ε_4 (mm)	ε_5 (mm)	ε_6 (mm)
Angeli &Hewitt	O/W	199.32	199.32	65.83	1.17	1.17	0.16

Table 14 - Maximum Diameter Model Evaluation for W/O Dispersions

Model	Flow Pattern	ε_1 (%)	ε_2 (%)	ε_3 (%)	ε_4 (mm)	ε_5 (mm)	ε_6 (mm)
Hinze	W/O	-44.52	44.52	15.80	-0.82	0.82	0.68
Kubie & Gardner	W/O	205.04	205.04	84.70	3.31	3.31	1.84
Angeli & Hewitt	W/O	-57.88	57.88	13.04	-1.04	1.04	0.58
Kouba	W/O	-90.44	90.44	2.74	-1.54	1.54	0.65
Brauner	W/O	-40.60	41.46	17.86	-0.77	0.78	0.54

Table 15 - Minimum Diameter Model Evaluation for W/O Dispersions

Model	Flow Pattern	ε_1 (%)	ε_2 (%)	ε_3 (%)	ε_4 (mm)	ε_5 (mm)	ε_6 (mm)
Kouba	W/O	13.11	57.55	76.46	-0.01	0.03	0.04

Table 16 - SMD Model Evaluation for W/O Dispersions

Model	Flow Pattern	ε_1 (%)	ε_2 (%)	ε_3 (%)	ε_4 (mm)	ε_5 (mm)	ε_6 (mm)
Angeli &Hewitt	W/O	-61.74	61.74	11.72	-0.54	0.54	0.21

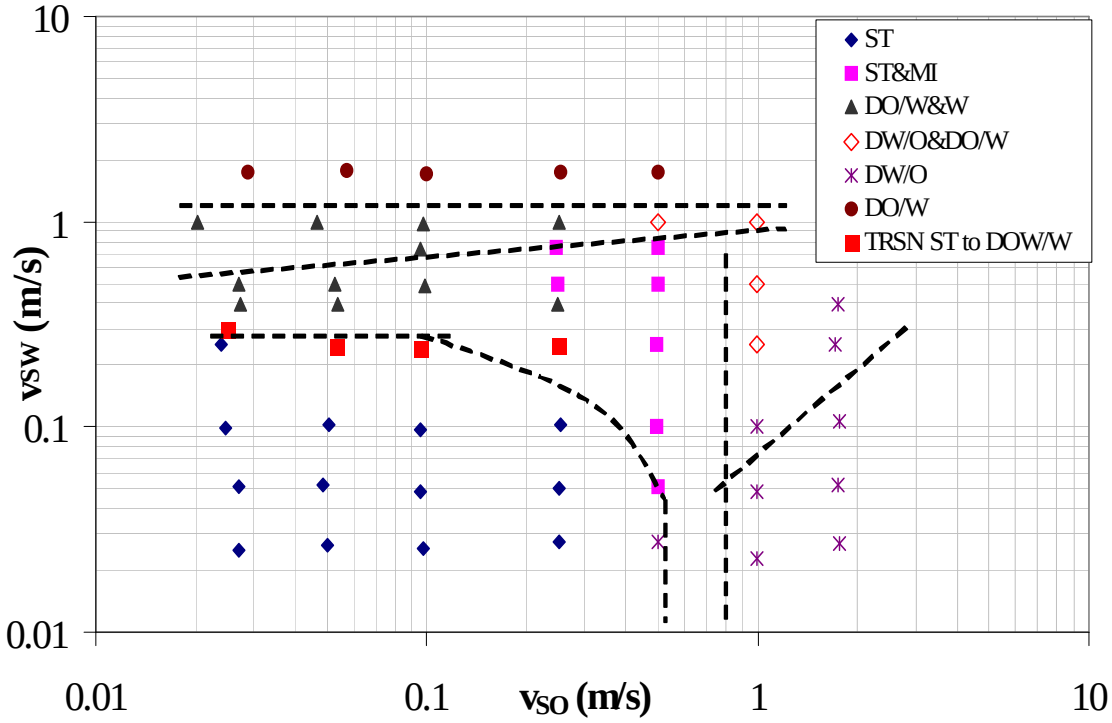

Figure 28 - Experimental Flow Pattern Map (-1° Downward)

Figure 29 - v_{so}=0.025 m/s v_{sw}=0.025 m/s (ST)

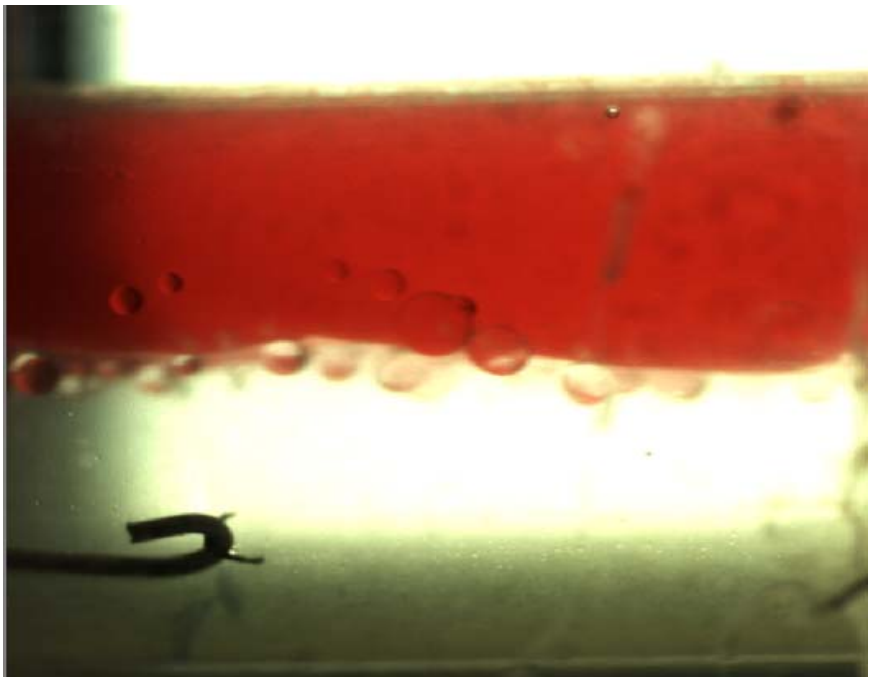

Figure 30 - v_{so}=0.250 m/s v_{sw}=0.500 m/s (ST&MI)

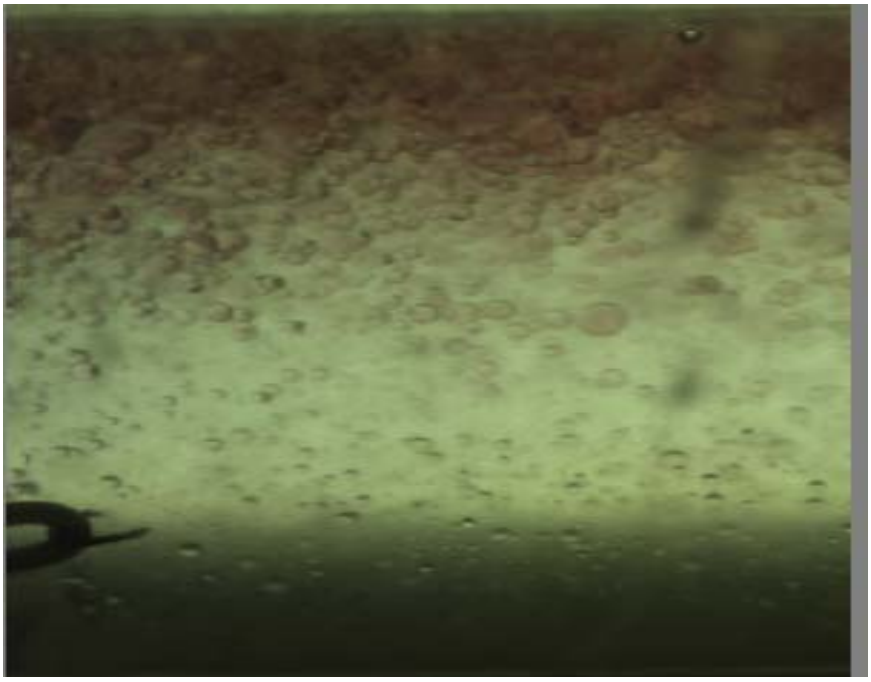

Figure 31 - v_{so}=0.050 m/s v_{sw}=1.000 m/s (DO/W&W)

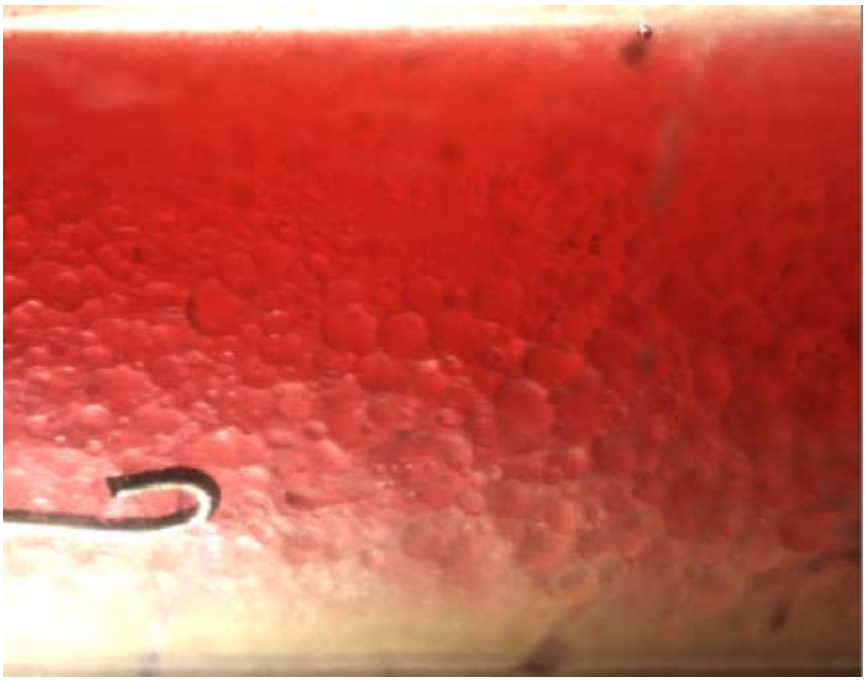

Figure 32 - v_{so}= 1.000 m/s v_{sw}=0.400 m/s (DO/W&DW/O)

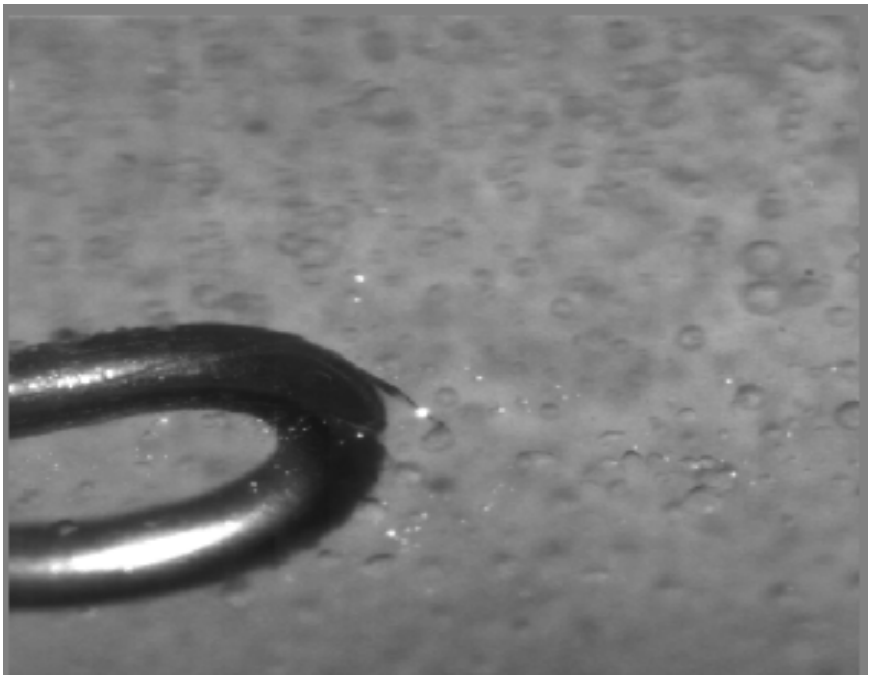

Figure 33 - v_{so}= 0.050 m/s v_{sw}=1.750 m/s (DO/W)

Figure 34 - v_{so}= 1.750 m/s v_{sw}=0.100 m/s (DW/O)

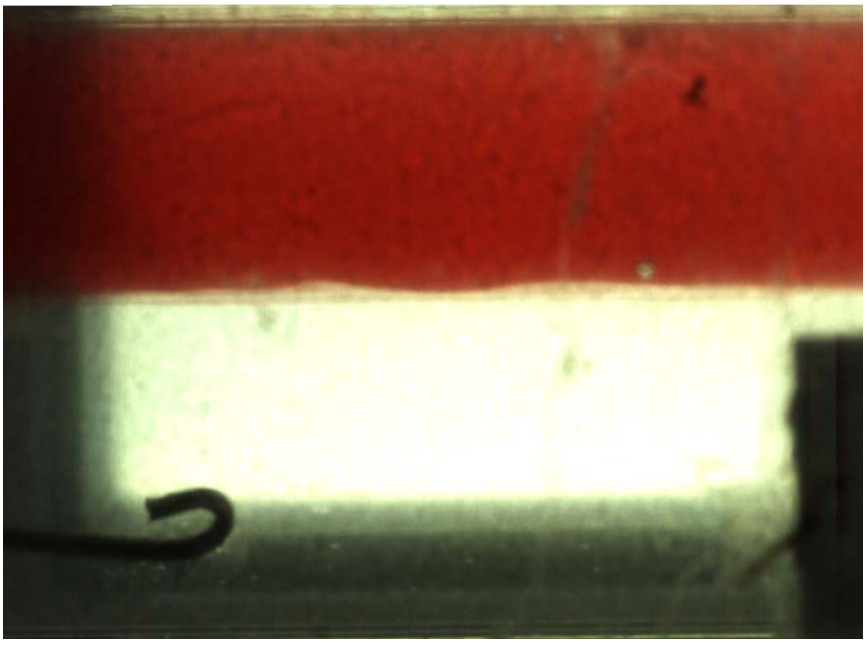

Figure 35 - v_{so}=0.100 m/s v_{sw}=0.250 m/s (TRNS ST to ST&MI)

Figure 36 - v_{so}=0.500 m/s v_{sw}=0.025 m/s (DW/O&O)

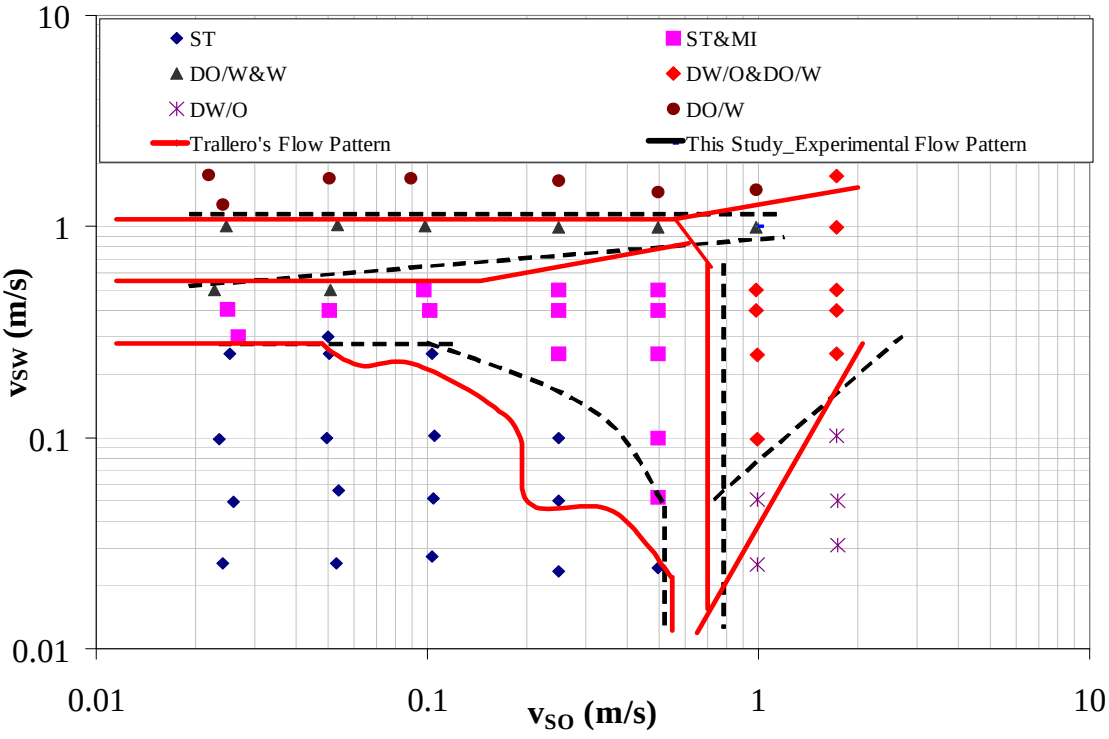

Figure 37 - Comparison of Flow Pattern Boundaries (Model) Horizontal

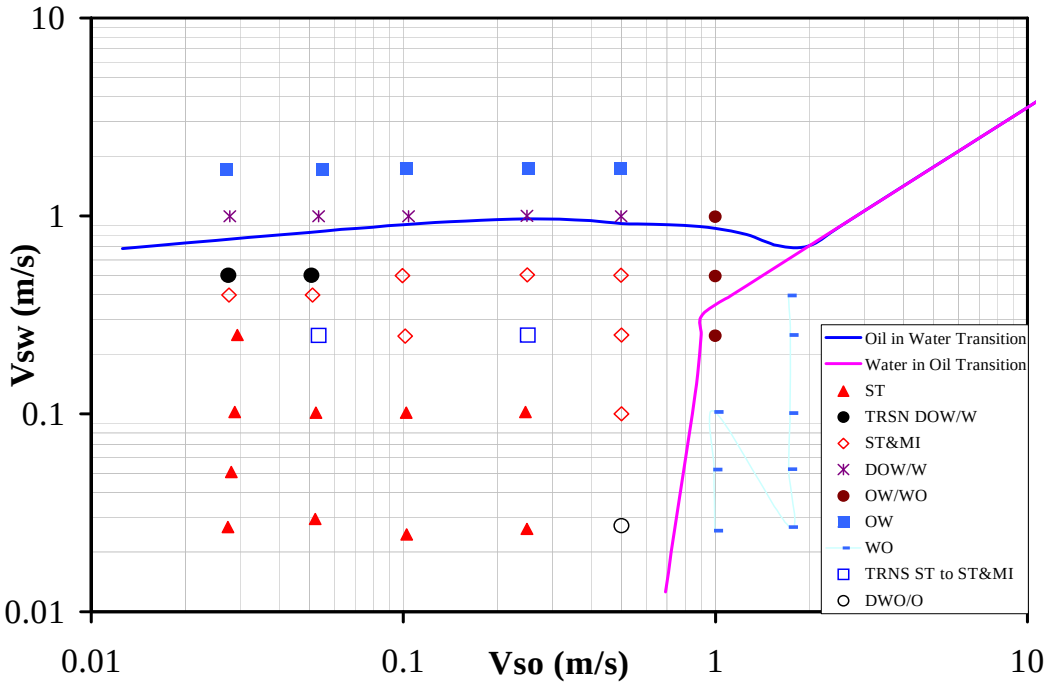

Figure 38 - Comparison of Flow Pattern Boundaries (-2° Downward)

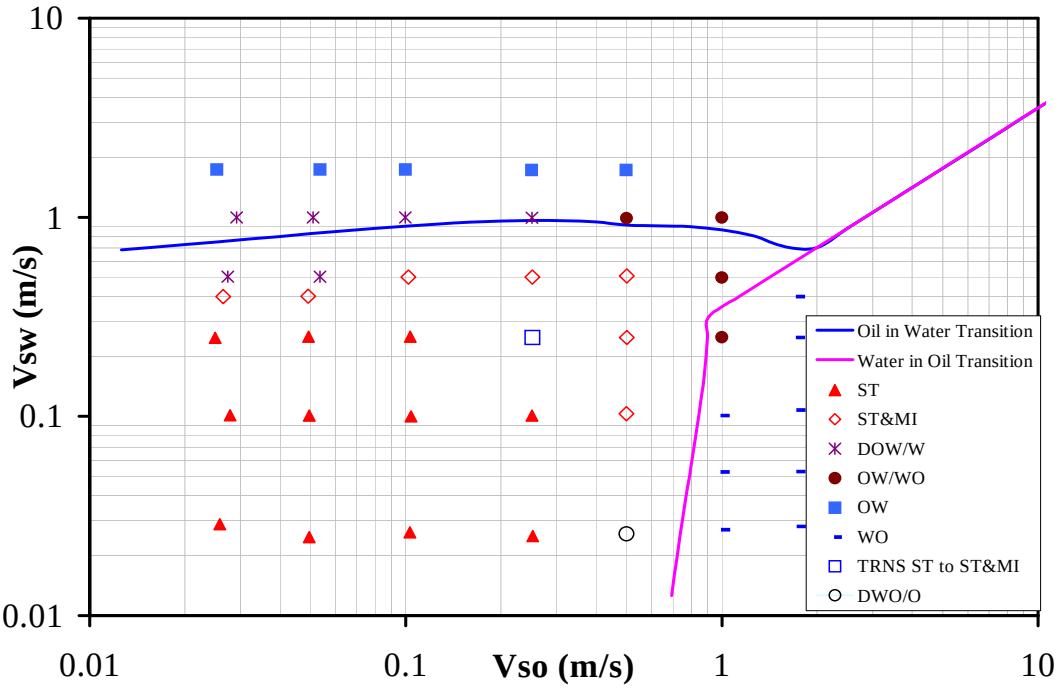

Figure 39 - Comparison of Flow Pattern Boundaries (+2° Upward)

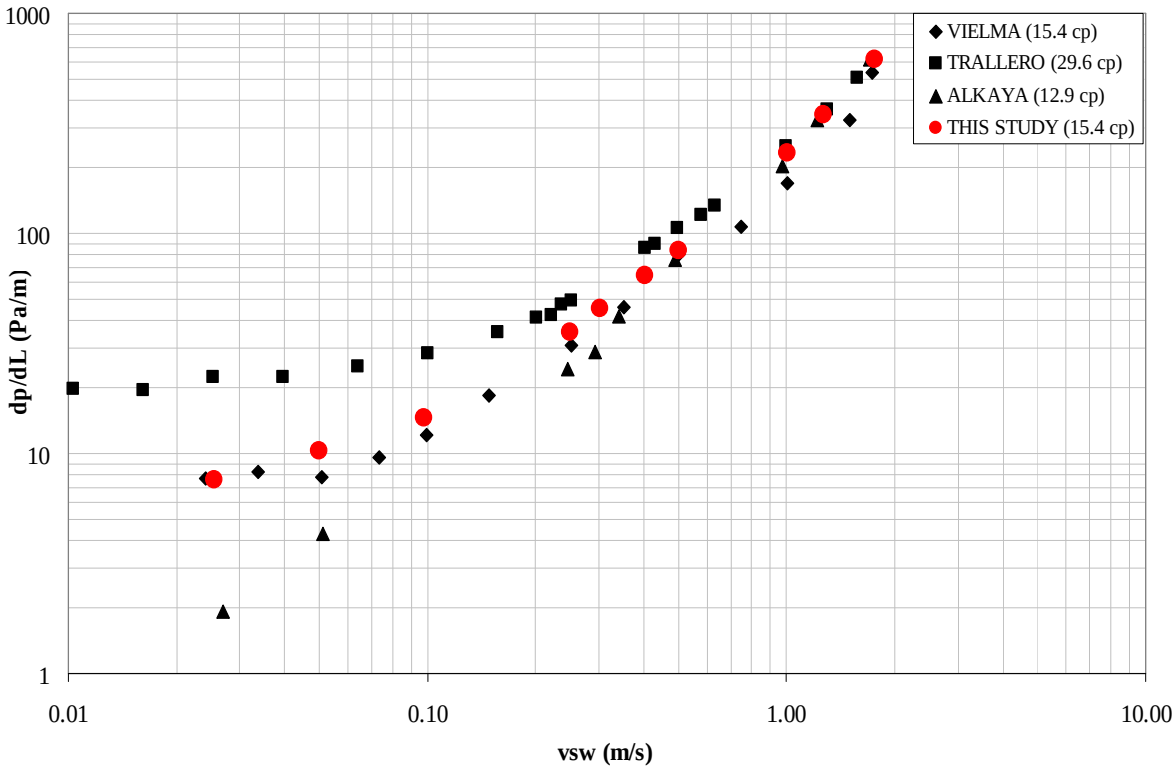

Figure 40 - Pressure Drop Comparison (v_{so}=0.025 m/s)

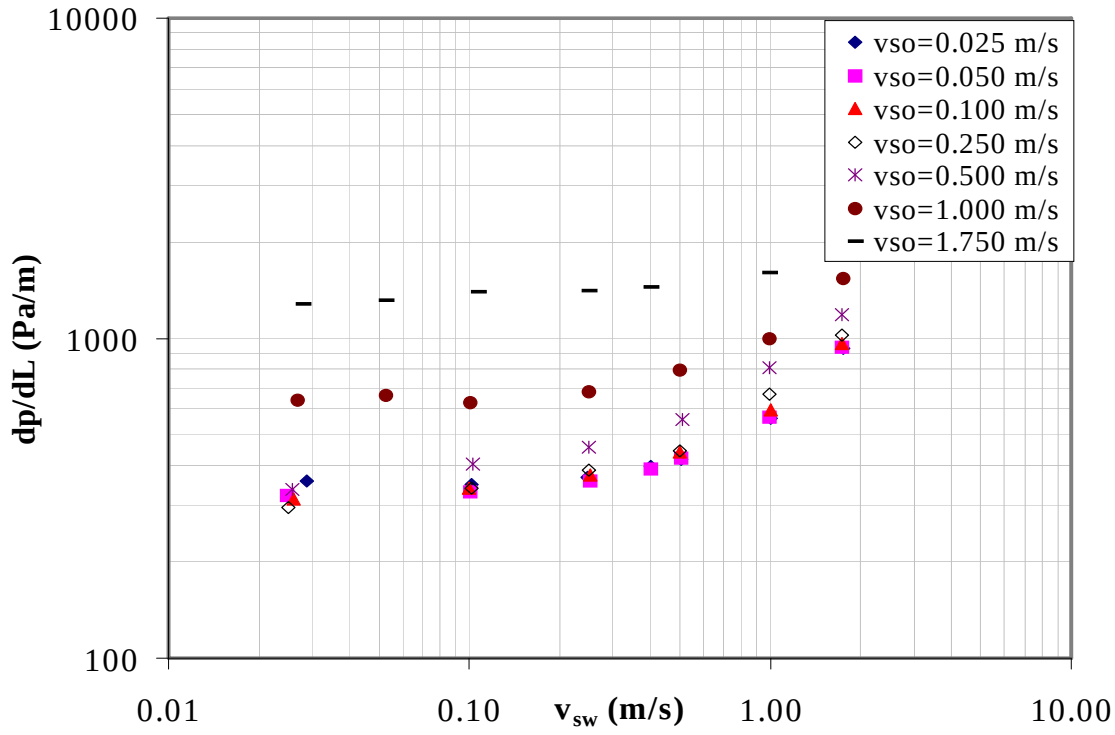

Figure 41 - Experimental Pressure Gradients (+2° Upward)

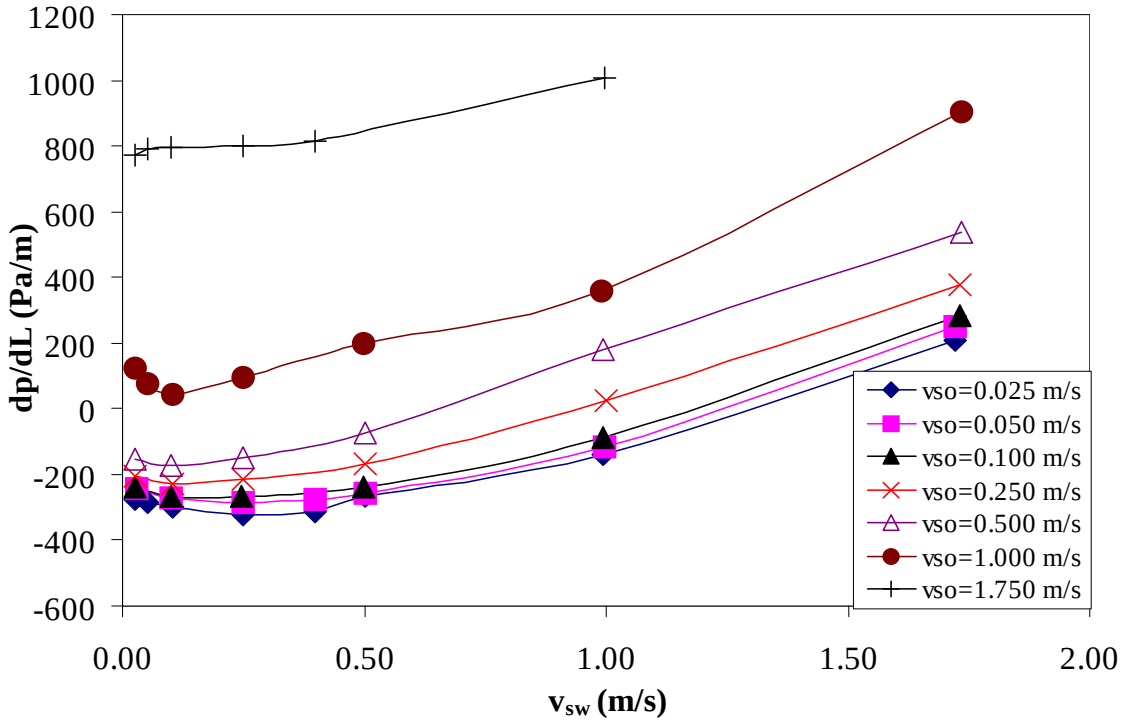

Figure 42 - Experimental Pressure Gradients (-2° Downward)

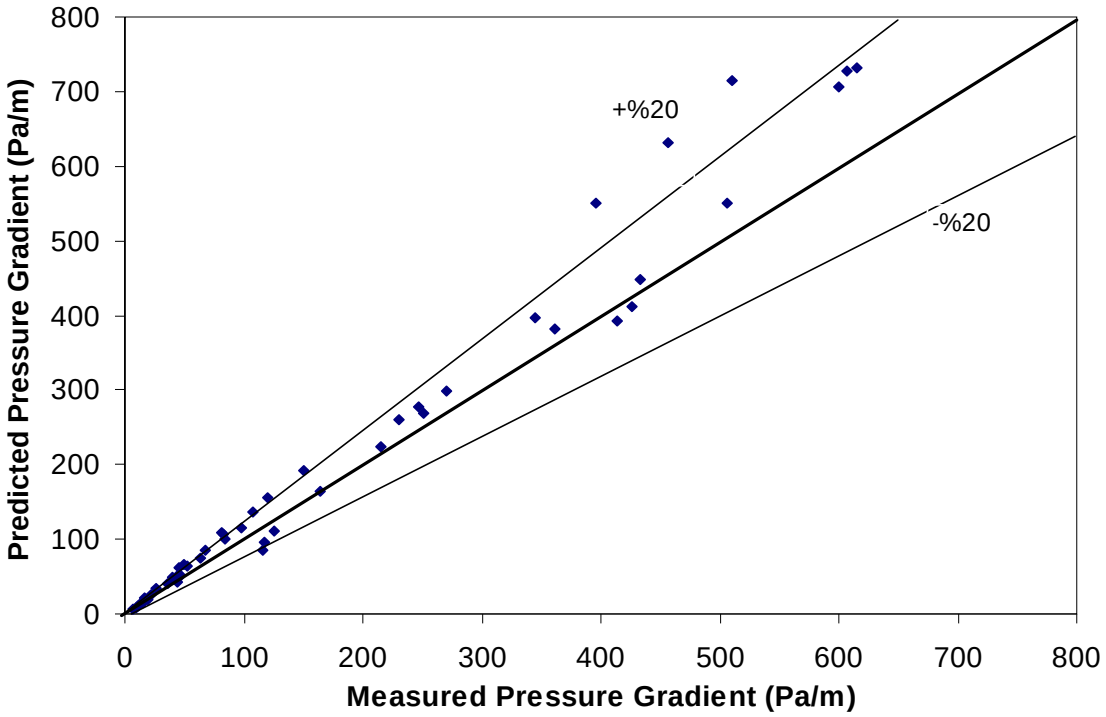

Figure 43 - Unified Model Pressure Gradient Comparisons (Horizontal)

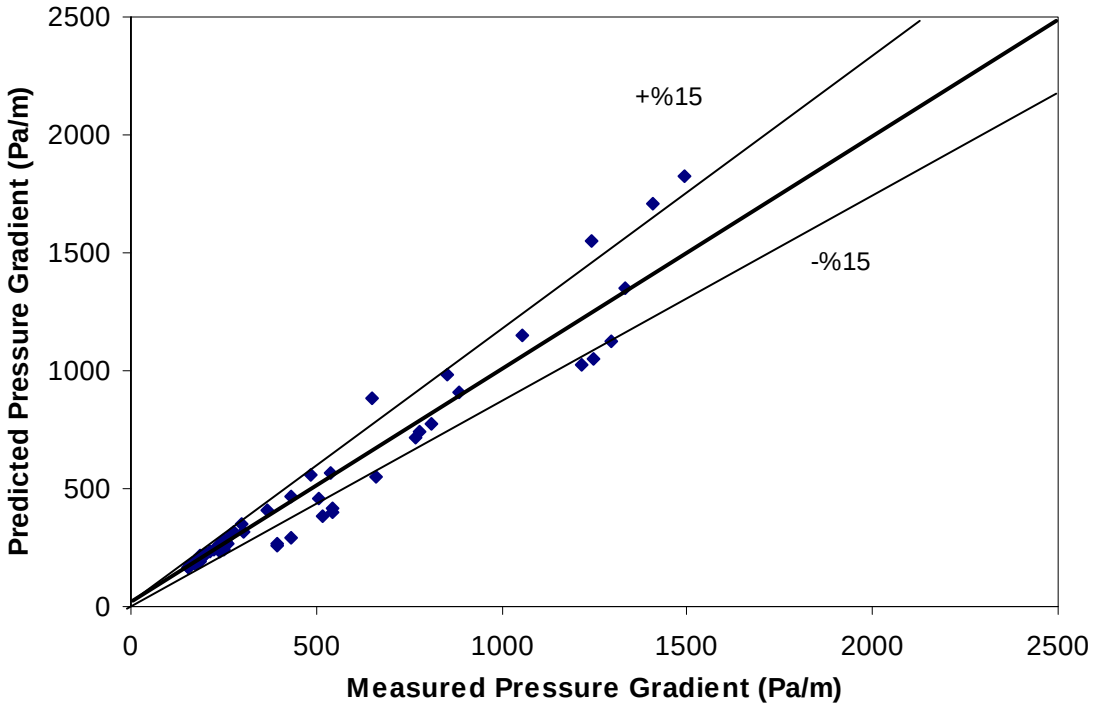

Figure 44 - Unified Model Pressure Gradient Comparisons (+1° Upward)

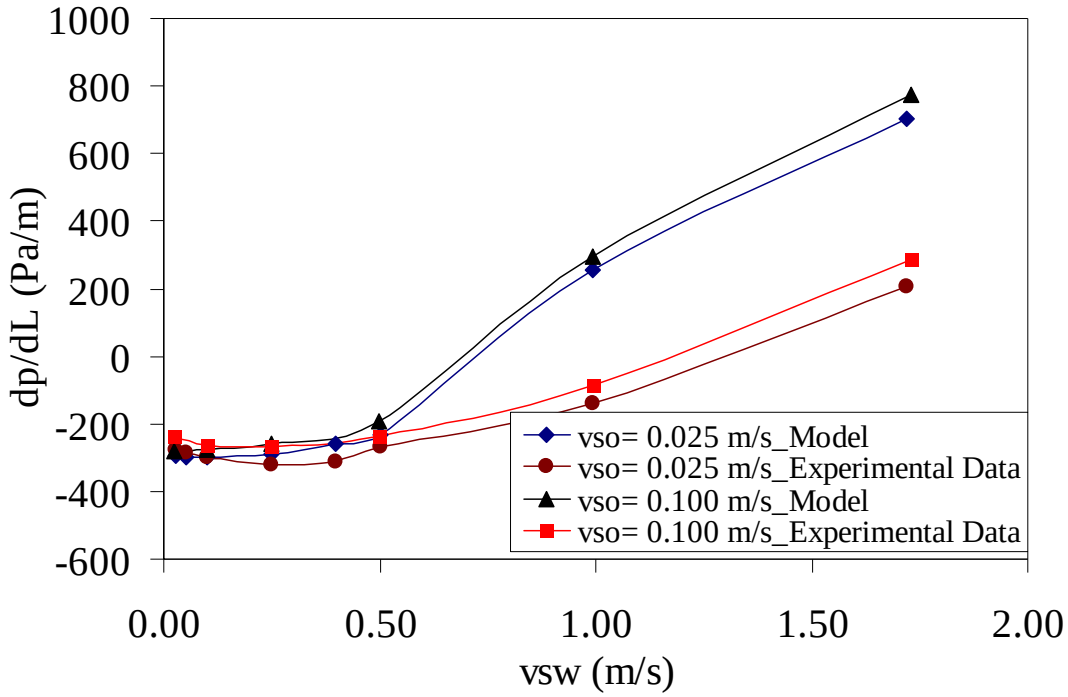

Figure 45 - Minimum Pressure Gradient Comparison against Zhang et al. Unified Model (2003b) (-2° Downward)

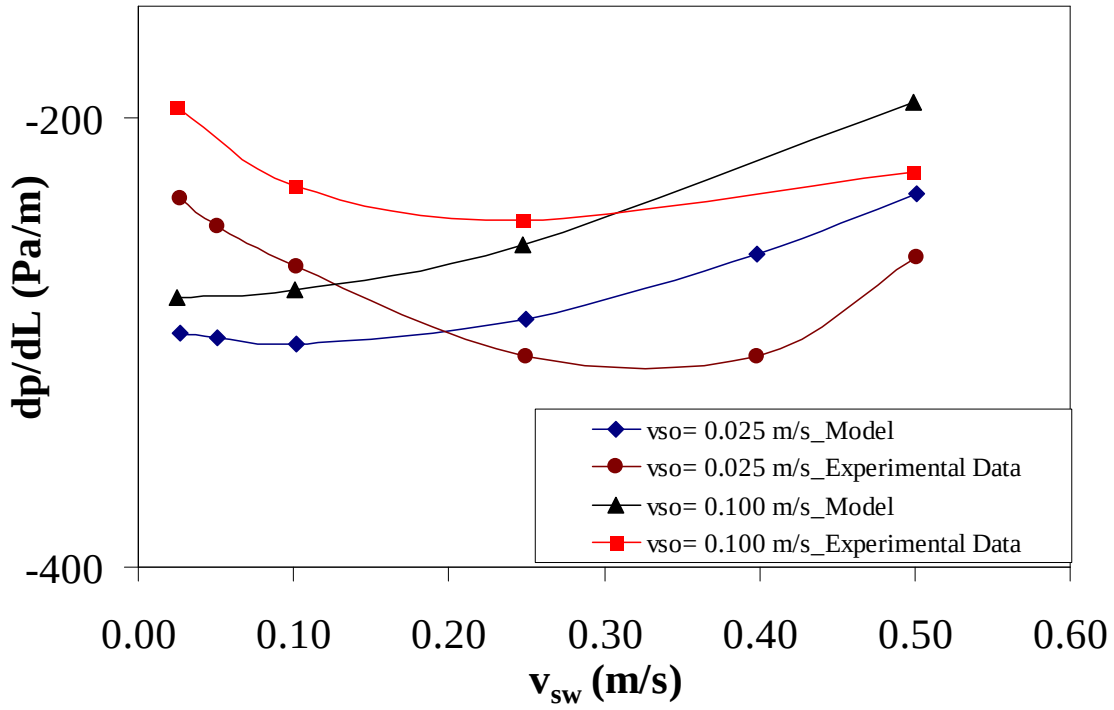

Figure 46 - Minimum Pressure Gradient Comparison against Zhang et al. Unified Model (2003b) (Small Area -2° Downward)

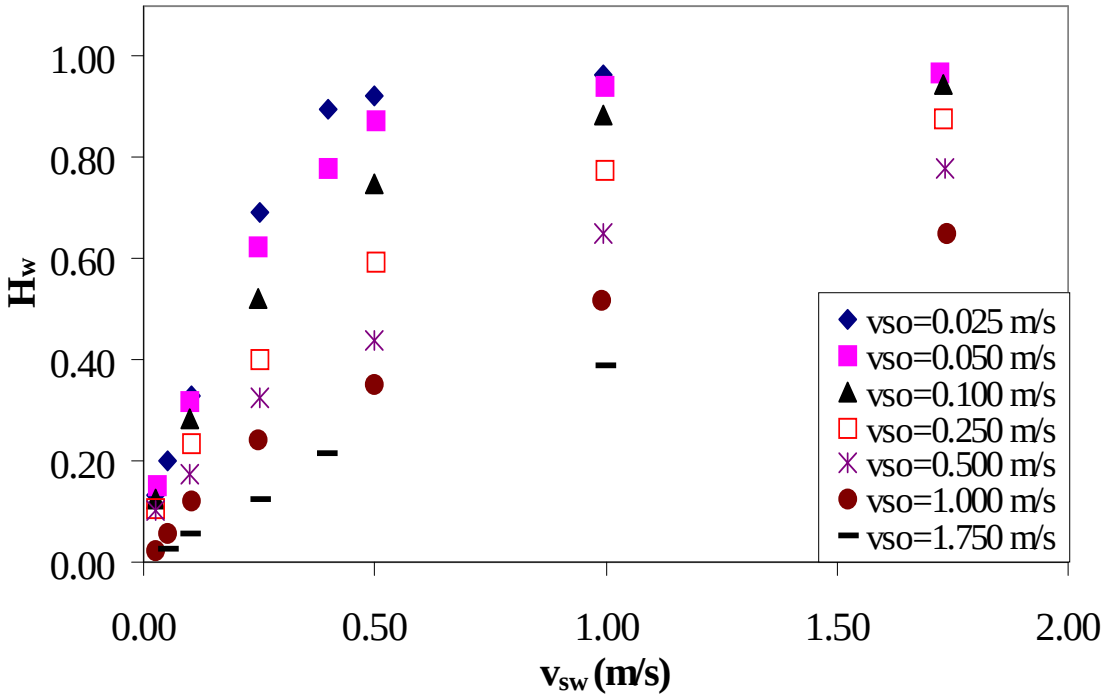

Figure 47 - Experimental Water Holdup (-2° Downward)

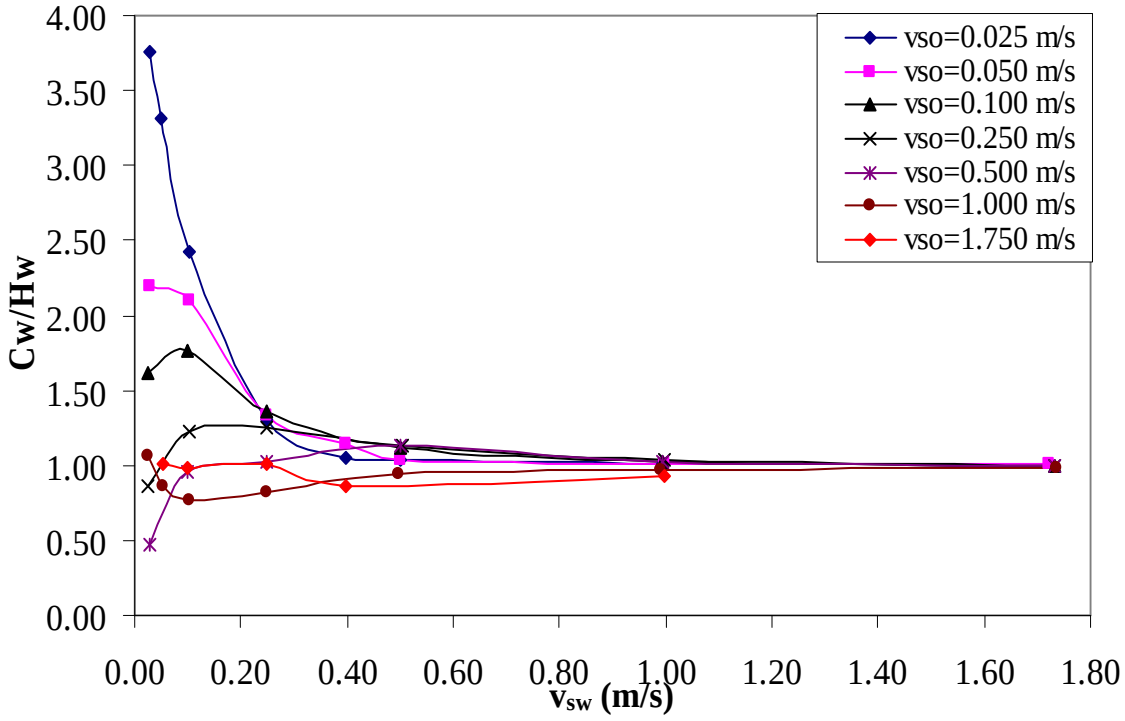

Figure 48 - Experimental Water Holdup Ratio (-2° Downward)

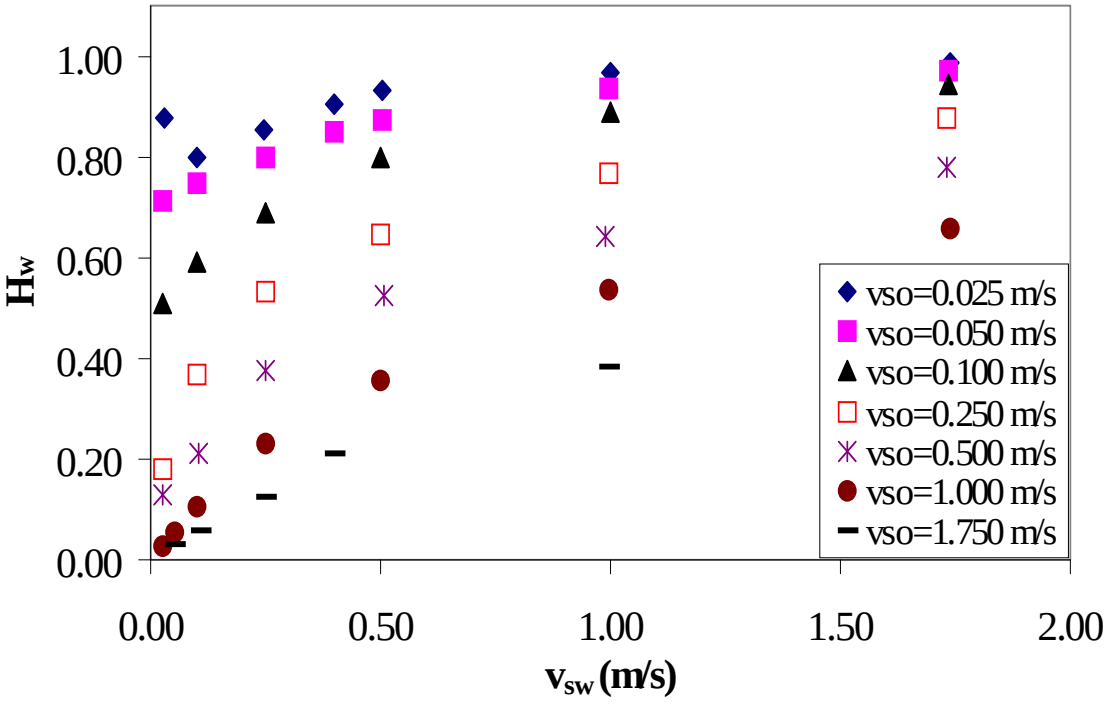

Figure 49 - Experimental Water Holdup (+2° Upward)

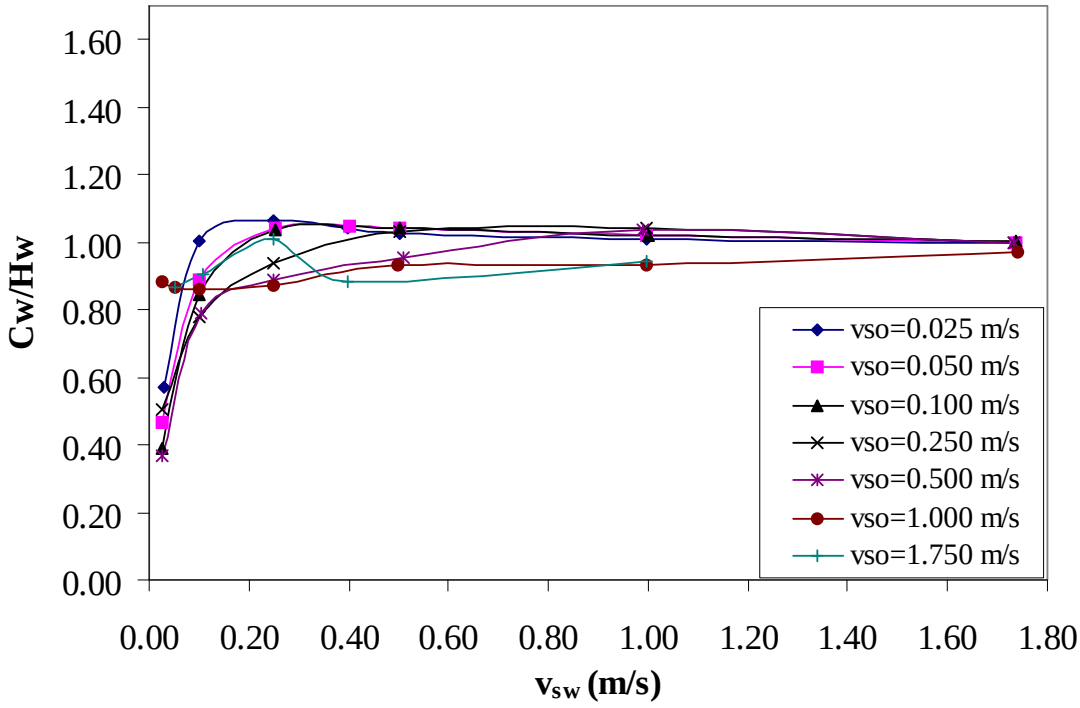

Figure 50 - Experimental Water Holdup Ratio (+2° Upward)

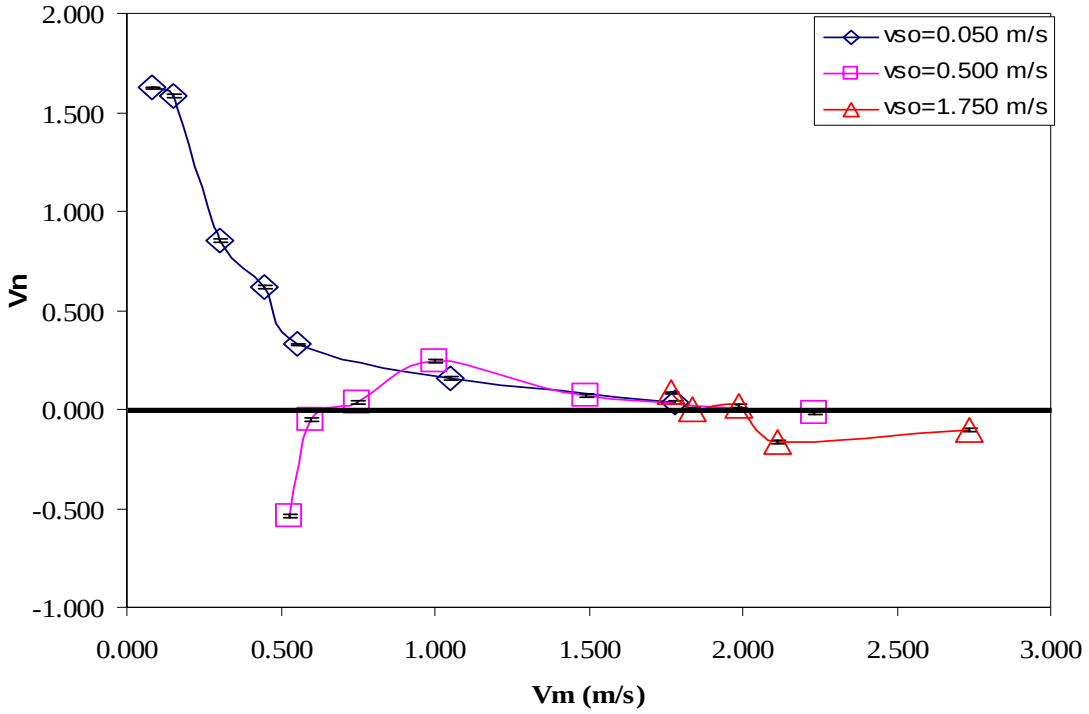

Figure 51 - Normalized Drift Velocity (-2° Downward)

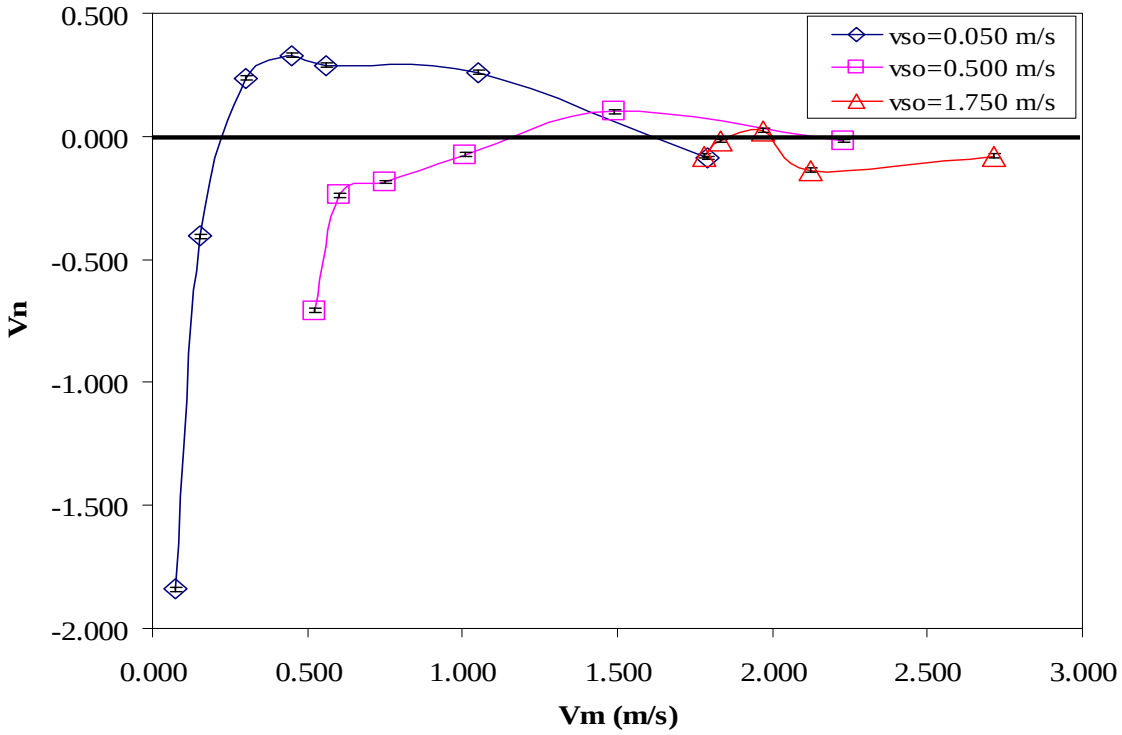

Figure 52 - Normalized Drift Velocity (+2° Upward)

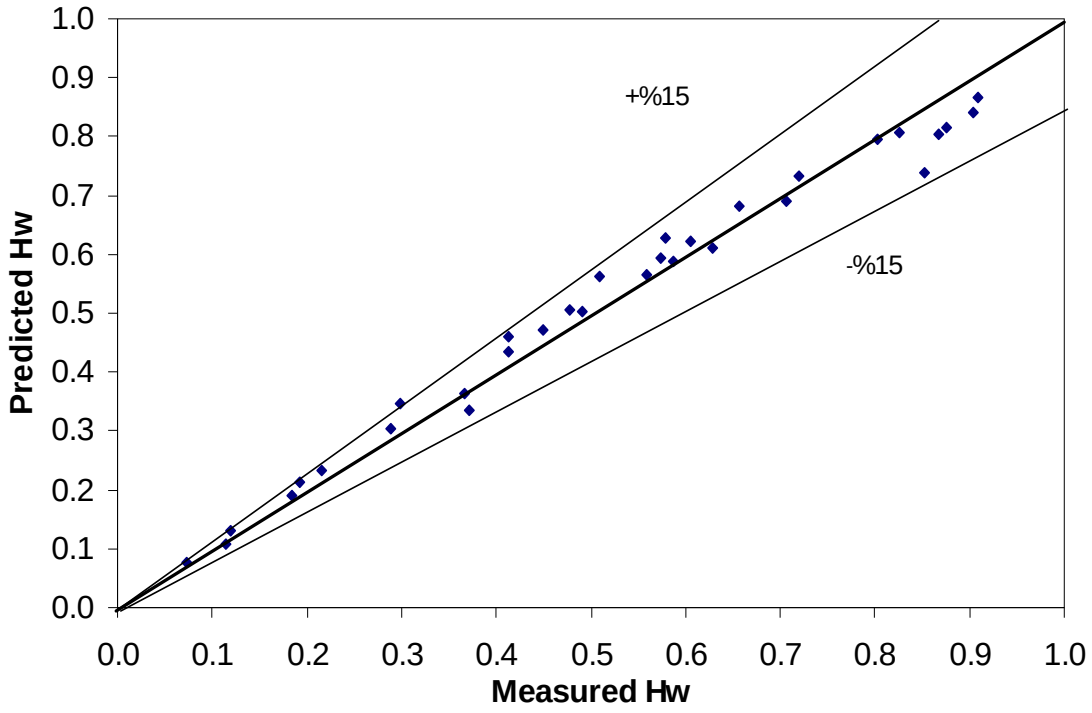

Figure 53 - Unified Model Water Holdup Comparisons (+1° Upward)

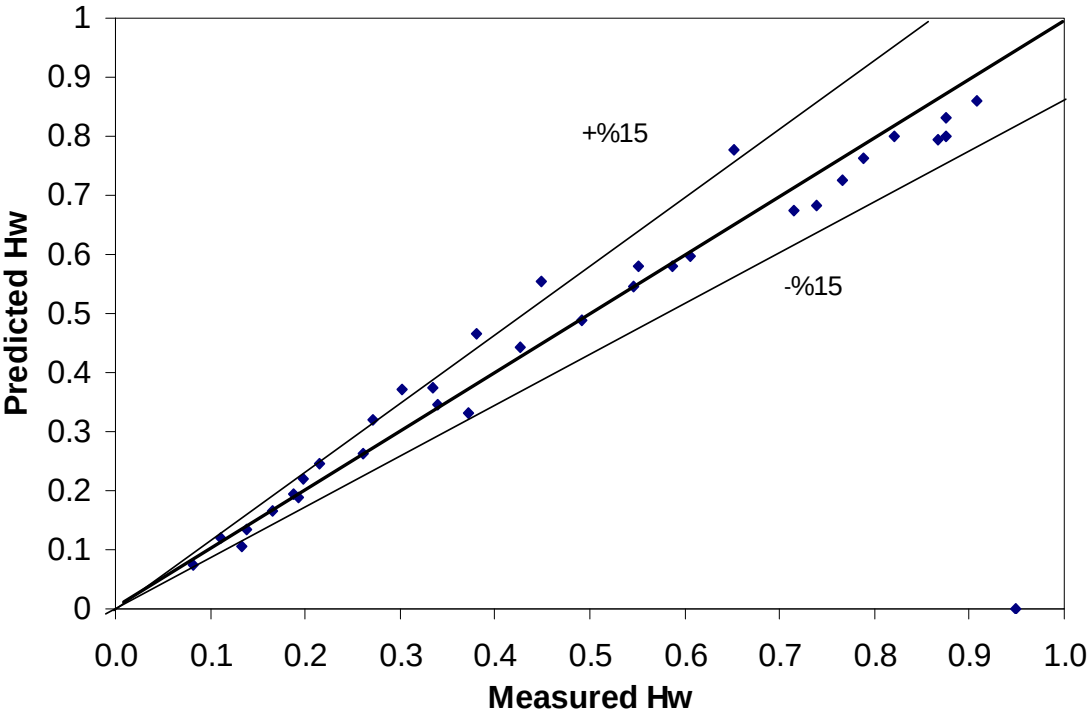

Figure 54 - Unified Model Water Holdup Comparisons (-1° Downward)

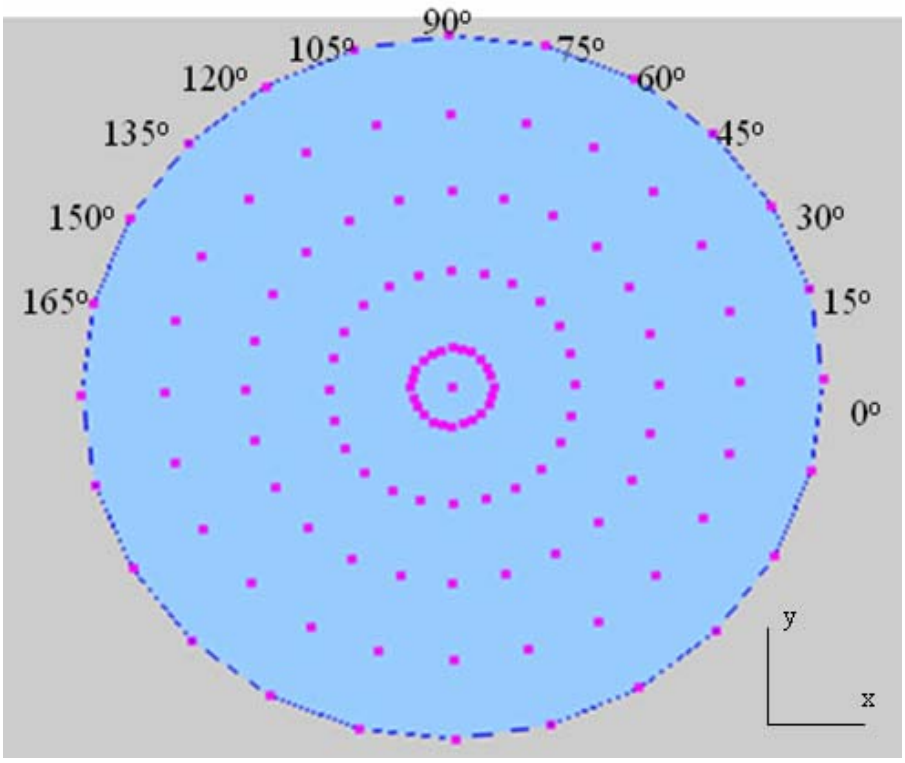

Figure 55 - New Model for Phase Distribution

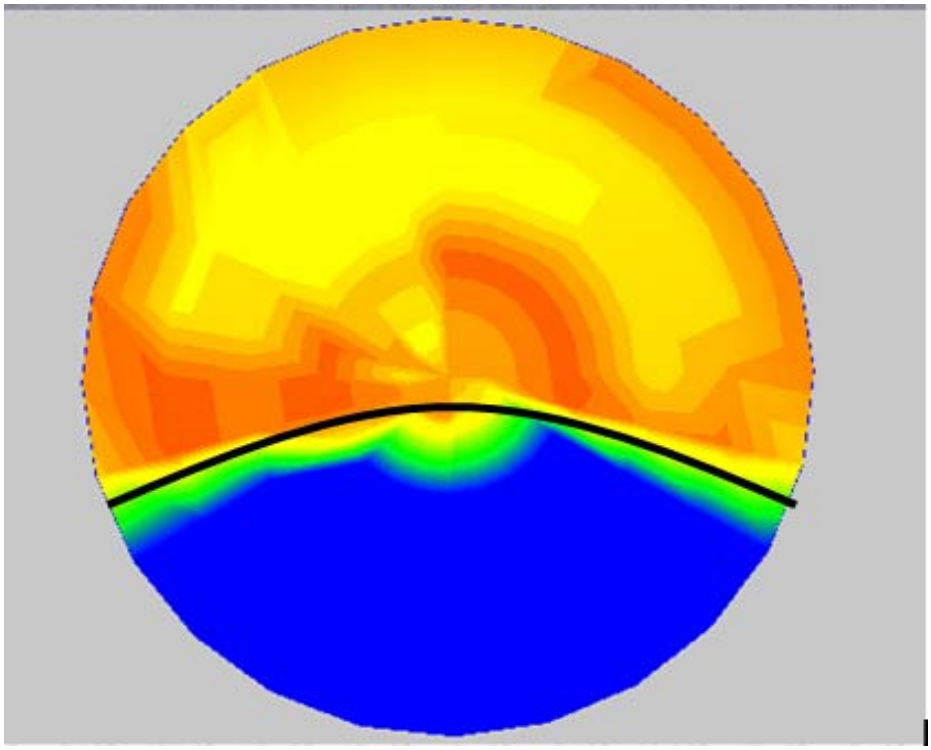

Figure 56 - Phase Distribution for v_{so} = 0.050 m/s, v_{sw} = 0.050 m/s (-2° Downward)

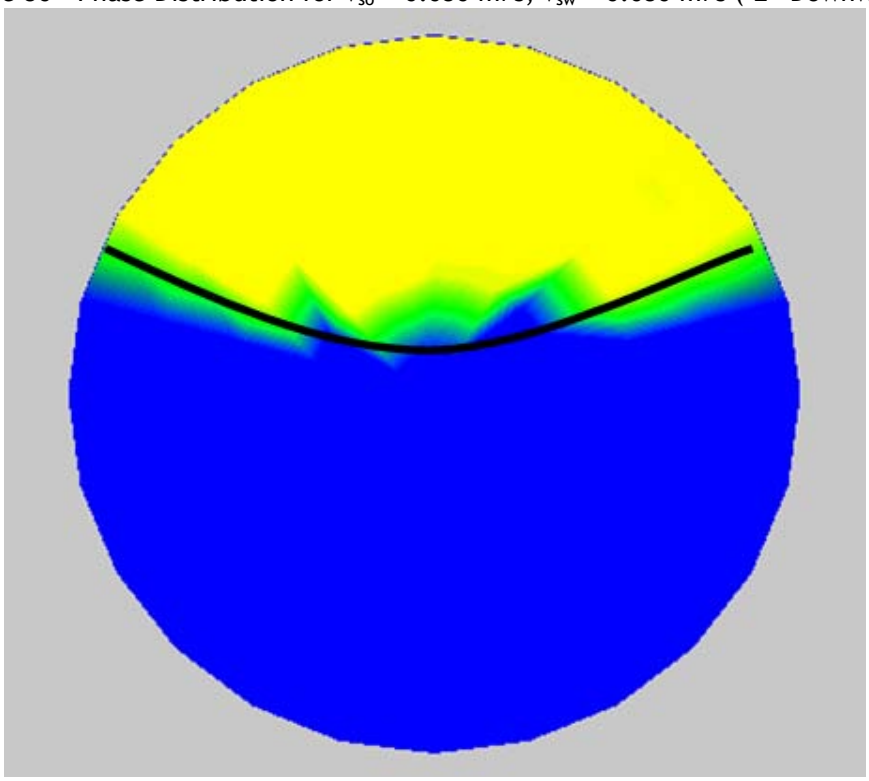

Figure 57 - Phase Distribution for v_{so}=0.050 m/s, v_{sw}=0.050 m/s (+2° Upward)

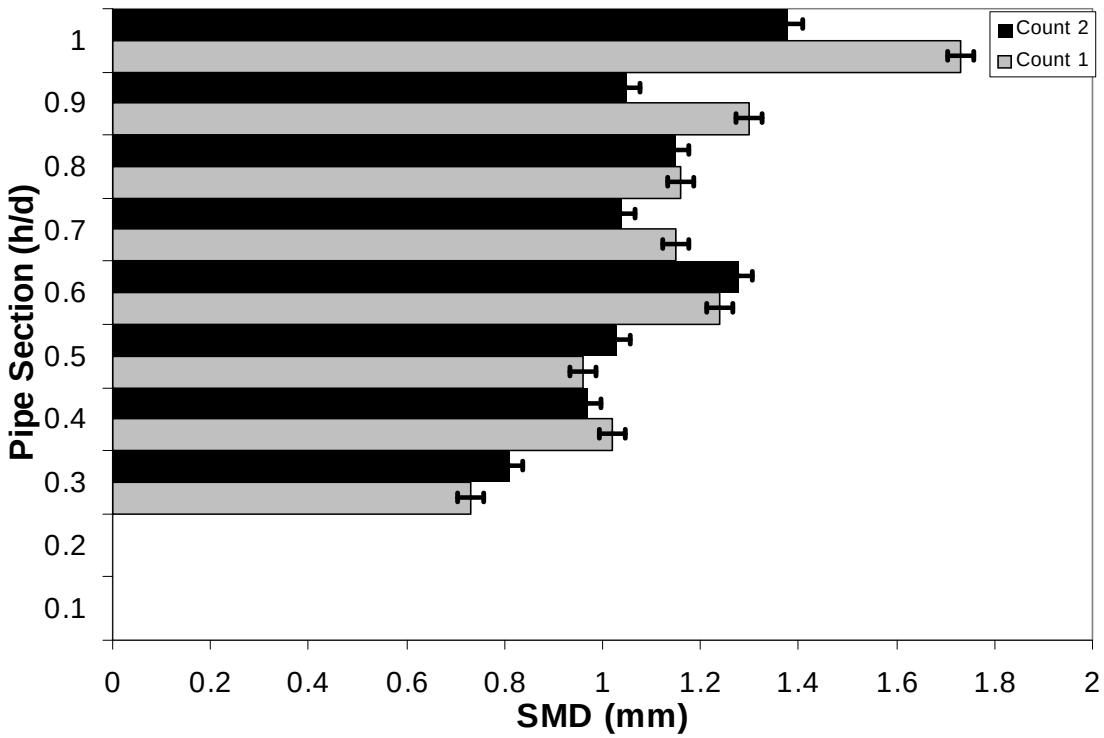

Figure 58 - Repeatability of Counting Droplets

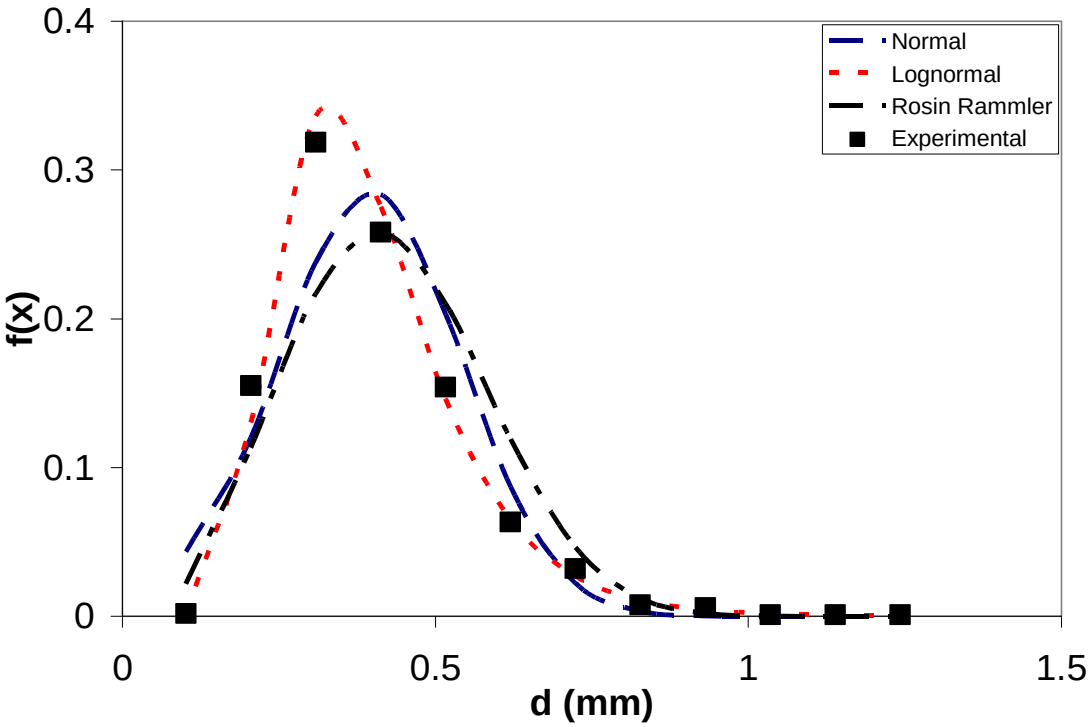

Figure 59 - Droplet Size Distributions (v_{so}=0.025 m/s, v_{sw}=1.750 m/s, +2° Upward)

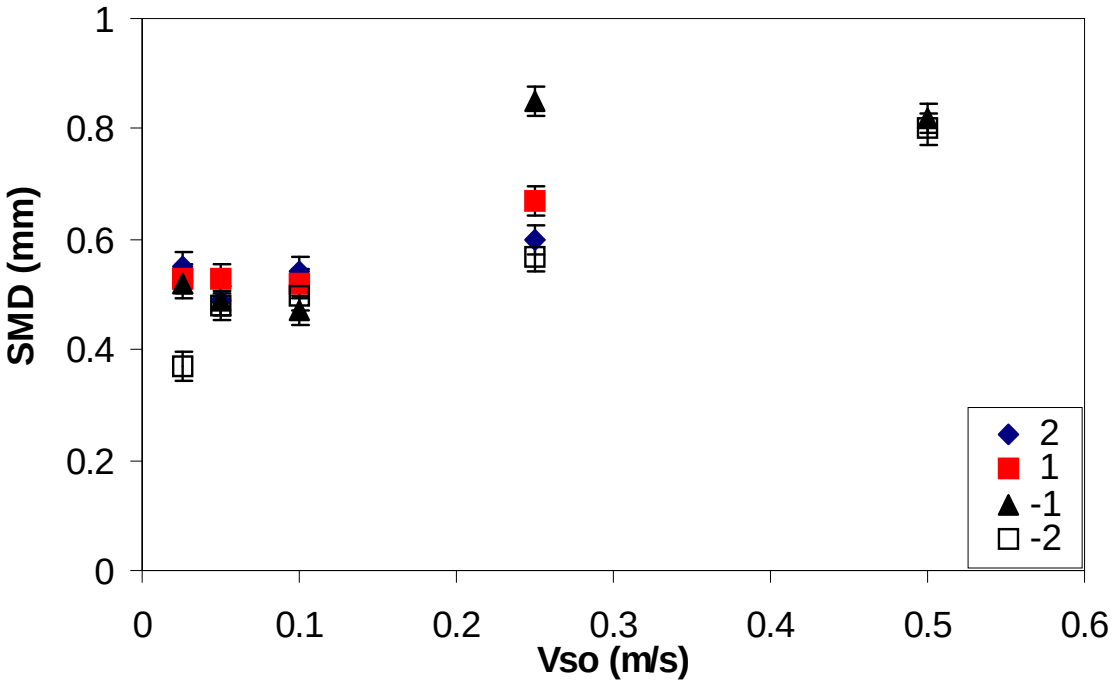

Figure 60 - Figure 60: Variation of SMD with v_{so} and Inclination Angles for O/W Dispersions

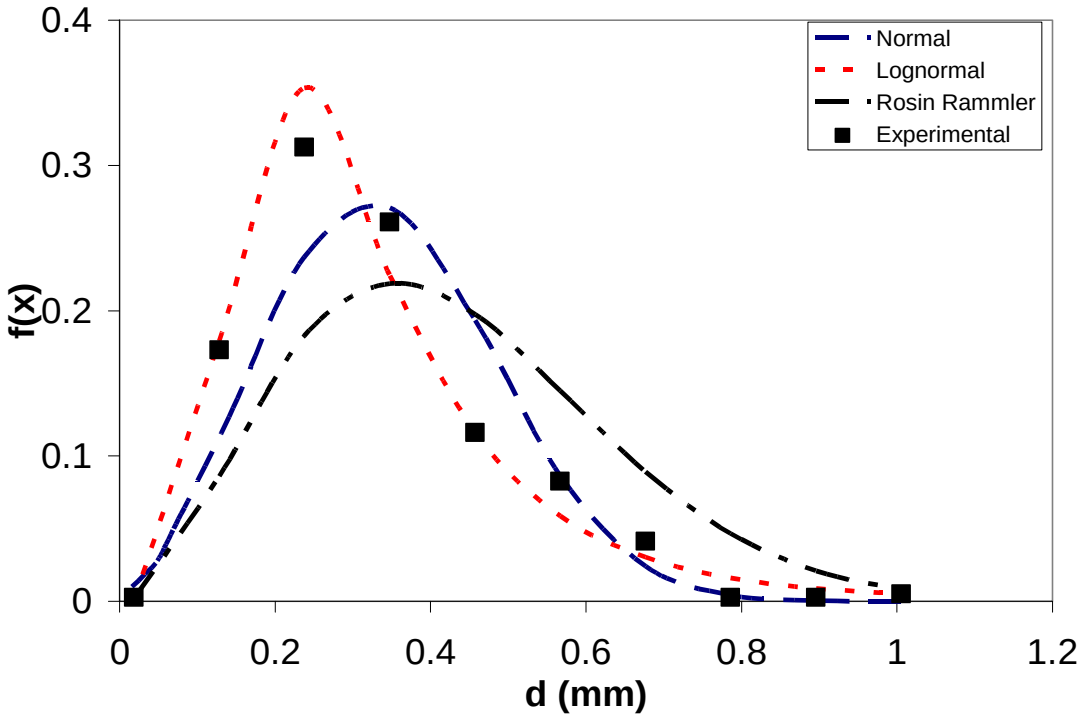

Figure 61 - Droplet Size Distributions (v_s=1.750 m/s, v_{sw}=0.100 m/s, +2° Upward)

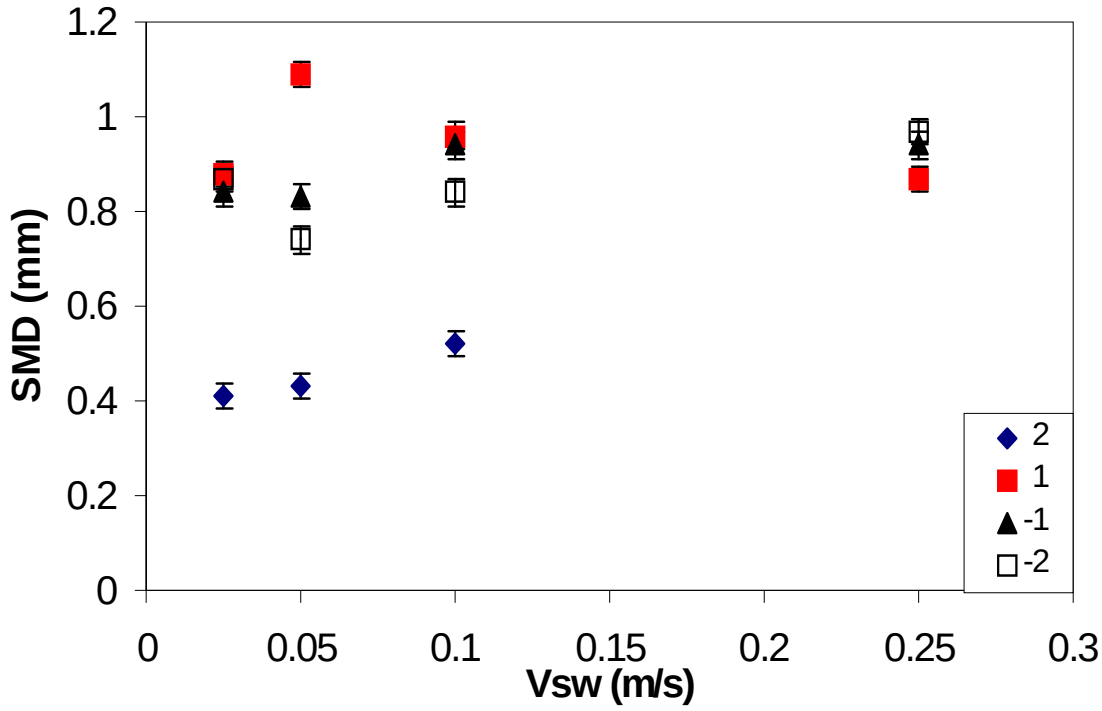

Figure 62 - Variation of SMD with v_{sw} and Inclination Angles for W/O Dispersions

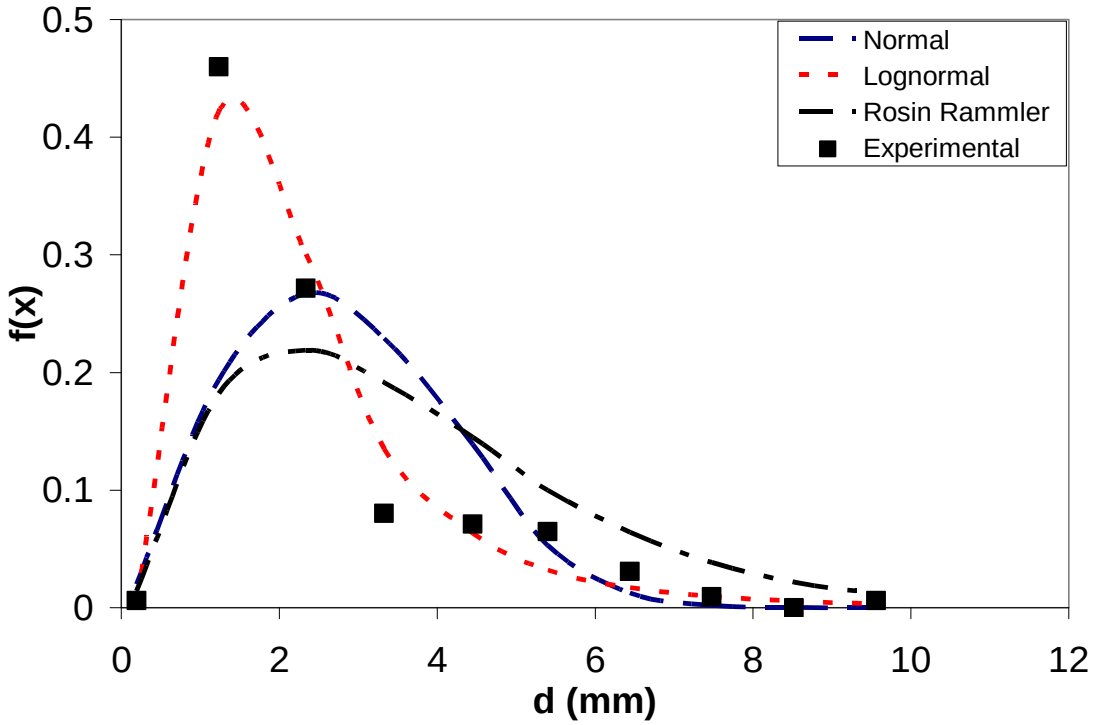

Figure 63 - Droplet Size Distributions (v_{so}=0.500 m/s, v_{sw}=0.100 m/s, +2° Upward)

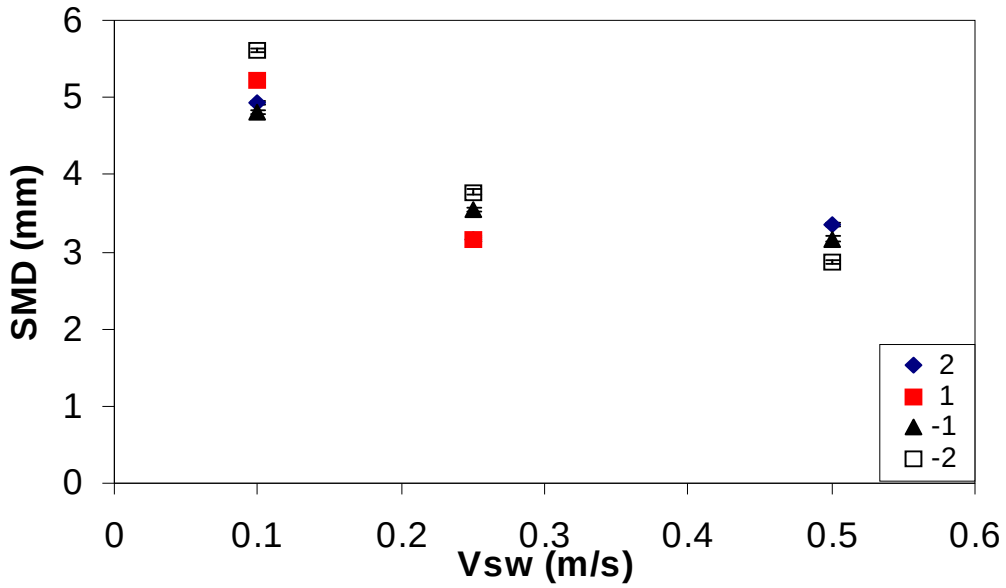

Figure 64 - Variation of SMD with v_{sw} and Inclination Angles for ST&MI Dispersions

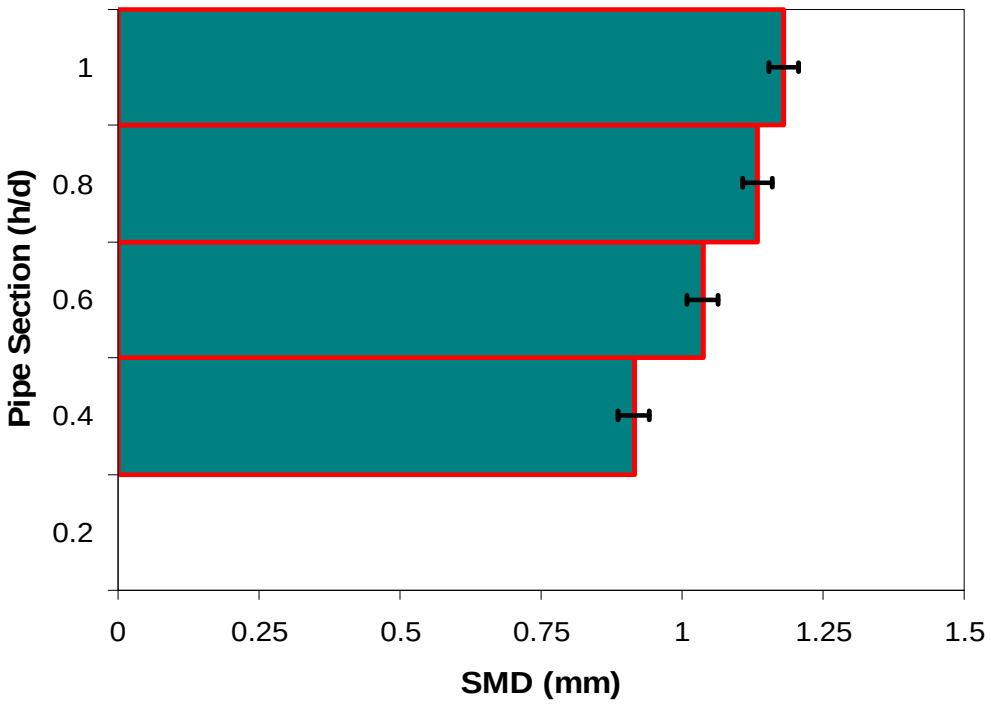

Figure 65 - SMD vs. h/D for D O/W & W (v_{so}=0.050 m/s, v_{sw}=1.000 m/s, +2° Upward)

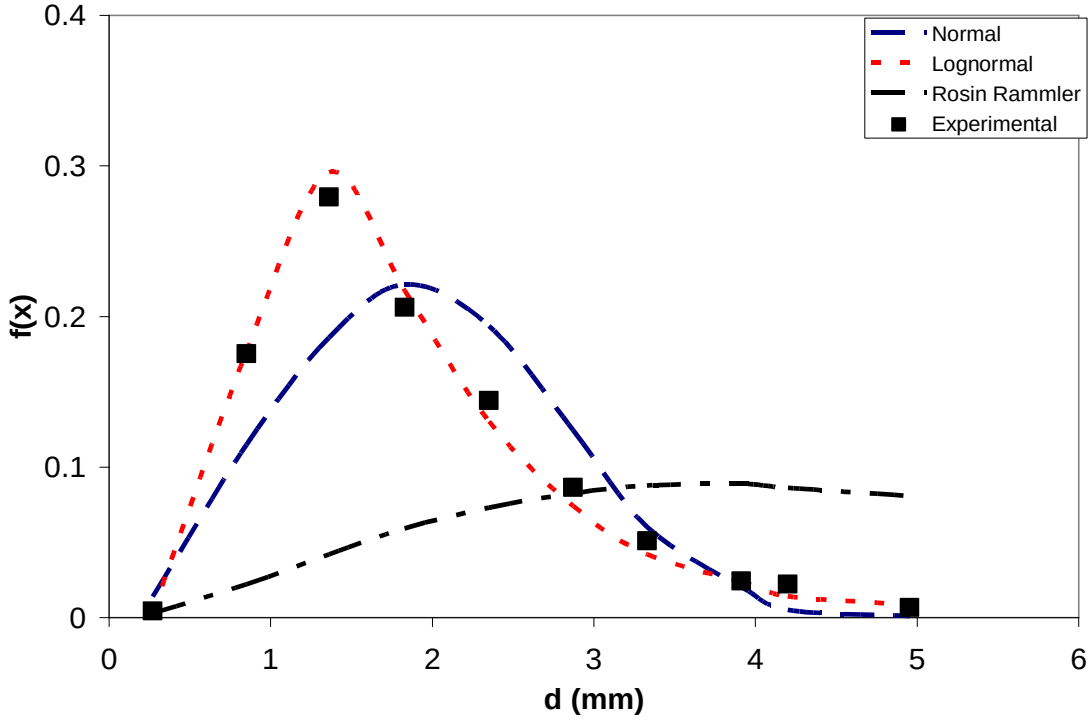

Figure 66 - Oil Droplet Size Distributions (v_{so}=1.000 m/s, v_{sw}=0.500 m/s, -1° Downward)

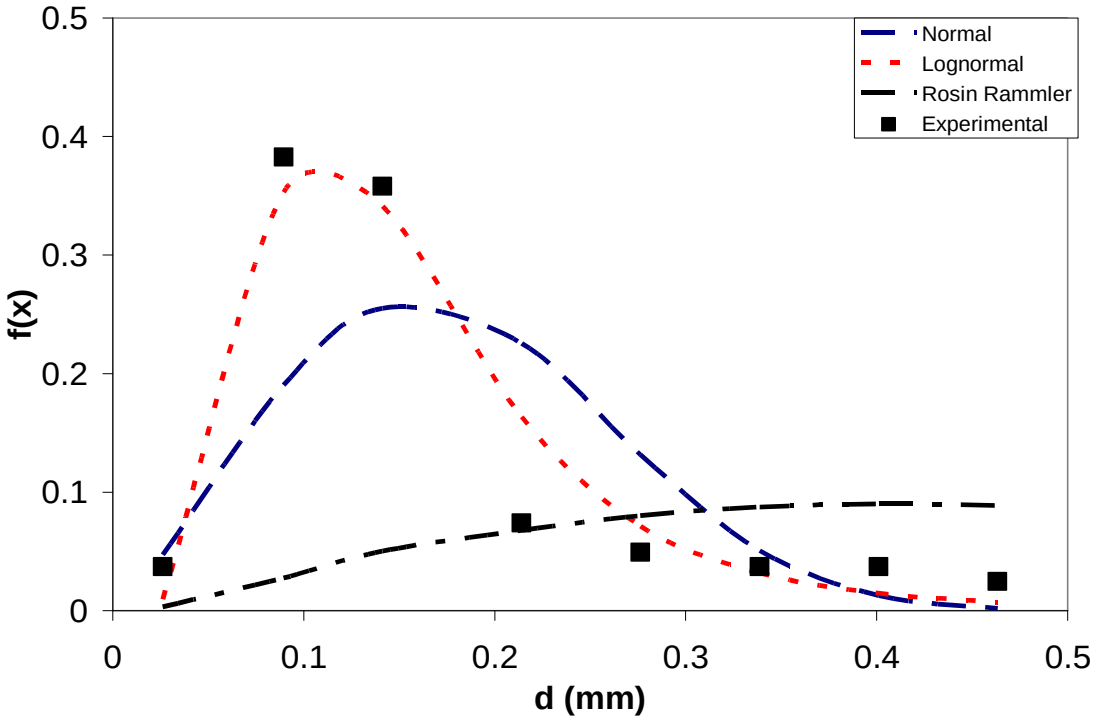

Figure 67 - Water Droplet Size Distribution (v_{so}=1.000 m/s, v_{sw}=0.500 m/s, -1° Downward)

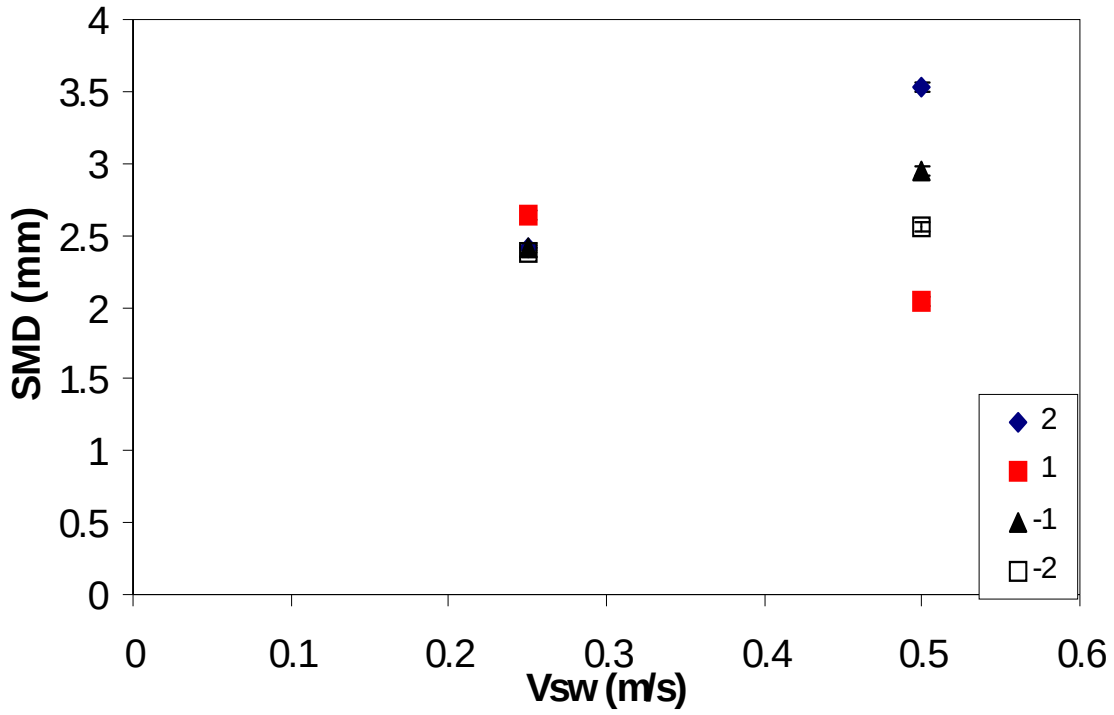

Figure 68 - Variation of SMD with v_{sw} and Inclination Angles for Oil Droplets

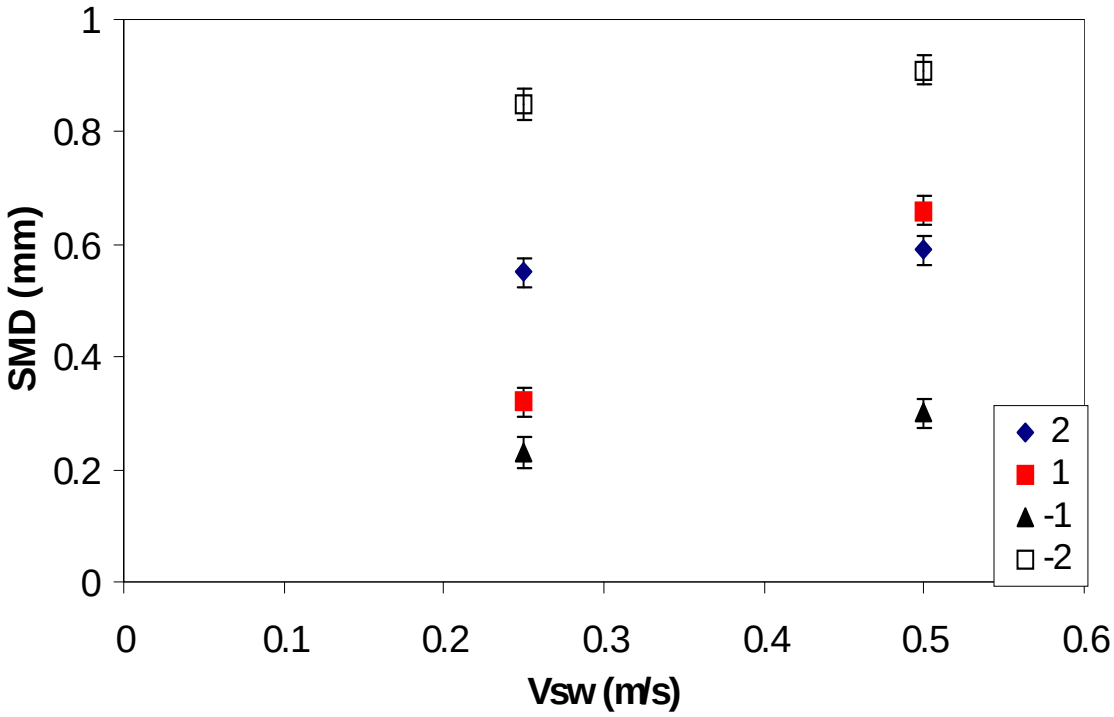

Figure 69 - Variation of SMD with v_{sw} and Inclination Angles for Water Droplets

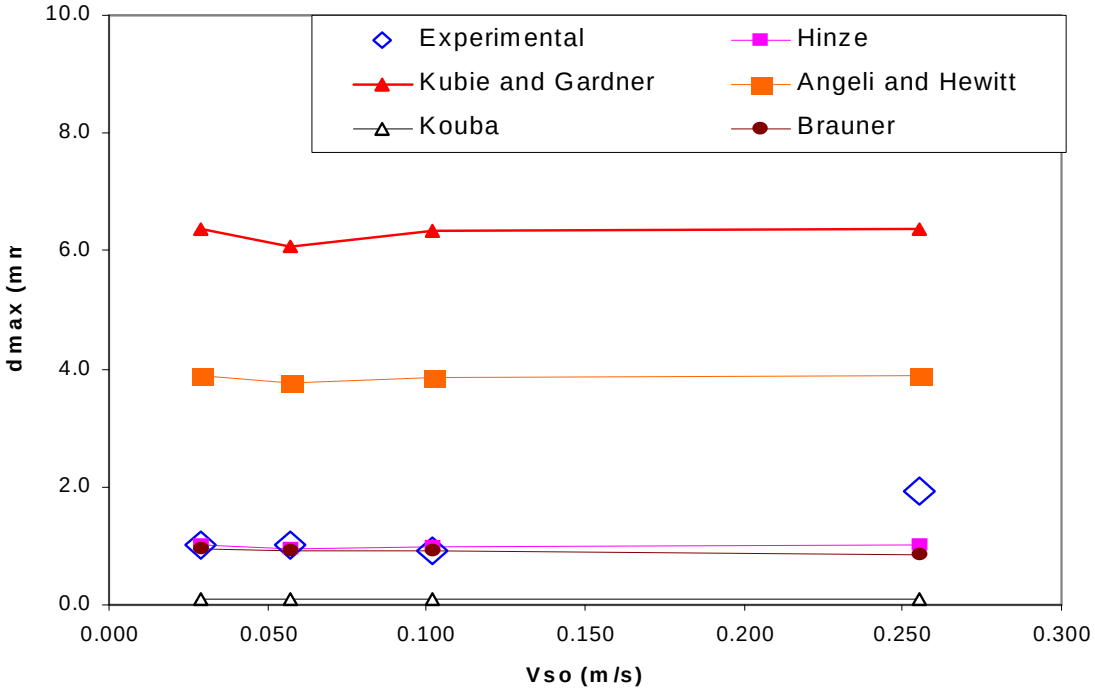

Figure 70 - Maximum Diameter Comparisons for v_{sw}=1.750 m/s (-1° Downward)

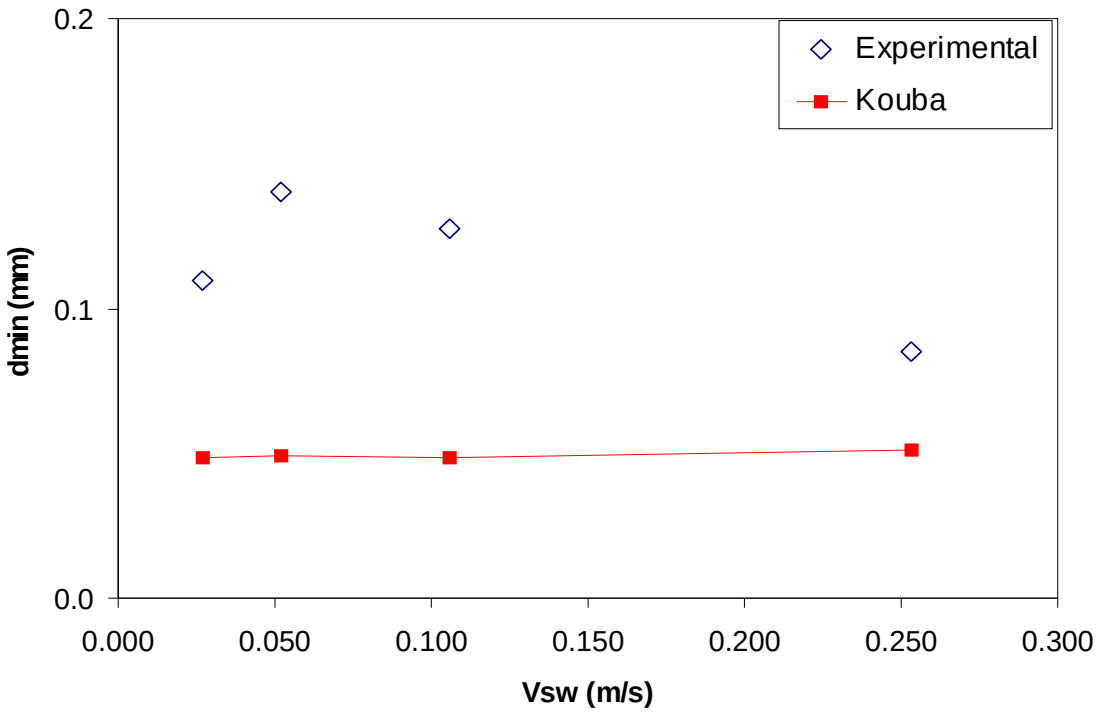

Figure 71 - Minimum Diameter Comparisons for v_{sw}=1.750 m/s (-1° Downward)

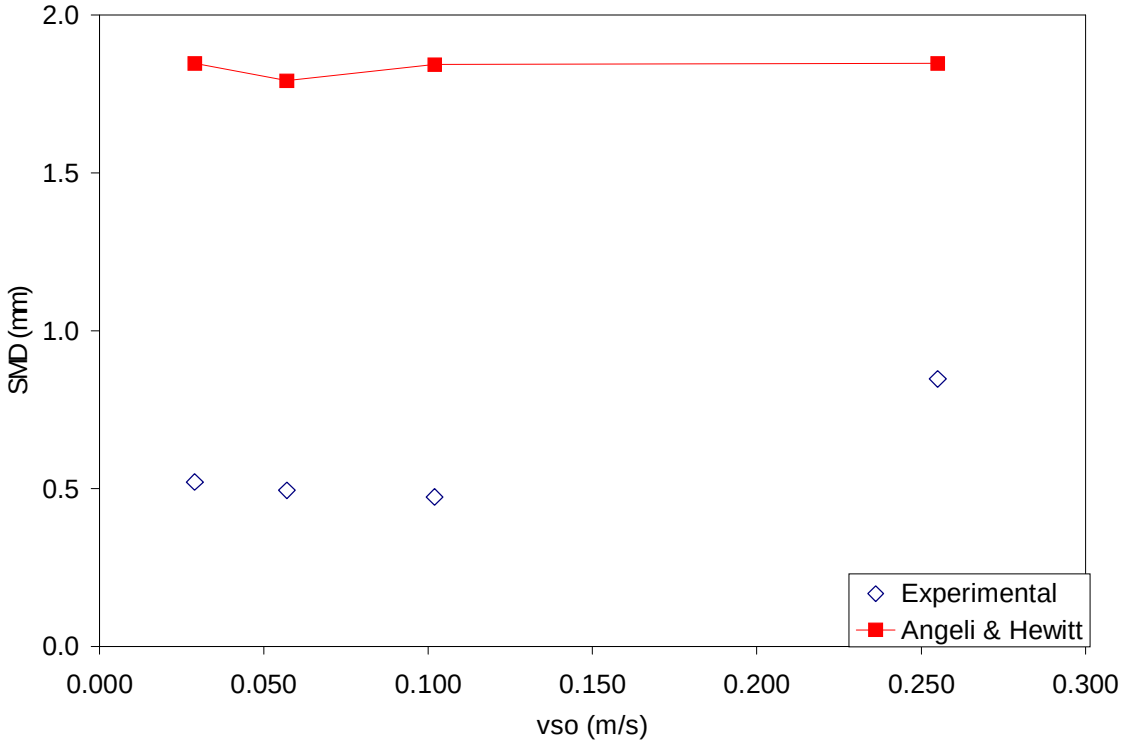

Figure 72 - SMD Comparisons for v_{sw}=1.750 m/s (-1° Downward)

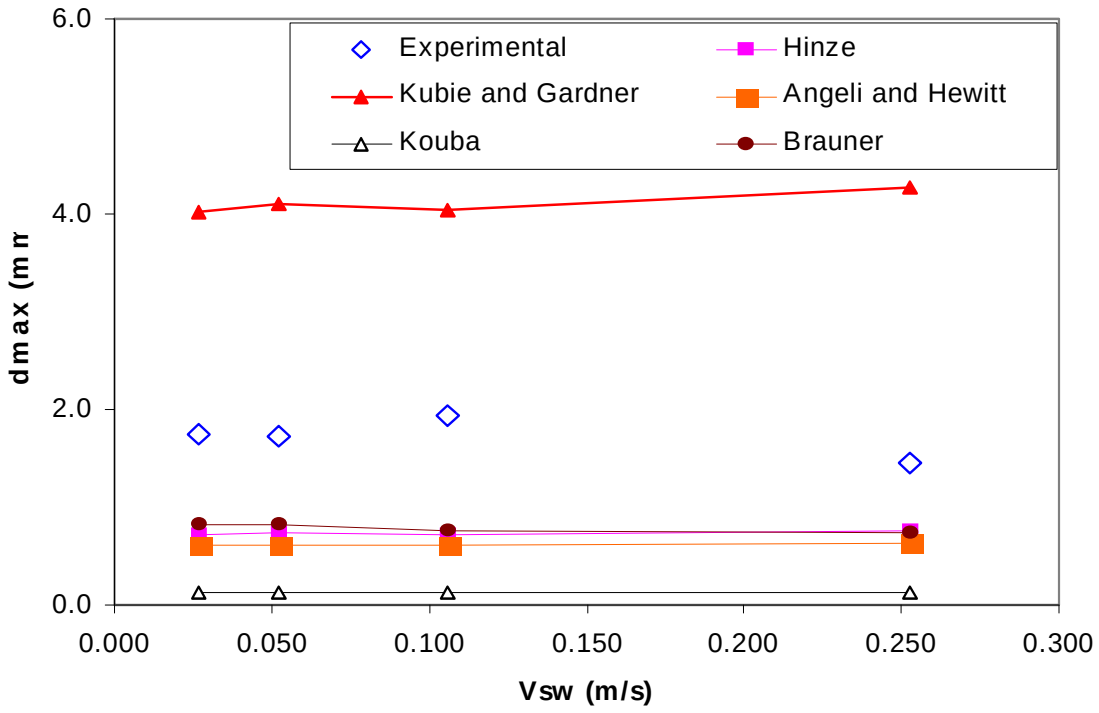

Figure 73 - Maximum Diameter Comparisons for v_{so}=1.750 m/s (-1° Downward)

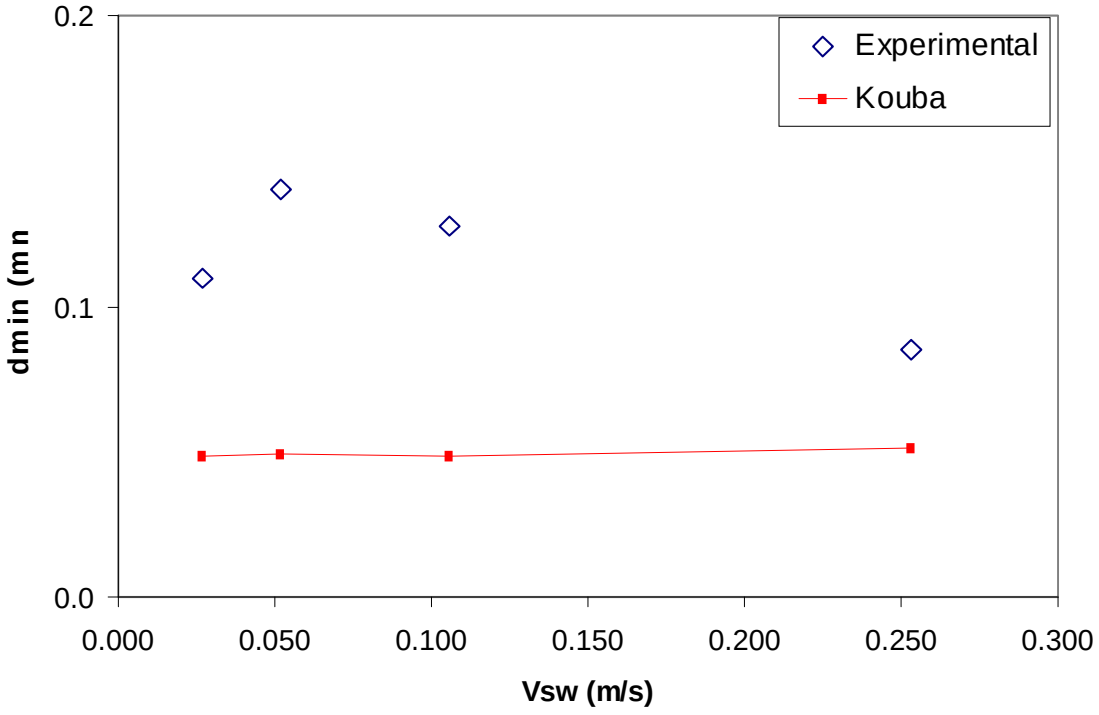

Figure 74 - Minimum Diameter Comparisons for v_{so}=1.750 m/s (-1° Downward)

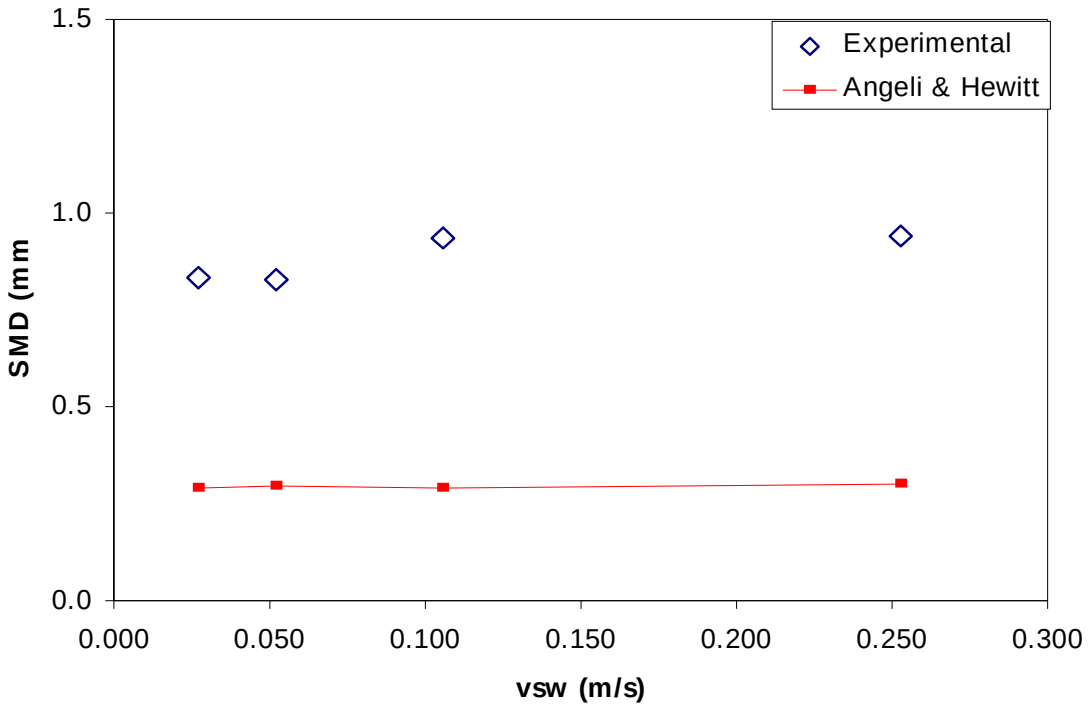

Figure 75 - SMD Comparisons for v_{so}=1.750 m/s (-1° Downward)

THREE-PHASE GAS-OIL-WATER PIPE FLOW DATABANK DEVELOPMENT AND MODEL PERFORMANCE

NEW DATABASE

The databank that was available at the start of this project was composed of 438 data points as given in the technology assessment section of this report. During the final year (Budget Period-2) of this project, the data base is expanded to 1013, 301 of which are generated with this study. The composition of the databank is given below.

- 392 data points from TUFFP Well Databank, vertical or deviated flow, pipe diameter ranges from 2 to 7 inches;
- 88 data points from TUFFP Dong (2007) low liquid loading data for 6 inches pipe horizontal flow;
- 213 data points from TUFFP Keskin (2005) data for 2 inches pipe horizontal flow;
- 93 data points from Hall (1992) for 3 inches pipe horizontal flow;
- 79 data points from TUFFP Laflin and Oglesby (1976) for 1.5 inches pipe horizontal flow;
- 34 data points from Malinowski (1975) for 1.5 inches pipe horizontal flow;
- 114 data points from Sobocinski (1955) for 3 inches pipe horizontal flow.

COMPARISON OF THE TESTING RESULTS

Both two-phase and three-phase flow models were used for the prediction of liquid holdup and pressure gradient, and the results were compared with the experimental data.

LIQUID HOLDUP

Figure 76 shows the comparison of liquid holdups from model prediction and experimental results with Dong's low liquid loading data. In this case, the three phase flow modeling gives much better predictions than the two-phase flow modeling.

Figure 77 shows the comparison of liquid holdups from model prediction and experimental results with Keskin (???) data for pipe horizontal flow. In this case, the three-phase and two-phase flow modeling give similar predictions.

PRESSURE GRADIENT

Figures 78–84 show the comparison of pressure gradient from model prediction and experimental results for all the data sets.

For the well data, Dong (2007) data and Laflin & Oglesby (1976) data, three-phase flow modeling give better predictions than the corresponding two phase flow modeling. For all the other cases, the predictions from both models are similar.

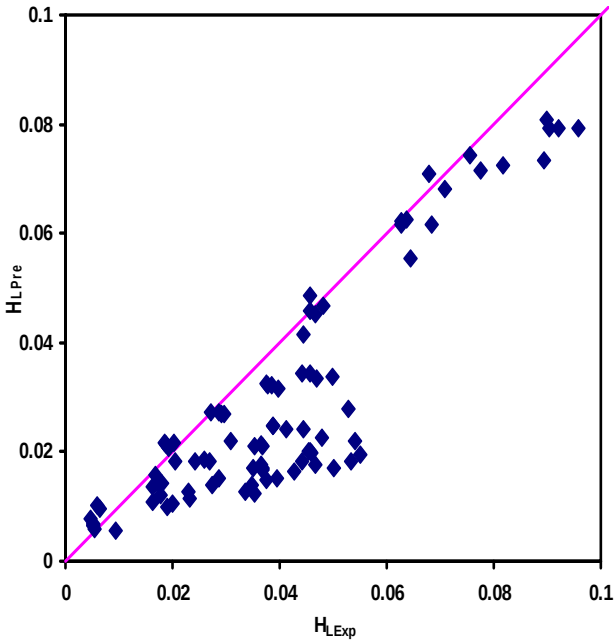

(a)

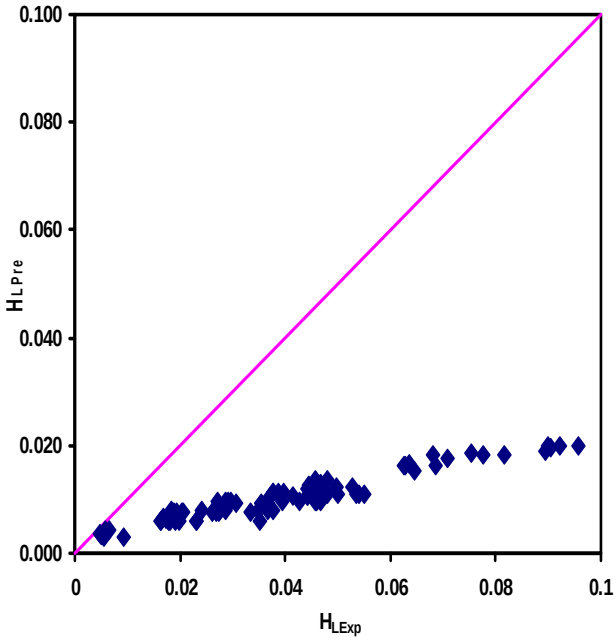

(b)

Figure 76 - Dong data – liquid holdup (a) Three-phase flow model results; (b) Two-phase flow model results compared with experimental data

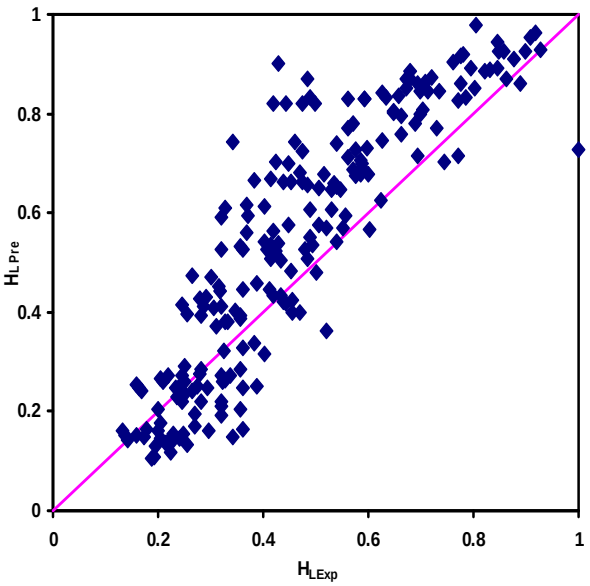

(a)

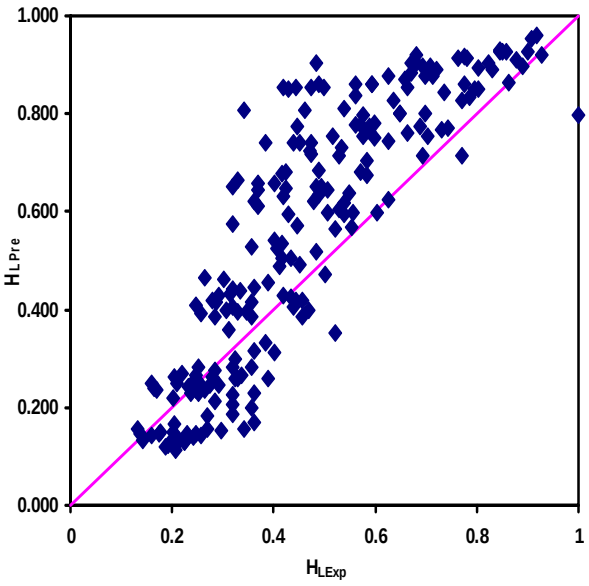

(b)

Figure 77 - Keskin data – liquid holdup (a) Three-phase flow model results (b) Two-phase flow model results compared with experimental data

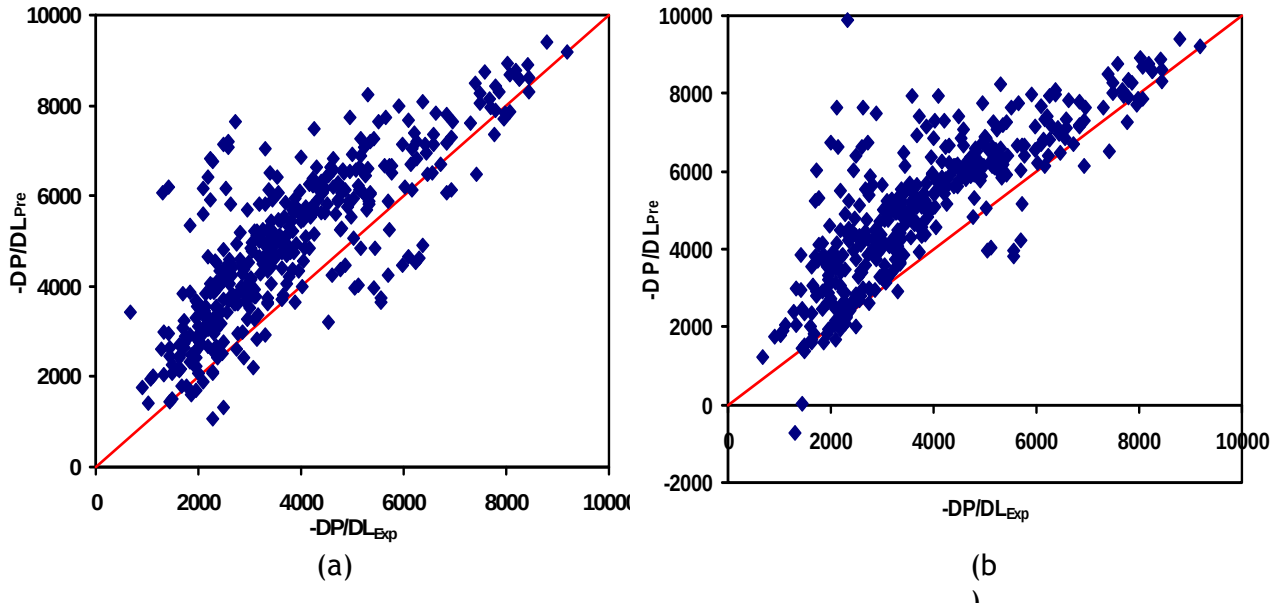

Figure 78 - Well databank – pressure gradient (a) Three-phase flow model results; (b) Two-phase flow model results compared with experimental data

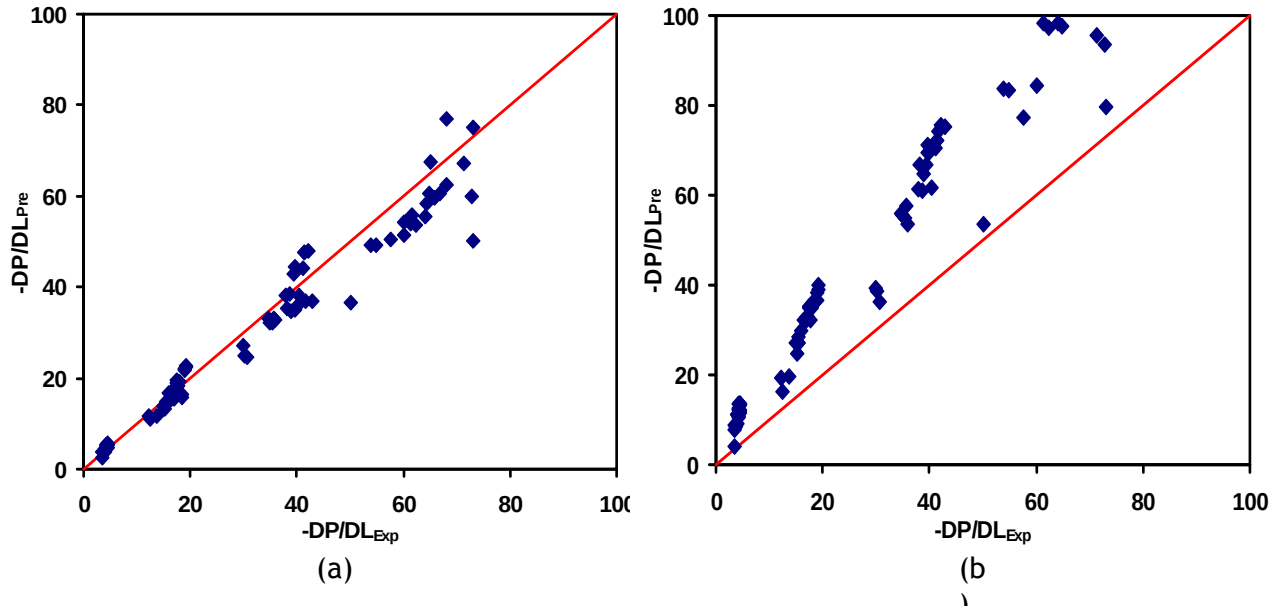

Figure 79 - Dong data – pressure gradient (a) Three-phase flow model results; (b) Two-phase flow model results compared with experimental data

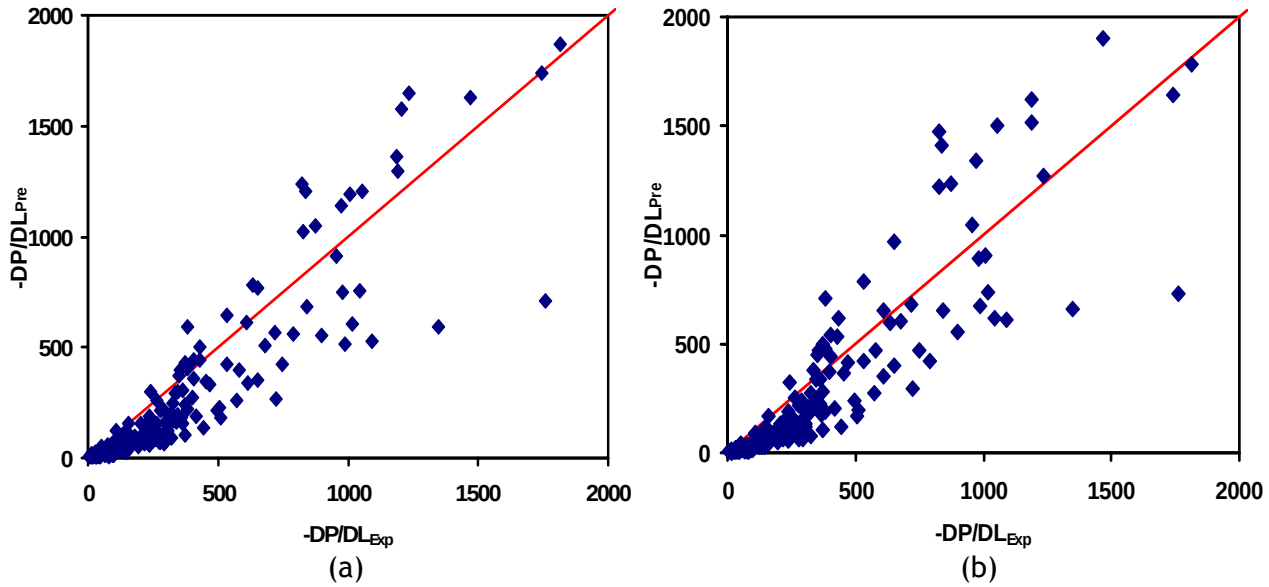

Figure 80 - Keskin – pressure gradient (a) Three-phase flow model results; (b) Two-phase flow model results compared with experimental data

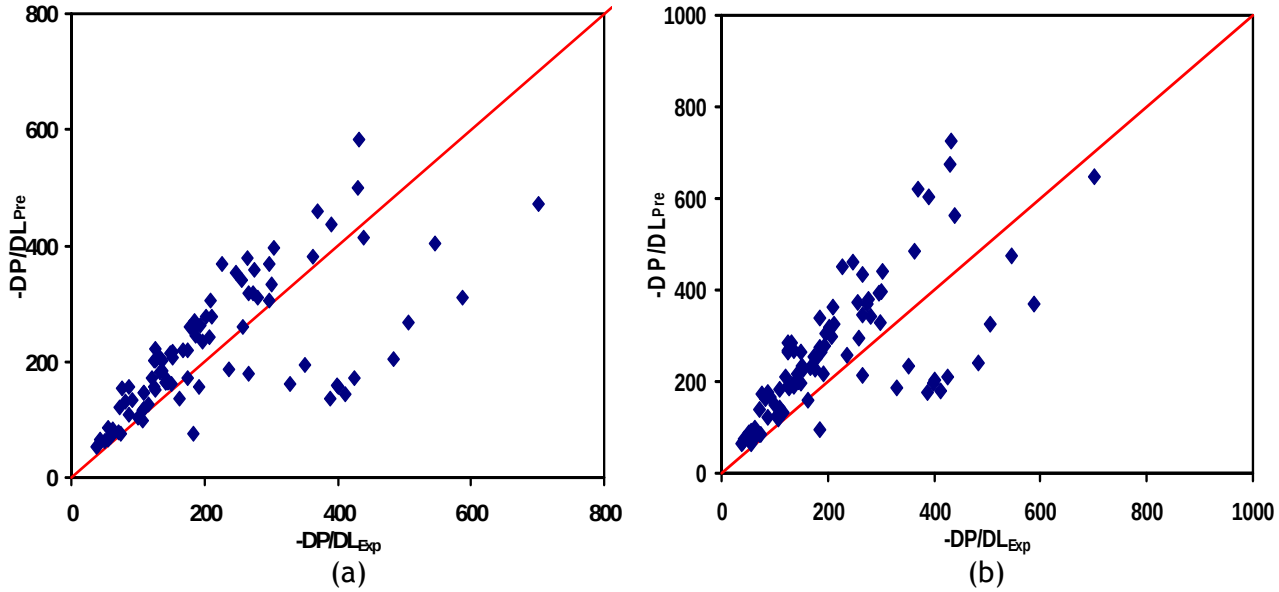

Figure 81 - Hall – pressure gradient (a) Three-phase flow model results; (b) Two-phase flow model results compared with experimental data

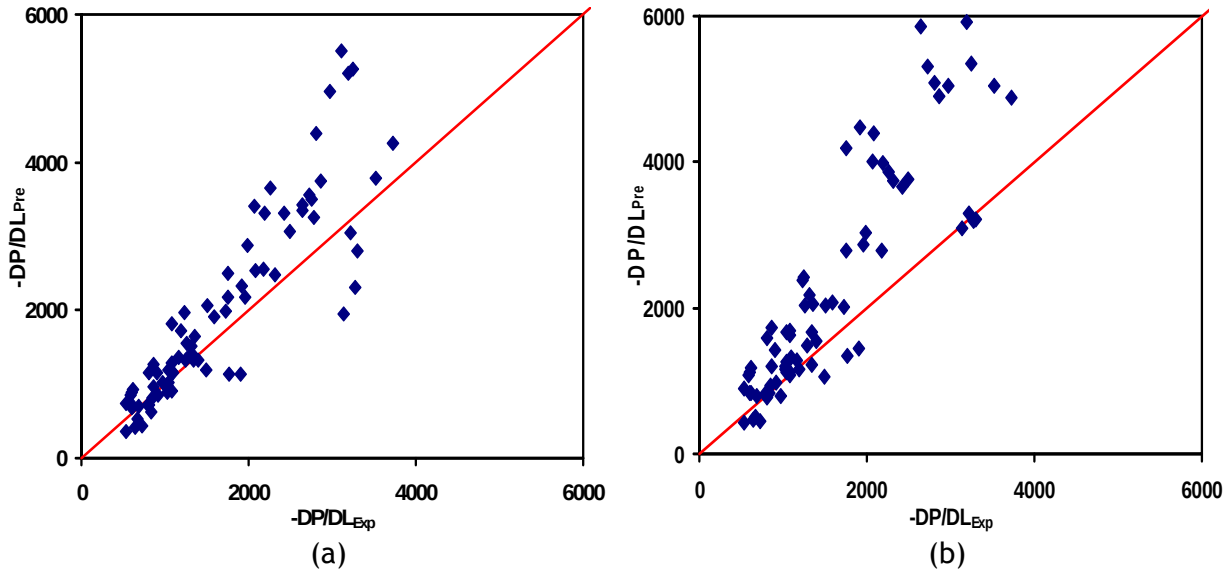

Figure 82 - Laflin & Oglesby –pressure gradient (a) Three-phase flow model results; (b) Two-phase flow model results compared with experimental data

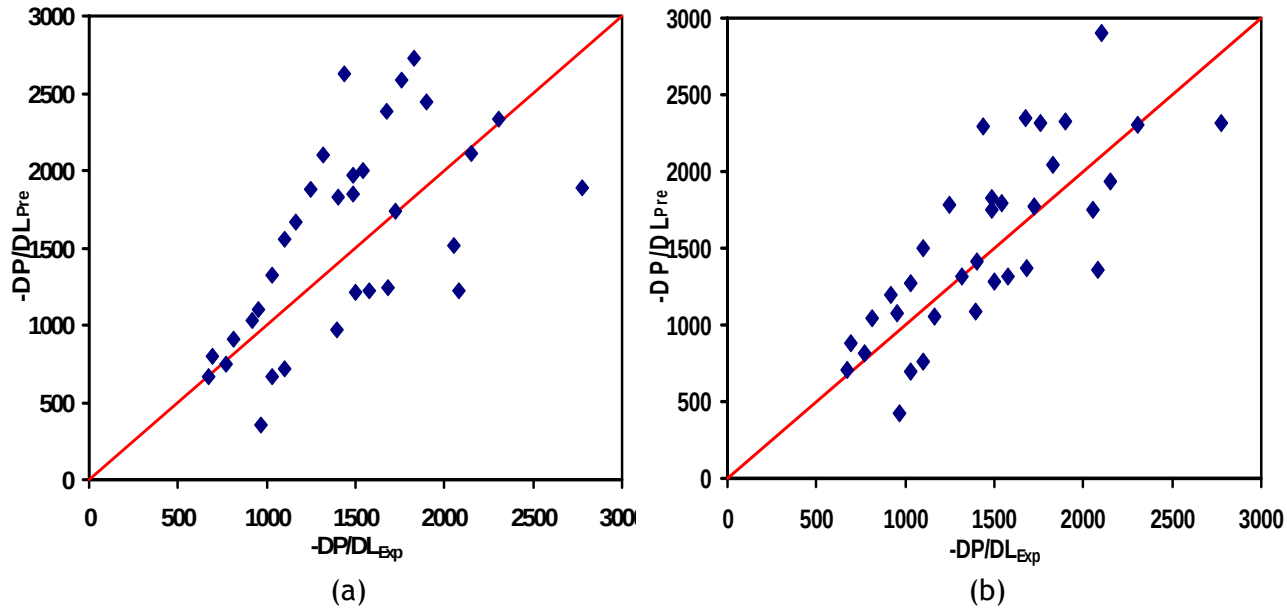

Figure 83 - Malinowski – pressure gradient (a) Three-phase flow model results; (b) Two-phase flow model results compared with experimental data

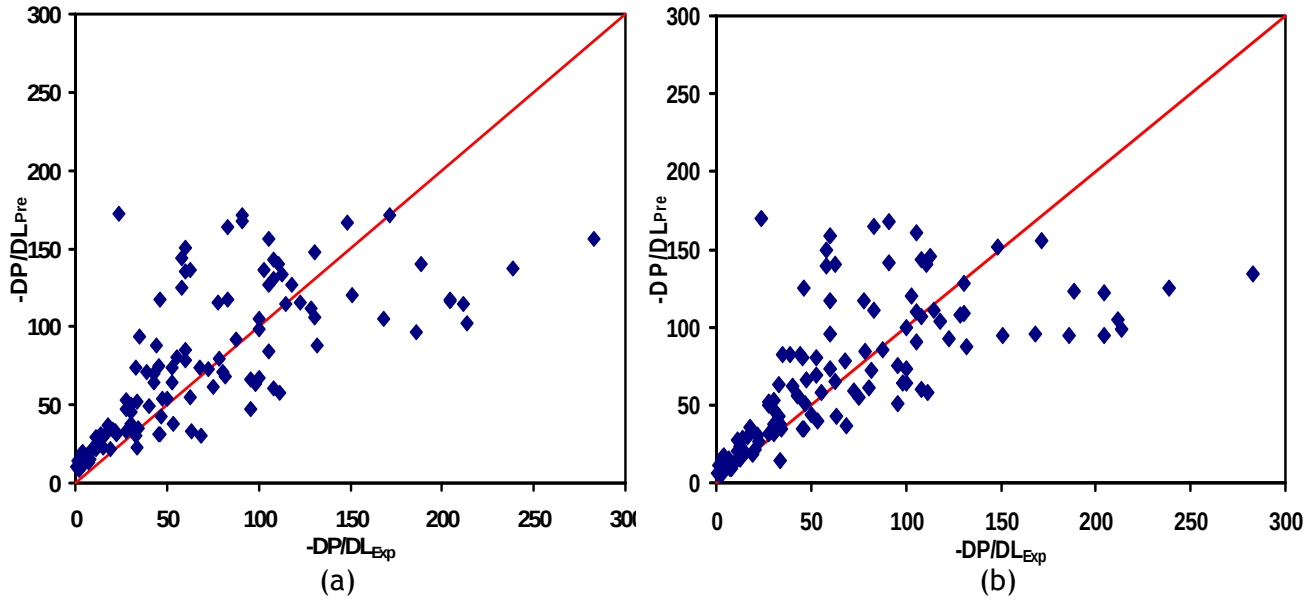

Figure 84 - Sobocinski – pressure gradient (a) Three-phase flow model; (b) Two-phase flow model results compared with experimental data

CONCLUSIONS

TECHNOLOGY ASSESSMENT

Gas-liquid two-phase flow models can be used to predict gas-oil-water three-phase flow pressure gradient (or pressure drop) if the oil and water can be assumed as a fully mixed single phase liquid. Comparisons have been made between two-phase model predictions and three-phase experimental data for upward vertical flows and horizontal/near-horizontal flows.

Model predictions agreed with experimental data better for vertical flows than for horizontal flows, and better for slug flows than for stratified flows. This was probably related to the mixing between oil and water. Oil and water are normally better mixed for vertical flows and for slug flows. Therefore, it is more valid to assume oil and water as a pseudo single phase liquid in these cases.

On the other hand, the comparison results indicated that, the stratification between the oil and water layers had to be considered at relatively low flow rates, especially for horizontal and near-horizontal flows.

When oil and water are fully mixed, they can be treated as a single-phase liquid. Better prediction methods need to be implemented for the inversion of the continuous phase and the effective viscosity of the liquid mixture.

UNIFIED MODEL (NEXT GENERATION MULTIPHASE PIPE FLOW PREDICTION TOOL) DEVELOPMENT

A unified model for gas-oil-water three-phase pipe flow has been developed. The model is based on the dynamics of slug flow, which shares transition boundaries with all the other flow patterns. The equations of slug flow are used not only to calculate the slug characteristics, but also to predict transitions from slug flow to other flow patterns.

The model requires closure relationships such as the gas-liquid interfacial friction factor, liquid entrainment fraction in the gas core, gas void fractions in oil and water in the slug body, slug translational velocity, and slug length) were implemented by using the corresponding gas-liquid two-phase closure relationships with necessary modifications. The other closure relationships (such as oil-water interfacial friction factor, oil water mixing, and phase inversion) were newly developed.

EXPERIMENTAL STUDY

Three-phase gas-oil-water horizontal flow and two-phase horizontal and inclined oil-water flow testing were conducted utilizing Tulsa University Fluid Flow Projects Three-phase Flow Facility. The objectives of the testing program were three-fold: 1. Observation and better description of the flows; 2. Acquire data to test the performance of the newly developed next generation multiphase flow prediction tool; 3. Acquire data to develop new closure relationships. Main highlights of the experimental study are given below.

Three-phase gas-oil-water tests were conducted for 20, 40, 50, 60 and 80 % water fractions. Based on the observations and high speed video recordings, three-phase gas-oil-water flow patterns in horizontal pipes were identified, and a new classification was proposed. 12

individual three-phase gas-oil-water flow patterns in horizontal pipes have been identified.

Pressure drop, holdup and wetted perimeter data were acquired for all of the tests. It can be concluded that pressure gradients increase with increasing gas and liquid flow rates and in general, the pressure gradients for water in oil dispersions are relatively higher than the pressure gradients for oil in water dispersions at similar gas and liquid flow rates most probably due to the change of the continuous phase.

Total liquid holdups generally increase with increasing liquid flow rates and decrease with increasing gas flow rate. Similar to that, wetted wall fractions increase when the superficial liquid velocities increase. At the same superficial liquid velocity, wetted wall fraction decreases with increasing superficial gas velocity.

Most of the three-phase gas-oil-water flow closure relationships require the information on oil-water flow. Therefore, an oil-water flow study has been conducted. The two-phase oil-water tests which cover the inclined pipe configuration have been conducted. The data has been analyzed. Flow patterns, pressure and holdup behavior of oil-water were studied.

An experimental study on flow pattern transition boundaries, pressure gradients, water holdups, phase distributions, droplet size and its distribution was successfully completed. 324 new oil-water data points were collected for 6 different inclination angles (0^o, $\pm1^o$, $\pm2^o$ and -5^o) for different superficial liquid velocities varying from 0.025 m/s to 1.750 m/s. An uncertainty analyses was performed in terms of random, systematic and combined uncertainties for all data collected. Pressure gradients, holdups, droplet size and phase distribution data was collected for horizontal configuration for comparison and repeatability reasons.

New experimental pressure gradient and water holdup data were compared against Zhang et al. unified model. Holdups were measured by raising the boom in order to decrease the uncertainty in measurement. Normalized velocity term was created to show no-slip velocity for different inclination angles.

Droplets were captured by using high speed camera. Each picture was analyzed carefully for different flow patterns and inclination angles. Videos were recorded for all 324 data points. Log-normal distribution was found to represent the droplet size distribution. The performance of the existing maximum diameter and Sauter Mean Diameter (SMD) correlations were tested and the best ones were identified.

DATABANK DEVELOPMENT AND MODEL PERFORMANCE

A new three-phase databank has been developed using the data generated during this project and additional data available in the literature. The unified model to predict the gas-oil-water three phase flow characteristics was tested by comparing the prediction results with the data. The results showed good agreements.

NOMENCLATURE

a, b, c	=	Example variables in uncertainty analysis
A	=	Cross-sectional area
b_i	=	Elemental systematic uncertainty
B	=	Combined systematic uncertainty
C_e	=	Coefficient in Eq. 32
C_H	=	Constant in Eq. 45
C_S	=	Constant in Eq. 55
C_w	=	Water cut
d	=	Droplet diameter (mm), differential
d	=	differential
D	=	Pipe diameter
D_{32}, SMD		Sauter Mean Diameter
e_{rj}	=	percentage error for component j
e_i	=	error for component i
$\bar{e}$	=	Rate of turbulent energy dissipation per unit mass
$\dot{E}_s$	=	Rate of surface free energy
f	=	friction factor
Fr	=	Froude number
g	=	gravity acceleration
H	=	holdup
h	=	height
l	=	Length
L	=	Pipe length
N	=	Number of data points
p	=	Pressure
Q	=	volume flow rate
Re	=	Reynolds number
RPF	=	relative performance factor
S	=	perimeter
S_x	=	Standard deviation of a population

$S_{\bar{x}}$	=	Standard deviation of a population average
$t_{95,\upsilon}$	=	Student's *t*
U	=	Uncertainty
U_{95}	=	Combined uncertainty with 95% confidence
v	=	velocity
v'	=	Velocity fluctuation
$\overline{X}$	=	Sample average
X_i	=	The *i*th data point
We	=	Weber number

SUBSCRIPTS

0	=	page 16, Eq. 39
c	=	Continuous phase
C	=	gas core
calc	=	calculated value
crit	=	critical
d	=	Dispersed phase
D	=	Drift
F	=	liquid film
G,g	=	gas
i	=	interface
I0	=	oil-water interface in slug body
I1	=	gas-oil interface in gas pocket region of slug flow
I2	=	oil-water interface in gas pocket region of slug flow
I	=	inversion
Int	=	internal phase
L	=	liquid
M	=	mixture
MAX	=	maximum
MIN	=	minimum
meas	=	measured value
N	=	normalized
O	=	Oil

OF	=	oil phase in slug body
OG	=	oil phase with entrapped gas
OS	=	oil phase in slug body
R	=	Random
S	=	slug
sc	=	superficial continuous
sd	=	superficial dispersed
SG	=	superficial gas
SO	=	superficial oil
SW	=	superficial water
t	=	total
T	=	translational
U	=	slug unit
W	=	water
WF	=	water phase in film region
WG	=	water phase in gas core
WGS	=	water and gas holdup in slug body, page 11-13
WS	=	water phase in slug body

GREEK SYMBOLS

α_{OS}	=	gas volume fraction in oil of slug body
α_{WS}	=	gas volume fraction in water of slug body
Δp_t	=	Total differential pressure
Δp_m	=	Measured differential pressure
ΔL	=	Differential distance
ε	=	absolute roughness of pipe inside wall
ε_1	=	average percentage error
ε_2	=	absolute average percentage error
ε_3	=	standard deviation of percentage errors
ε_4	=	average error
ε_5	=	absolute average error
ε_6	=	standard deviation of errors
ϕ	=	volumetric phase fraction

θ	=	inclination angle
λ	=	No-slip holdup
μ	=	dynamic viscosity
ρ	=	density
σ	=	Interfacial surface tension
τ	=	Shear stress

REFERENCES

Acikgoz, M, F. Franca and R, Lahey Jr.:" An Experimental Study of Three-Phase Flow Regimes." International Journal of Multiphase Flow, Vol-18, No. 3, P327-336 (1992).

Alkaya, B.: "Oil-Water Flow Patterns and Pressure Gradients in Slightly Inclined Pipes", M.S. Thesis, The University of Tulsa (2000).

Angeli, P and Hewitt, G.F.: "Drop Size Distributions in Horizontal Oil-Water Dispersed Flows," Chemical Engineering Science (2000) **26**, 1117-1140.

Atmaca, S.: "Characterization of Oil-Water Flows in Inclined Pipes," M.S. Thesis, The University of Tulsa (2007).

Barnea, D.: "A Unified Model for Predicting Flow-Pattern Transitions for the Whole Range of Pipe Inclinations," *Int. J. Multiphase Flow*, Vol. 11, pp. 1-12 (1987).

Beggs, D and J. Brill.: "A Study of Two Phase Flow in Inclined Pipes," Journal of Petroleum Technology, SPE-4007 (1973).

Brauner, N. and Ullmann, A., 2002, "Modeling of Phase Inversion Phenomenon in Two-Phase Pipe Flows," *Int. J. Multiphase Flow*, Vol. 28, pp. 1177-1204.

Brauner, N., 2001, "The Prediction of Dispersed Flows Boundaries in Liquid-Liquid and Gas-Liquid Systems," *Int. J. Multiphase Flow*, Vol. 27, pp. 885-910.

Brauner, N.: "Modeling and Control of Two Phase Flow Phenomena: Liquid-Liquid Two Phase Flow Systems," School of Engineering, Tel-Aviv University, Tel-Aviv 69978, Israel (2002).

Brinkman, H.C., 1952, "The Viscosity of Concentrated Suspensions and Solutions," *J. Chemical Physics*, Vol. 20, No. 4, p. 571.

Brodkey, R. S.: The Phenomena of Fluid Motions, Addison-Wesley (1969).

Chierici, G. L., Ciucii, G. M and Sclocchi, G.: "Two-Phase Vertical Flow in Oil Wells – Prediction of Pressure Drop," *J. Pet. Tech.*, 927-938, Aug. (1974).

Churchill, S.W.: "Frictional Equation Spans All Fluid Flow Regions," *Chem. Eng.* (1977)**84**(24), 91.

Dong, H.: "An Experimental Study of Low Liquid Loading Gas-Oil-Water Flow in Horizontal Pipes,",M.S. Thesis, U. of Tulsa, Tulsa, OK (2007).

Espanol, H. J. H.: "Comparison of Three Methods for Calculating a Pressure Traverse in Vertical Multi-Phase Flow," M.S. Thesis, The University of Tulsa, (1968).

Fancher, G. H., Jr. and Brown, K. E.: "Prediction of Pressure Gradients for Multi-Phase Flow in Tubing," *Soc. Pet. Eng. J.*, 3, 59-69, Trans. AIME, 228, March (1963)

Flores, J. G.: "Oil-Water Flow in Vertical and Deviated Wells", Ph.D. Dissertation, The University of Tulsa (1997).

Govier, G. W. and Fogarasi, M.: "Pressure Drop in Wells Producing Gas and Condensate," *J. Can. Pet. Tech.,* 28-41, Oct – Dec (1975).

Grolman, E., 1994, "Gas-Liquid Flow with Low Liquid Loading in Slightly Inclined Pipes," PhD Dissertation, U. of Amsterdam, The Netherlands, ISBN 90-9007470-8.

Hagedorn, A. and K. Brown.: "Experimental Study of Pressure Gradients Occurring During Continuous Two-Phase Flow in Small Diameter Vertical Conduits," SPE-940 (1965).

Hall, A. R. W.: "Multiphase Flow of Oil, Water and Gas in Horizontal Pipes," Ph.D. Thesis, Imperial College of Science, Technology and Medicine, University of London (1992).

Hinze, J.O., 1955. "Fundamentals of the Hydrodynamic Mechanism of Splitting in Dispersion Processes," AIChE J. Vol. 1, p. 289.

Kaya, A. S.: Comprehensive Mechanistic Modeling of Two-Phase Flow in Deviated Wells, M.S. Thesis, The University of Tulsa (1998).

Keskin, C.: "An Experimental and Modeling Study of Gas-Oil-Water Flow in Horizontal Pipes," Progress Report, Fall 2005 TUFFP ABM Brochure, Tulsa OK (2005).

Khor, S. H., "Three-Phase Liquid-Liquid-Gas Stratified Flow in Pipelines," PhD Thesis, Imperial College of Science, Technology and Medicine, University of London (1998).

Khor, S.H., Mendes-Tatsis, M.A. and Hewitt, G.F., 1997, "One-Dimensional Modeling of Phase Holdups in Three-Phase Stratified Flow," *Int. J. Multiphase Flow*, Vol. 23, No. 5, pp. 885-897.

Kouba, G.: "Mechanistic Models for Droplet Formation and Breakup," *Proceedings of ASME* (2003), 1-9.

Kubie, J. and Gardner, G.C.: "Drop Sizes and Drop Dispersion in Straight Horizontal Tubes and Helical Coils," *Chem. Eng. Sci.* (1977) 32, 195-202.

Kvandal, H., A. Valle, B. Robole and T. Arvesen.: "Comparison between Three-phase Field Tests and Multiphase Simulation Code," SPE-49159 (1998).

Laflin, G. C. and Oglesby, K. D.: "An Experimental Study on the Effects of Flow Rate, Water Fraction and Gas-Liquid Ratio on Air-Oil-Water Flow in Horizontal Pipes," B.S. Thesis, The University of Tulsa (1976).

Langsholt, M. and Holm, H.: "Oil-Water-Gas Flow in Steeply Inclined Pipes," BHR Group Multiphase '01, pp. 279-291 (2001).

Malinowsky, M. S.: "An Experimental Study of Oil-Water and Air-Oil-Water Flowing Mixtures in Horizontal Pipes," M.S. Thesis, The University of Tulsa (1975).

Malinowsky, M. S.: An Experimental Study of Oil-Water and Air-Oil-Water Flowing Mixtures in Horizontal Pipes, M.S. Thesis, The University of Tulsa (1975).

Nicklin, D. J.: "Two-Phase Bubble Flow," *Chem. Eng. Sci.*, Vol. 17, pp. 693-702 (1962).

Oliemans, R.V., Pots, B.F.M. and Trompe, N., 1986, "Modeling of Annular Dispersed Two-Phase Flow in Vertical Pipes," *Int. J. Multiphase Flow*, **12**(5), pp. 711-732.

Orkiszewski, J.: "Predicting Two-Phase Pressure Drops in Vertical Pipes," *J. Pet. Tech.* 19, 829-838, June (1967)

Pan, L., Jayanti, S. and Hewitt, G.F., 1995, "Flow Patterns, Phase Inversion and Pressure Gradient in Air-Oil-Water Flow in a Horizontal Pipe," Proceedings of the 2nd International Conference on Multiphase Flow '95-Kyoto, April 3-7, 1995, Kyoto, Japan.

Poettmann, F. H. and Carpenter, P.G.: "The Multi-Phase Flow of Gas, Oil and Water through Vertical Flow String with Application to the Design of Gas Lift Installations," *Drill. And Prod. Prac., API*, 257-317 (1952).

Sobocinski, D. P.: "Horizontal Co-current Flow of Water, Gas-Oil, and Air" Master's Thesis, University of Oklahoma, (1955).

Stapelberg, H.: "The Slug Flow of Oil, Water and Air in Horizontal Tubes," PhD Dissertation, University of Hannover (1991)

Taitel, Y., Barnea, D. and Brill, J. P.: "Stratified Three Phase Flow in Pipes," *Int. J. Multiphase Flow*, Vol. 21, No. 1, pp. 53-60 (1995).

Trallero, J. L.: "Oil-Water Flow Patterns in Horizontal Pipes", Ph.D. Dissertation, The University of Tulsa (1995).

Valle, Arne.: "Three Phase Gas-Oil-Water Pipe Flow," Ph/D Thesis, Imperial College of Science, Technology and Medicine, University of London (2000).

Vielma, M.: "Characterization of Oil-Water Flows in Horizontal Pipes," M.S. Thesis, The University of Tulsa (2006).

Woods, G.S., Spedding, P.L., Watterson, J.K. and Raghunathan, R.S., 1998, "Three-Phase Oil/Water/Air Vertical Flow," *Trans IChemE*, Vol. 76, Part A, pp. 571-584.

Zhang, H.-Q., Wang, Q. and Brill, J.P., 2003a, "A Unified Mechanistic Model for Slug Liquid Holdup and Transition between Slug and Dispersed Bubble Flows," *Int. J. Multiphase Flow*, **29**, pp. 97-107.

Zhang, H.-Q., Wang, Q., Sarica, C. and Brill, J.P., 2003b, "A Unified Mechanistic Model for Slug Liquid Holdup and Transition Between Slug and Dispersed Bubble Flows," *Int. J. Multiphase Flow*, Vol. 29. pp. 97-107.

Zhang, H.-Q., Wang, Q., Sarica, C. and Brill, J.P., 2003b, "Unified Model for Gas-Liquid Pipe Flow via Slug Dynamics — Part 1: Model Development," ASME *J. Energy Res. Tech.*, **125**(4), pp. 266-273.

National Energy Technology Laboratory

626 Cochrans Mill Road
P.O. Box 10940
Pittsburgh, PA 15236-0940

3610 Collins Ferry Road
P.O. Box 880
Morgantown, WV 26507-0880

One West Third Street, Suite 1400
Tulsa, OK 74103-3519

1450 Queen Avenue SW
Albany, OR 97321-2198

539 Duckering Bldg./UAF Campus
P.O. Box 750172
Fairbanks, AK 99775-0172

Visit the NETL website at:
www.netl.doe.gov

Customer Service:
1-800-553-7681